LICENTIATE THESIS

Oxidation and Alpha–Case Phenomena in Titanium Alloys used in Aerospace Industry: Ti–6Al–2Sn–4Zr–2Mo and Ti–6Al–4V

Birhan Sefer

LULEÅ UNIVERSITY OF TECHNOLOGY

LICENTIATE THESIS

Oxidation and Alpha–Case Phenomena in Titanium Alloys used in Aerospace Industry:

Ti–6Al–2Sn–4Zr–2Mo and Ti–6Al–4V

Birhan Sefer

Division of Materials Science

Department of Engineering Sciences and Mathematics

Luleå University of Technology

Engineering Materials

Division of Materials Science

Department of Engineering Sciences and Mathematics

Luleå University of Technology

SE–971 87 Luleå

Printed by Luleå University of Technology, Graphic Production 2014

ISSN 1402-1757
ISBN 978-91-7439-927-1 (print)
ISBN 978-91-7439-928-8 (pdf)

Luleå 2014

www.ltu.se

To my parents, my brother and my wife Elma

ABSTRACT

Titanium and its alloys are attractive engineering materials in aerospace industry because of their outstanding mechanical properties such as high specific strength and excellent corrosion resistance. Ti–6Al–2Sn–4Zr–2Mo (Ti–6242) and Ti–6Al–4V (Ti–64) are two alloys commonly used for manufacturing components in jet engines, such as fan blades, disks, wheels and sections of the compressor where the maximum temperature is in the range of 300–450 °C. At temperatures above 500 °C and in oxygen containing environments, these alloys are oxidizing rapidly. Oxidation normally involves formation of an oxide scale on top of the metal and a hard and brittle oxygen enriched layer beneath the scale which is known as "alpha–case". The alpha–case layer has a detrimental effect on important mechanical properties such as ductility, fracture toughness and especially the fatigue life when an engine component is subjected to dynamic loading. In order to increase the understanding of the oxidation and alpha–case phenomena, the behaviour of these two alloys after long time exposure in air at elevated temperature has been investigated.

Heat treatments were performed on Ti–6242 and Ti–64 alloys in ambient air at 500, 593 and 700 °C for times up to 500 hours. The oxide scale and the alpha–case layer were analysed, characterized and compared for both alloys. It was found that the oxide scale and alpha–case thickness are functions of temperature and time. Faster and more complex oxidation kinetics was noted in Ti–64, whereas in Ti–6242 the oxidation kinetics was found moderate at all tested temperatures and times. Discrepancies in the oxidation kinetics are believed to be because of the differences in the chemical composition and the microstructure of the two alloys. In addition, different morphology of the oxide scales was observed after 500 hours exposure time at 700 °C.

The thickness of the alpha–case layer was measured using conventional metallographic and microscopic techniques. It was found that in both alloys the alpha–case growth obeys parabolic law with respect to time at all three tested temperatures. In addition, the diffusion coefficients and the activation energy of oxygen diffusion were estimated in the temperature range of 500–700 °C for the two alloys. Electron probe micro analyser (EPMA) was used to measure the oxygen concentration along the thickness of the alpha–case layer. It was found that the oxygen concentration decreases along the alpha–case layer. The oxygen concentration profiles were used to estimate the alpha–case thicknesses and it was found good agreement with the optically measured values for almost all investigated temperatures and times. Only at 700 °C in the time interval 300–500 hours in Ti–6242 a difference between the results from the two methods was found. Moreover, the EPMA concentration profiles of the main α and β alloying elements, before and after heat treatment at 700 °C for 500 hours, revealed microstructural changes and an increase of the α–phase volume fraction in the two investigated alloys.

Keywords: Titanium alloys, Microstructure, Oxidation, Oxygen diffusion, Oxide Scale, Alpha–case, SEM and EPMA.

PREFACE

The research described in this thesis has been carried out at the Division of Materials Science, Luleå University of Technology (LTU) between September 2012 and May 2014. Three collaborators are involved in this project: Luleå University of Technology (LTU), the Polytechnical University of Catalonia (UPC) and GKN Aerospace Engine Systems in Trollhättan, Sweden.

The thesis comprises of introduction to the research field and compilation of the following papers:

Paper I

Raghuveer Gaddam, Birhan Sefer, Robert Pederson, Marta–Lena Antti, Study of alpha–case depth in Ti–6Al–2Sn–4Zr–2Mo and Ti–6Al–4V, Institute of Physics Conference Series: Materials Science and Engineering, 2013 (In Press).

Paper II

Raghuveer Gaddam, Birhan Sefer, Robert Pederson, Marta–Lena Antti, Oxidation and alpha–case formation in Ti–6Al–2Sn–4Zr–2Mo alloy, submitted for publication.

Paper III

Birhan Sefer, Raghuveer Gaddam, Antonio Mateo, Robert Pederson, Marta–Lena Antti, Characterization of the oxide scale and alpha–case layer in Ti–6Al–4V and Ti–6Al–2Sn–4Zr–2Mo in the temperature range 500–700 °C, to be submitted for publication.

Luleå, May 2014

Birhan Sefer

ACKNOWLEDGMENTS

At the beginning, I would like to express my gratitude to my supervisors, Marta–Lena Antti and Robert Pederson for their guidance, support and sharing their knowledge in this field. Also, I am very thankful to my former colleague and closest collaborator Raghuveer Gaddam, for his help, suggestions and long fruitful discussions. Big thanks go to Pia Åkerfeldt for being my PhD adviser and sharing her knowledge and experience in titanium alloys field.

I also want to thank all my PhD colleagues and all staff members of Division of Materials Science at LTU, for creating pleasant working environment. I am very thankful to Esa Vuorinen and Ragnar Tegman, always willing to help with their suggestions and discussions. Special thanks go to Johnny Grahn and Lars Frisk for sharing their experience in the labs and helping me with the instruments. Big thanks go to all my friends in Luleå and Macedonia, for their support, motivation and encouragement.

I would like to acknowledge the Joint European Doctoral Programme in Materials Science and Engineering (DocMASE) for providing me with financial support.

I would also like to express my gratitude to my parents and my brother for providing me with support, inspiration and motivation through the years.

Finally, I am very lucky and happy to have Elma and I am very thankful for her love, understanding, support and motivation that guide me and give me strength to overcome all obstacles in my life.

Contents

CHAPTER 1

INTRODUCTION

High specific strength, low density and excellent corrosion resistance of titanium and its alloys, compared to steel, aluminium (Al) and nickel (Ni)–based superalloys, make them attractive to be used as structural materials in aerospace applications [1]. The main reasons for using titanium alloys in aerospace applications include [2]:

- Weight savings (replacement of steel and Ni–based superalloys)
- Space savings due to high specific strength (replacement of Al alloys)
- Better fatigue strength than Al alloys
- Low susceptibility to corrosion in different environments (compared to Al alloys and low carbon steels)
- Good temperature stability at elevated temperatures (replacement of steel, Al alloys and Ni–based superalloys)
- Composite compatibility (replacement of Al alloys)

Through the years the application of titanium alloys in commercial aircrafts has been increasing significantly, reaching approximately 9 % of the total weight in Boeing 777 and Airbus aircrafts. Moreover, nowadays titanium alloys are representing the second most abundant material used in jet engines, after Ni–based superalloys [3]. This has been attained due to development of numerous titanium alloys, which meet the high demanding application requirements such as high strength, ductility and creep resistance at elevated pressure/temperature conditions. However, one of the major drawbacks of titanium alloys is their low oxidation resistance when they are exposed for long–term at elevated temperatures and oxygen containing environments. In such conditions titanium reacts readily with oxygen, thereby forming an oxide scale on the surface and a hard and brittle oxygen enriched layer beneath the scale, known as “alpha–case” [1,3,4]. It is well known that alpha–case significantly reduces the mechanical properties of titanium, such as ductility, fracture toughness and fatigue life [1,3,4] and therefore is undesirable in the jet engine components. Figure 1.1 shows development of titanium alloys together with their maximum application temperatures [5]. Adding different alloying elements in various quantities significantly expands the maximum application temperature of the titanium alloys, which today is ranging between 300–600 °C, depending on the alloy.

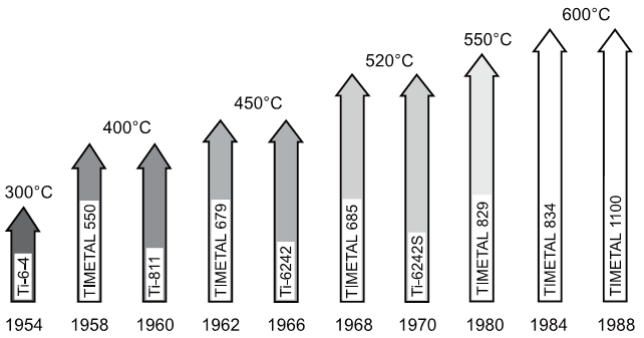

Figure 1.1 *Thirty years of development of titanium alloys used in jet aero engines and their maximum application temperature [5]*

The jet engine designers are working intensively on the new design of future engines with primary objective to improve the efficiency, but also to maintain the environmental and economic restrictions. One way to improve efficiency is to increase the pressure in the engines, which is resulting also with increase of the temperature. Therefore, there is a need to introduce new materials or expand the thermal stability of already known titanium alloys at higher temperatures, with goal to replace the heavier Ni–based superalloys in the jet engines. In order to accomplish this, better knowledge and understanding of the phenomena of oxidation and alpha–case formation and its effect on the mechanical properties in various titanium alloys are needed.

1.1 Aim and objective of the research

The present research was initiated by GKN Aerospace Sweden to evaluate the effect of elevated temperature (500–700 °C) and long exposure time (up to 500 hours) in ambient air on the oxidation and alpha–case phenomena in Ti–6Al–2Sn–4Zr–2Mo (Ti–6242) and Ti–6Al–4V (Ti–64) alloys. The objectives of the research were as follows:

- To investigate and compare the oxidation behaviour of the two alloys.
- To characterize and compare the oxide scales in the two alloys.
- To measure and compare the thickness of the alpha–case layer developed in both alloys.
- To estimate and compare the diffusion kinetics of oxygen, such as diffusion coefficients and activation energy of oxygen diffusion in both alloys.
- To evaluate and compare any metallurgical and/or microstructural changes in both alloys, dependent on oxidation temperature, time and alloying chemistry.

CHAPTER 2

BACKGROUND

This chapter describes the background theory to the research field and includes a literature review for the investigated alloys.

Several names in the history are responsible for today's importance of titanium and its alloys in numerous disciplines. Titanium was discovered in 1791 by William Gregor in England. Four years later, the German chemist Martin Heinrich Klaproth isolated titanium oxide from the mineral "rutile" and he named the element Titanium after the Titans from the Greek mythology. However, production of titanium in larger scales was initiated even in 1932 by Wilhelm Justin Kroll, who introduced a method for production of pure titanium by combining $TiCl_4$ and magnesium. Even today this method is widely used and therefore Kroll is recognized as the father of titanium industry.

Titanium is the ninth abundant element and the fourth most prevalent structural element in the Earth's crust after aluminum, iron and magnesium. However, it is never found in pure state and therefore its processing is difficult and expensive. The high processing expenses, but also the impressive properties compared to other structural materials, explains the preferential use of titanium and its alloys in the aerospace industry.

Pure titanium exists in two allotropic forms, α–titanium (α–phase) with hexagonal close–packed (HCP) crystal structure and β–titanium (β–phase) with body centred–cubic (BCC) crystal structure. Figure 2.1 shows the unit cells of α and β–phase of titanium, together with some crystallographic parameters. In Figure 2.1 a) one of the three most densely packed (0002) planes are shown, also known as basal plane, one of the three $\{10\bar{1}0\}$ planes, called prismatic planes and one of the six $\{10\bar{1}1\}$ pyramidal planes for the HCP crystal structure of titanium. The axes a_1, a_2 and a_3 are the close packed directions with indices $<11\bar{2}0>$. On the other hand, in Figure 2 b) is illustrated one of the six most densely packed {110} planes in the BCC crystal structure of titanium.

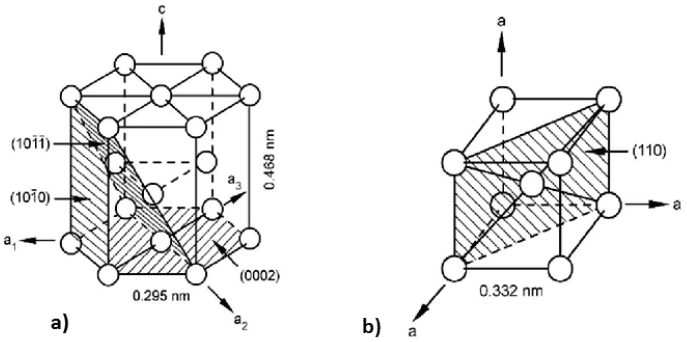

Figure 2.1 *Cristal structures of titanium, a) hexagonal close–packed (α–phase) and b) body centred–cubic (β–phase) [1]*

At 882 ± 2 °C an allotropic phase transformation from α to β–phase occurs and this temperature is recognized as the β–transus temperature. At room temperature and temperatures up to the β–transus temperature the α–phase is stable, whereas at temperatures above the β–transus the β–phase is stable. The allotropic phase transformation temperature is strongly dependent on the alloying elements present in the metal and is therefore a factor of the purity of the metal [1]. The occurrence of titanium in two phases together with the corresponding allotropic phase transformation temperature is of particular importance for the processing metallurgy of titanium and its alloys, since that is the basis for achieving good mechanical properties [5].

2.1 Manufacturing of titanium alloys

The procedure of manufacturing titanium alloys includes several steps [4]:

1) Reduction of the titanium ore, i.e. rutile (TiO_2) or ilmenite ($TiFeO_3$) to impure titanium sponge
2) Purification of the obtained titanium sponge
3) Melting of the sponge with or without added alloying elements in order to obtain ingots
4) Processing of the ingots to obtain mill products such as bar, plate, sheet, strip, wire etc.

A schematic overview of the manufacturing steps of titanium alloys is shown in Figure 2.2. The Kroll process is the starting step used to obtain "raw" titanium and includes reduction of $TiCl_4$ with magnesium that results in formation of titanium sponge. The reduction of $TiCl_4$ can also be performed with sodium and this process is known as Hunter process [1,4,7]. In the next step the titanium sponge is purified through vacuum distilling process, which completely removes the present byproducts (magnesium chloride) formed in the previous Kroll process. The purified titanium sponge is then blended in small particles with master alloy granules of the same size. The master alloy is a mixture that contains the alloying elements in higher concentrations than the final alloy and helps to minimize segregation and obtain the correct alloy composition. Both the blended titanium sponge and the master alloy granules are pressed together into briquettes and then welded together to form electrodes.

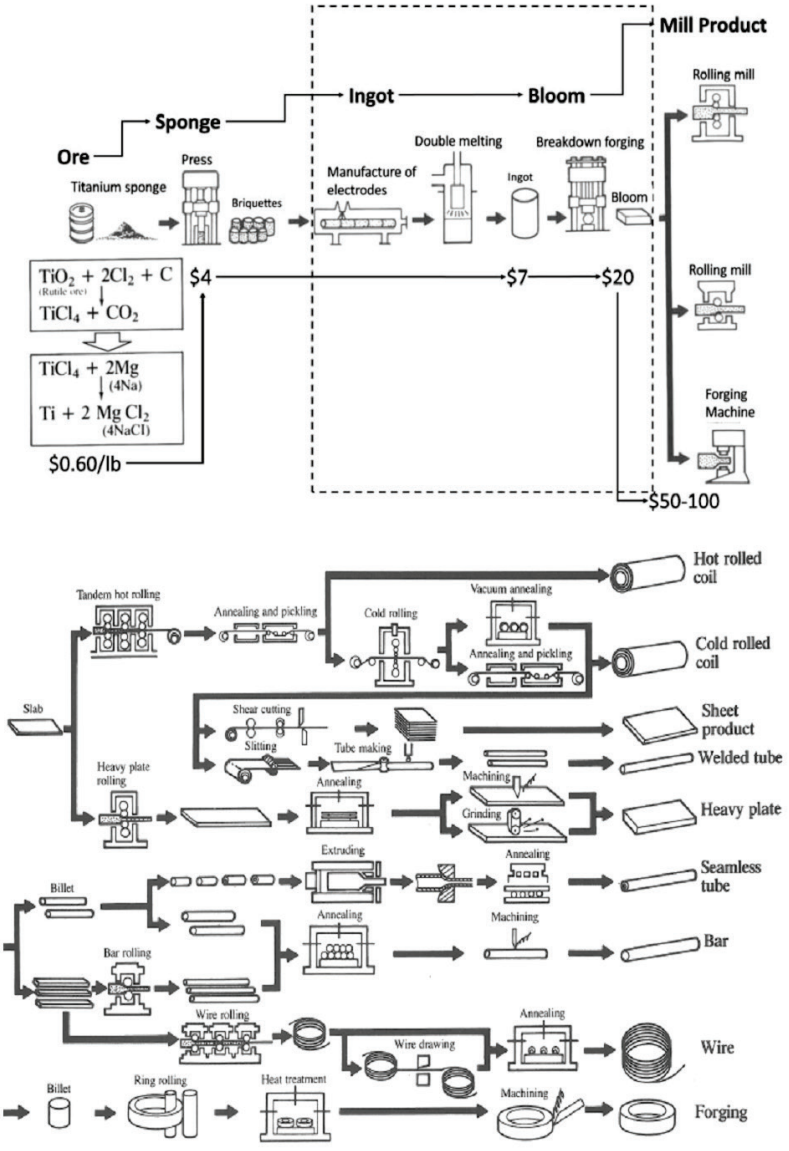

Figure 2.2 *Overview of the manufacturing pathway of titanium alloys [4]*

In the next step, the obtained electrode with a length of 4.5 meters and a diameter of more than half a meter is melted using a process known as vacuum arc remelting (VAR). Vacuum arc remelting (see Figure 2.3) contributes in removal of hydrogen and other volatiles picked up from the previous steps and also minimize the alloy segregation. During melting the electrode plays a role as anode and the water cooled copper crucible as cathode. The titanium electrode is consumed during the VAR in the water cooled copper crucible and the produced

ingot serves as electrode for the next VAR process. This process of remelting of the ingot is repeated twice in order to eliminate segregation of the alloy.

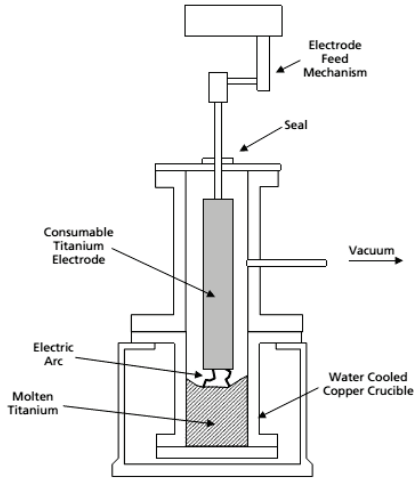

Figure 2.3 *Vacuum arc melting of titanium ingots [7]*

Titanium alloys are available in many mill product forms such as: billet, bar, plate, sheet, strip, foil, extrusion, wires and tubing. Various processing operations are applied to convert the obtained ingots into mill products. Hot working is used to refine the grain size, to obtain uniform microstructure and reduce segregation. Prior to thermo–mechanical processing, the as–cast ingots are subjected to grinding in order to remove any surface defects. The first deforming step of the as–cast ingots involves forging, pressing and cogging in order to achieve homogenization of the structure and to break–up the transformed beta structure. Most of these operations are initially performed above the β–transus temperature, but some of them are in later stages also performed below the β–transus temperature in order to refine the microstructure and to avoid surface rupturing. The obtained billets and bars from the forging operations are later subjected to straightening, annealing, grinding and ultrasonic inspection. Additionally, the slabs are hot rolled into plate or sheet forms, followed by finishing operations such as annealing, descaling in hot caustic baths, straightening, grinding, pickling and ultrasonic inspection.

Before obtaining the final products the titanium alloys are subjected to heat treatments. Some of the heat treatments for titanium alloys include stress relieving, annealing and solution treating and aging (STA). Stress relief is used in order to remove the residual stresses from the mechanical processing, cooling of the castings and the heat treatment. Combinations of different temperatures and times are used for the stress relief heat treatments. Temperatures in the range of 450–800 °C are commonly used for stress relief of the near–α and α+β titanium alloys. On the other hand, annealing is quite similar to stress relief except that it is performed at higher temperatures in order to remove all of the residual stresses and stresses caused by the cold working. Some of the frequently used annealing operations for titanium alloys are mill annealing, duplex annealing, recrystallization annealing and beta annealing. Mill annealing is performed at the mill and it is not full annealing which means that it can

leave traces of cold or warm working in the microstructure. Only near–α and α+β titanium alloys are mill annealed. The beta alloys are not annealed since this process can lead to formation of precipitations of embrittling phases. Duplex annealing is used to obtain better creep resistance and consists of a two stage annealing processes. The first annealing is performed at high temperature in the alpha + beta field and is followed by air cooling. The second annealing is conducted at lower temperature in order to obtain thermal stability and is followed by air cooling. Recrystallization annealing is commonly used for improvement of the fracture toughness and consists of heating the titanium part at temperatures in the upper range of the alpha + beta field, holding for some time and then slow cooling. In contrast, the beta annealing is performed at temperatures above the β–transus temperature followed by air cooling or water quenching to avoid formation of grain boundary alpha. Such treatment maximizes the fracture toughness, but also significantly decreases the fatigue strength of the alloy. Solution treating and aging (STA) is used to obtain high strength levels of the alloys. Solution treating consists of heating the part high in the alpha + beta phase field and then followed by quenching. During solution treating the ratio of beta phase to alpha phase is increasing and maintained afterward by the quenching. Aging, on the other hand, consists of reheating the solution treated part. During this heat treatment alpha phase precipitates from the retained beta in the structure. For example, typical STA treatment for Ti–64 would be solution treating at 905–930 °C followed by water quenching. Thereafter, the aging would be conducted at 539 °C for 4 hours and followed by air cooling. The best practice is to conduct the heat treatments in vacuum furnaces in order to avoid contamination with oxygen, hydrogen and nitrogen.

2.2 Metallurgy of titanium alloys

As mentioned before pure titanium exists in two phases with respect to the temperature. The stability of the phases and their amount at room temperature can be changed by adding different alloying elements. Moreover, adding alloying elements to titanium also changes the β–transus temperature. Figure 2.4 shows the effect of some alloying elements on the β–transus temperature.

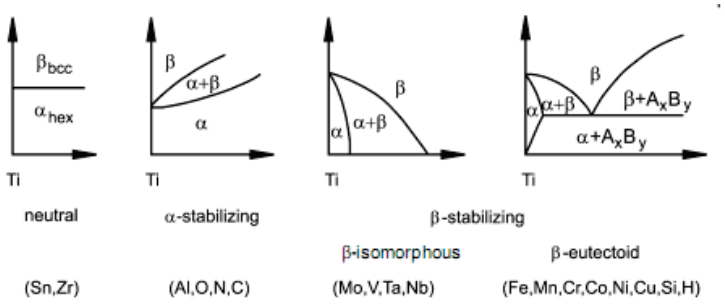

Figure 2.4 *Effect of alloying elements on phase diagrams of titanium alloys [1]*

As seen from Figure 2.4 there are elements that added to titanium increase the β–transus temperature through stabilizing the α–phase and those elements are called *α–stabilizers*. In contrast, there are elements known as *β–stabilizers* that are stabilizing β–phase thereby decreasing the β–transus temperature. The β–stabilizing elements are divided into β–isomorphous and β–eutectoid elements. Those elements that have high solubility in titanium are β–isomorphous, whereas the β–eutectoid elements have limited solubility and tend to form

intermetalics. On other hand, there are also elements that do not affect the β–transus temperature and they are called neutral elements.

Aluminum is the most common used α–stabilizing alloying element, because it is the only element that raises the β–transus temperature and has large solubility in both α and β–phase (see Figure 2.5). However, its content in most titanium alloys is limited to about 6 wt. % in order to avoid formation of Ti_3Al precipitates in the α–phase. From the Ti–Al phase diagram shown in Figure 2.5, it can be seen that for about 6 wt. % aluminium the β–transus temperature is elevated from 882 to about 1000 °C. Moreover, the Ti–Al phase diagram is also basis for development of titanium–aluminum intermetallics that are characterized with high strength at high temperatures, but also with very low ductility and fracture toughness compared to the conventional titanium alloys.

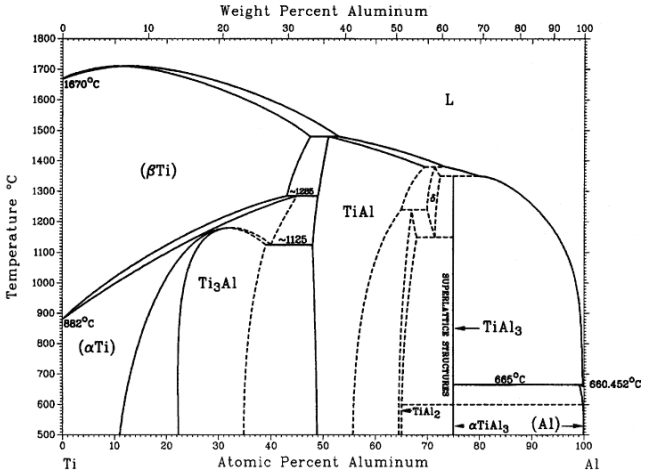

Figure 2.5 *Ti–Al phase diagram [6]*

Oxygen is also an important alloying element that has significant impact by increasing the strength of titanium alloys and is used to obtain the desired strength levels. Other α–stabilizing elements include B, Ga, Ge and some rare earth elements, but because of their low solubility they are not commonly used as alloying elements.

Most frequently used β–isomorphous stabilizing elements include V, Mo and Nb that in sufficient amounts stabilize the β–phase at room temperature. In the group of β–eutectoid stabilizing elements that are used in many titanium alloys belong Cr, Fe and Si, whereas Zr, Hf and Sn behave neutral i.e. do not have strong impact on the β–transus temperature.

2.2.1 Alloy classification

The titanium alloys are divided into three main classes, α, α+β and β alloys, which are further subdivided into two more subclasses, near–α and metastable or near–β alloys (see Figure 2.6). The classification is based on the type and amount of alloying elements which determines the dominate phase at room temperature.

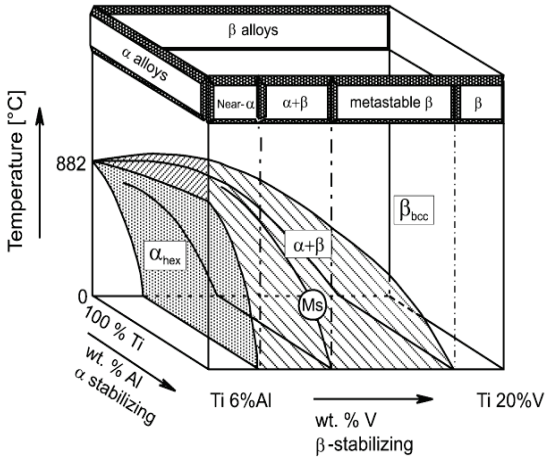

Figure 2.6 *Schematic three–dimensional phase diagram for classification of titanium alloys [5]*

α alloys and near α–alloys

This class of alloys comprises commercial pure titanium (CP–titanium) and alloys that contain α–stabilizing and/or neutral alloying elements such as oxygen, aluminum and tin. The CP–titanium grades differ only in the oxygen content that drastically increases the strength, but also reduces the ductility. Elements like iron and carbon are considered as impurities obtained mainly from the manufacturing process. These alloys are characterized with high corrosion resistance and deformability, thus are primarily used in the chemical and process engineering industry. The near α–alloys contain minor fractions of β–stabilizing alloying elements and are commonly referred as high–temperature alloys. These alloys are used in high temperature applications (500–550 °C) since they have excellent creep behaviour and high strength. The excellent creep properties at elevated temperatures are due to the small additions of Si that tend to segregate on dislocations and form TiSi precipitates in the grain boundaries thus preventing dislocation climb and deformation.

α+β alloys

The α+β class of titanium alloys contain α (e.g. aluminium) and β (e.g. molybdenum or vanadium) stabilizing elements in larger quantity than in near α–alloys. This class of alloys is recognized by the combination of high strength and ductility in comparison with the other two main classes of titanium alloys. Ti–6Al–4V is the most popular and most used alloy because of the good balance of properties such as good castability, plastic workability, heat treatability and weldability. Its production comprises more than 50 % of the total production of titanium alloys in the world.

β alloys and near β–alloys

This class of alloys is referred to as metastable β alloys, because they are located in the two phase (α+β) region (see Figure 2.6). β alloys do not form martensite upon fast cooling from the β phase field. This class of alloys usually contains more than 15 wt. % β–stabilizing alloying elements. The alloys that belong to this class possess good combinations of

properties including highest strength, low modulus, high toughness and fatigue strength. Some of the drawbacks compared to α+β class of titanium alloys are increased density, small processing window and high cost. In Table 2.1 some important commercial available titanium alloys with their characteristic β–transus temperatures are listed.

Table 2.1 *Important commercial titanium alloys [1]*

Commercial name	Composition (wt. %)	T_β (°C)
α alloys		
Grade 1	CP–Ti (0.2Fe, 0.18O)	890
Grade 2	CP–Ti (0.3Fe, 0.25O)	915
Grade 3	CP–Ti (0.2Fe, 0.35O)	920
Grade 4	CP–Ti (0.5Fe, 0.4O)	950
Grade 7	Ti–0.2Pd	915
Grade 12	Ti–0.3Mo–0.8Ni	880
Ti–8–2.5	Ti–5Al–2.5Sn	1040
Ti–3–2.5	Ti–3Al–2.5V	935
α + β alloys		
Ti–811	Ti–8Al–1V–1Mo	1040
TIMET 685	Ti–6Al–5Zr–0.5Mo–0.25Si	1020
TIMET 834	Ti–5.8Al–4Sn–3.5Zr–0.5Mo–0.7Nb–0.35Si–0.06C	1045
Ti–6242	Ti–6Al–2Sn–4Zr–2Mo–0.1Si	995
Ti–64	Ti–6Al–4V (0.20O)	995
Ti–64 ELI	Ti–6Al–4V (0.13O)	975
Ti–662	Ti–6Al–6V–2Sn	945
Ti–550	Ti–4Al–2Sn–4Mo–0.5Si	975
β alloys		
Ti–6246	Ti–6Al–2Sn–4Zr–6Mo	940
Ti–17	Ti–5Al–2Sn–2Zr–4Mo–4Cr	890
SP–700	Ti–4.5Al–3V–2Mo–2Fe	900
Beta–CEZ	Ti–5Al–2Sn–2Cr–4Mo–4Zr–1Fe	890
Ti–10–2–3	Ti–10V–2Fe–3Al	800
Beta 21S	Ti–15Mo–2.7Nb–3Al–0.2Si	810
Ti–LCB	Ti–4.5Fe–6.8Mo–1.5Al	810
Ti–15–3	Ti–15V–3Cr–3Al–3Sn	760
Beta C	Ti–3Al–8V–6Cr–4Mo–4Zr	730
B120VCA	Ti–13V–11Cr–3Al	700

2.2.2 Microstructure of titanium alloys

The microstructure determines the mechanical properties of the titanium alloys which depend on the size and the arrangement of α and β–phases present at room temperature. The different microstructures in titanium alloys are generated by thermo–mechanical treatments (TMT) that include heat treatment, thermo–mechanical processing, recrystallization, aging and annealing as stress relief treatment (see Figure 2.7). The β–transus temperature plays a central role in this TMT processes, because it separates the single β phase field from the two–phase α+β field. Three basic microstructures are found in titanium alloys lamellar, equiaxed and bimodal.

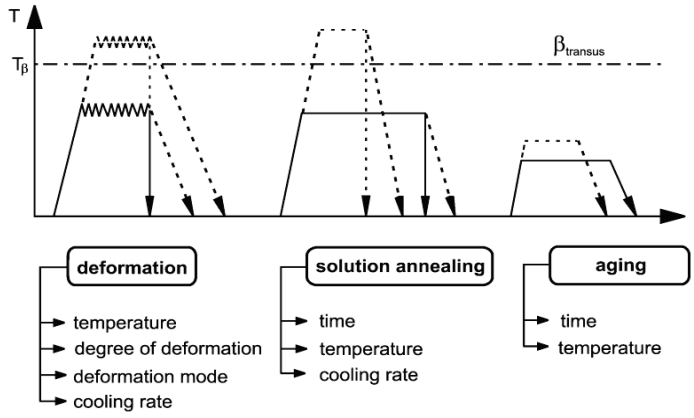

Figure 2.7 *Thermo–mechanical treatment of titanium alloys [5]*

Lamellar microstructure is generated upon cooling from the β phase field. Once the temperature falls below the β–transus temperature, α phase starts to nucleate at the grain boundaries and grows as lamellae into the prior β grains as shown in Figure 2.8.

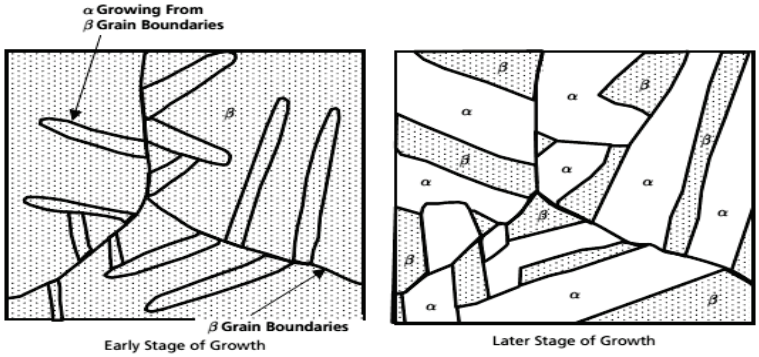

Figure 2.8 *Formation of lamellar microstructure in titanium alloys [7]*

The lamellar microstructure is dependent on the cooling rate. If the cooling rate is fast, then it forms fine needle–like microstructure known as "basket weave" or Widmanstätten microstructure (see Figure 2.9 a). On the other hand, if the cooling rate is slow the obtained microstructure will be fully lamellar, with lamellae being coarser with reducing cooling rate. This type of microstructure is known as colony microstructure (See Figure 2.9 b).

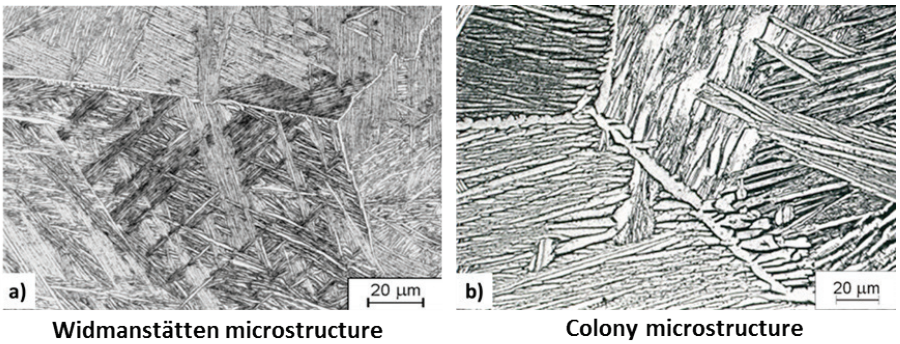

Figure 2.9 *Lamellar microstructures in titanium alloys, a) Widmanstätten microstructure and b) Colony microstructure [7]*

Euqiaxed microstructures are result of recrystallization process and therefore the alloy first has to be deformed in the α+β field in order to introduce enough cold work to the material. Upon subsequent solution heat treatment at temperatures in the α+β field, a recrystallized and equiaxed microstructure is developed (see Figure 2.10 a). Longer annealing results in coarsening of the microstructure (see Figure 2.10 b). The solution heat treatment temperature defines the volume fraction of primary α.

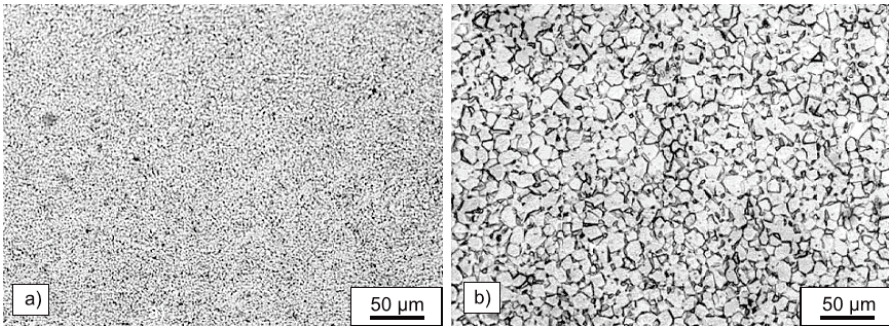

Figure 2.10 *Equiaxed microstructures in Ti–6Al–4V after recrystallization, a) fine equiaxed and b) coarse equiaxed [3]*

Bimodal microstructures are obtained when the solution heat treatment is performed at temperatures below the β–transus temperature. The bimodal microstructure consists of equiaxed α in a lamellar α+β matrix (see Figure 2.11) and can therefore be considered as a combination of lamellar and equiaxed microstructure.

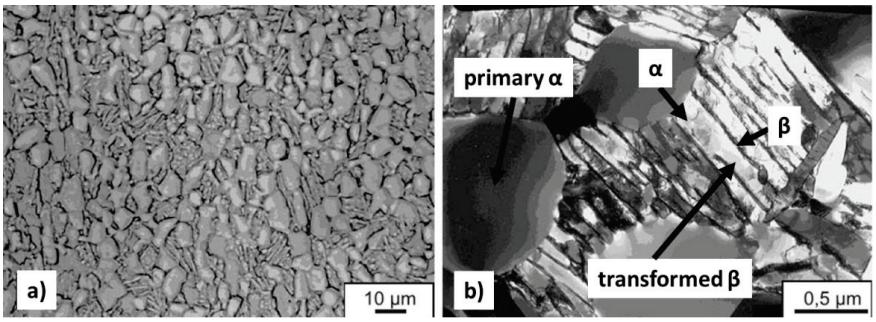

Figure 2.11 *Bimodal microstructure in Ti–6Al–4V after recrystallization, a) optical microscope and b) transmission electron microscope [3]*

In the present work the studied titanium alloys, Ti–6Al–2Sn–4Zr–2Mo (Ti–6242) and Ti–6Al–4V (Ti–64) have bimodal and equiaxed microstructure, respectively. Their microstructures are shown in Figure 2.12. As seen in Figure 2.12 a), the microstructure of Ti–6242 consists of primary α and transformed β grains, where the transformed β is composed of α and β lamellas oriented randomly. On the other hand, the microstructure of Ti–64 is composed of primary α grains and transformed β, where the transformed β consists of elongated α needles.

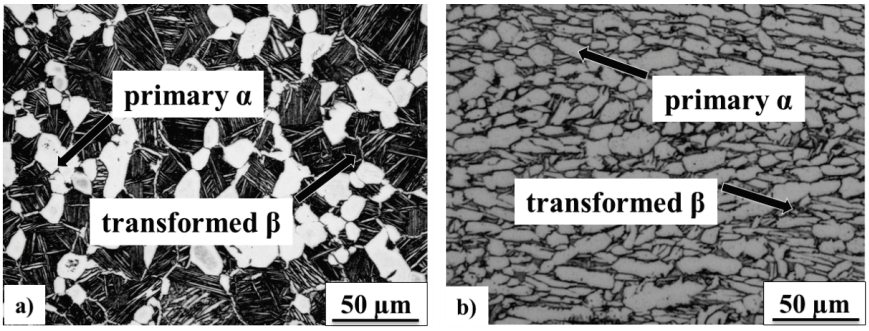

Figure 2.12 *a) bimodal microstructure in Ti–6242 and b) equiaxed microstructure in Ti–64* ***[Paper III]***

2.2.3 Mechanical properties of titanium alloys

The mechanical properties of titanium alloys can be adjusted through alloying and processing. Figure 2.13 shows schematically these relationships.

Alloying is the method used to adjust the properties through balancing the chemical composition of the alloy. Different elements are used to modify the strength via precipitation and/or solid solution hardening mechanisms. This type of modification also determines the physical properties such as density, Young's modulus and thermal expansion coefficient. Moreover, the alloying also determines the chemical resistance of the alloy such as oxidation and corrosion.

Processing is another important way to balance the mechanical properties of titanium alloys. This allows obtaining the desired type of microstructure that fulfils the specific properties required for the final application.

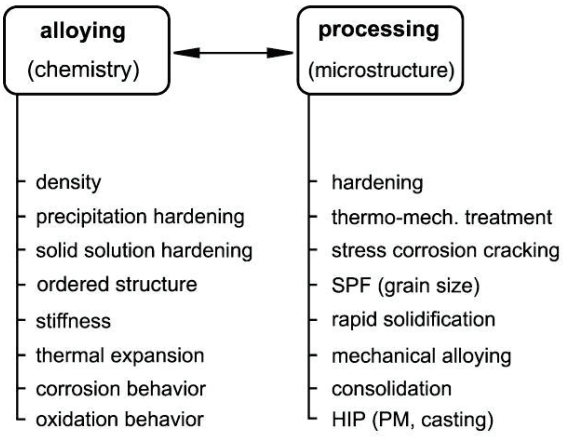

Figure 2.13 *Ways for modification of properties in titanium alloys [3]*

The properties of the different classes of titanium alloys are defined by the arrangement, the volume faction and the individual properties of α and β phases [1,3,4]. In Table 2.2 some of the basic physical, mechanical and technological properties of the three main classes of titanium alloys are shown and compared.

Table 2.2 *Properties of α, α+β and β titanium alloys [3]*

Properties	**Class of titanium alloys**		
	α	**α+β**	**β**
Density	+	+	–
Strength	–	+	++
Ductility	–/+	+	+/–
Fracture Toughness	+	–/+	+/–
Creep Resistance	+	+/–	–
Corrosion Resistance	++	+	+/–
Oxidation Resistance	++	+/–	–
Weldability	+	+/–	–
Cold Formability	– –	–	+/–

From the properties shown in Table 2.2 it can be summarized that α+β and β class of alloys have higher density than α alloys due to the alloying with heavy elements such as V and Mo. In terms of strength α alloys shows moderate strength, because they are built only of single α phase. In contrast, the α+β and β alloys consist of two phases and therefore can be hardened to higher strength levels. On the other hand, just because of the high strength, the β alloys are characterized with low ductility. Further on, the ductility and the fracture toughness are strongly dependent on the microstructure type (i.e fine, coarse, lamellar and equiaxed) and this relationship will be discussed more in detail later in this section. The excellent creep resistance of the near–α alloys is a result of the limited ability of atoms to diffuse and to deform the HCP in comparison to the BCC crystal structure of titanium. Therefore, increasing

the volume fraction of β phase in the titanium alloys results in lower creep resistance. The formation of very thin, dense and highly protective oxide layer (TiO_2), even at room temperature, is the main reason for the excellent corrosion resistance in different corrosive environments and is more efficient in the α than the β class of alloys. Titanium alloys exhibit poor oxidation resistance because of the high reactivity of titanium with oxygen even at room temperatures. β alloys are more susceptible than α alloys. Welding of titanium alloys is difficult due to the high reactivity of titanium with oxygen and hydrogen and therefore welding has to be performed in vacuum or inert gas environment. In general, α and α+β alloys are easier to weld than β alloys.

As mentioned before, the microstructure has considerable influence on the mechanical properties of the titanium alloys. The fine grain microstructure has more pronounced strength, ductility and fatigue strength. On the other hand, coarse grain microstructures have considerable better creep resistance. High ductility and high fatigue resistance are characteristics of the equiaxed microstructures, whereas the lamellar microstructures are featured with high fracture toughness and excellent creep resistance and fatigue crack growth. The high toughness of the lamellar structure can be explained by the easy ability to deflect propagating cracks along the different oriented lamella packets. Finally, the bimodal microstructures combine the advantages of the lamellar and equiaxed microstructures and therefore exhibit well balanced properties. Table 2.3 shows quantitatively how the fine, coarse, lamellar and equiaxed microstructures influence selected mechanical properties.

Table 2.3 *Influence of microstructure on selected mechanical properties of titanium alloys [3]*

Property	Lamellar	Equiaxed	Fine	Coarse
Young's Modulus	No effect	Positive/negative (texture)	No effect	No effect
Strength	Negative	Positive	Positive	Negative
Ductility	Negative	Positive	Positive	Negative
Fracture Toughness	Positive	Negative	Negative	Positive
Fracture Crack Initiation	Negative	Positive	Positive	Negative
Fracture Crack Propagation	Positive	Negative	Negative	Positive
Creep Strength	Positive	Negative	Negative	Positive
Super–plasticity	Negative	Positive	Positive	Negative
Oxidation rate	Positive	Negative	Positive	Negative

2.3 Interstitial elements and their effect on mechanical properties in titanium alloys

Oxygen, nitrogen and carbon are known as interstitial elements that cause solid solution strengthening in titanium alloys. All these elements stabilize the HCP crystal structure of titanium by occupying the free interstitial lattice positions. However, their individual effects on the mechanical properties are not the same. Finlay and Snyder [8] have studied the effects of the interstitial solutes on CP–titanium and they have reported increase of the strength and hardness with increasing interstitial element concentrations, accompanied with substantial decreasing of the ductility. They demonstrated that the individual effects of each element are different, with nitrogen having the largest effect followed by oxygen and carbon. Figure 2.14 shows the effect of the interstitial element concentrations on some important mechanical properties of CP–titanium. Detailed study of the effect of the interstitial elements on the mechanical properties of titanium and some titanium alloys was also performed by Ogden and Jaffe [9]. They reported that the effects of the interstitials on titanium alloys are similar to the

effects in CP–titanium and the magnitude of the effects is dependent on the amount and type of alloying elements present in the alloy. Another important property studied by these authors was the effect of interstitial elements on the thermal stability of the titanium alloys at elevated temperatures. It is known that the dissolved interstitial elements increase the rate of formation of α from β, causing detrimental effect on the thermal stability of the alloys and thereby reducing important mechanical properties such as ductility, strength, fracture toughness and fatigue life. They reported that the effect of the interstitial elements on the stability of two phase titanium alloys is directly related to their effects on the beta–decomposition reaction kinetics.

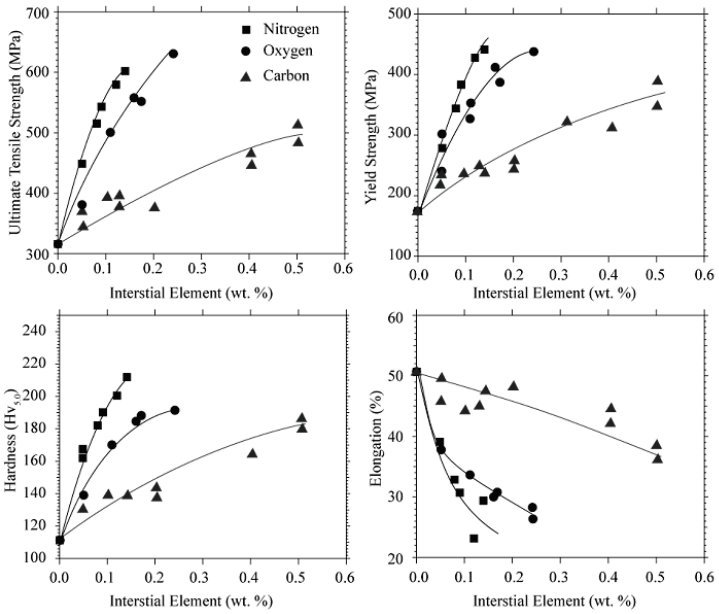

Figure 2.14 *Effects of interstitial elements on the mechanical properties of CP–titanium [8]*

Among the interstitial elements, oxygen is of particular interest because of the high chemical reactivity with titanium at elevated temperatures and the relative high solubility in α–titanium (14.3 wt. %). Kahveci and Welsch [10] have investigated the effect of oxygen concentrations on the hardness and the α/β–phase ratio in Ti–6Al–4V alloy. They showed that increase of oxygen concentrations significantly increases the hardness and the volume fraction of α–phase at given temperatures in this α+β alloy. A large number of studies can be found in the literature for different alloys that provide insight on the detrimental effect of oxygen uptake on several mechanical properties such as ductility, tensile strength, fatigue life and fracture toughness [11–23]. Shamblen and Redden [11] found a correlation between the increase of the oxygen contamination depth and the subsequent loss of ductility in the Ti–6Al–2Sn–4Zr–2Mo alloy. This was also confirmed by Shenoy et al. [13] for the same alloy, reporting reduction of the tensile elongation from 12.7 to 2.5 % dependent on the oxygen concentration and contamination depth. Liu and Welsch [14] studied the influence of the oxygen concentrations and the different heat treatment conditions on the hardness and the ductility in Ti–6Al–2V and Ti–2Al–16V alloys. They reported that the hardness is a function

of the square root of the oxygen concentration and that it is increasing in similar manner in the two alloys regardless of the differences in the chemical composition. The heat treatment conditions also affect the strength but in different ways in the two alloys. The strength of the Ti–6Al–2V alloy was not affected during the aging, whereas it was doubled in the Ti–2Al–16V alloy. Additionally, aging in combination with increased oxygen concentrations caused production of Ti_3Al precipitates in the alpha alloy, whereas alpha and omega or only alpha precipitates were formed in the beta alloy depending on the aging temperature. Moreover, they reported that the ductility is strongly decreasing by increase of oxygen concentration in the Ti–6Al–2V alloy leading to total brittleness at oxygen concentration of 0.65 wt. %. On the other hand, they reported that the ductility in the Ti–2Al–16V alloy was also decreased with the increase of oxygen concentrations, but did not embrittle the alloy even at 0.59 wt. % oxygen concentrations. A studies of Dong and Li [16] for Ti–6Al–4V and Ebrahimi et al. [18] for Ti–6Al–2V showed reduction of the fatigue limit of 27 % and 18 %, which was mainly due to the thermal oxidation and oxygen embrittlement of the alloys. The tensile properties dependent on the oxidation in TIMETAL 1100 and Ti60 were studied by Leyens et al. [23] and Jia et al. [19]. Both studies reported that the oxidation have significant effect on the tensile properties of the alloys featured with decreasing of the strength and the ductility of the alloys.

2.4 Oxidation

In this section fundamental aspects of metal oxidation and the oxidation of titanium and some of its alloys are presented.

2.4.1 Introduction

Under most of the ambient conditions metals are thermodynamically unstable [24]. This instability may be of little or no practical meaning at room temperature due to the slow reaction rate which becomes significant at elevated temperatures. High temperature oxidation of metals and alloys is a broad research field with scientific and technological importance [24–28]. Several aspects should be taken into account when the oxidation behaviour of metals at elevated temperatures is studied. It is important to know why the oxidation process is taking place, which are the products of the reaction, what are the kinetics and the mechanism of the oxidation process and on what they are dependent. Oxidation can be considered as a special type of corrosion degradation of metals and alloys that occurs when the metal or the alloy is exposed to air or in other oxidizing environments such as SO_2 and CO_2.The degradation results in oxide scale formation and sometimes also includes dissolution of the gas species into the metal substrate causing embrittlement. Moreover, if the formed oxide scales are thin, dense and adherent they provide protectiveness of the metal by inhibiting further oxidation, whereas if the formed oxide scales are porous and spall of the metal surface they act as non–protective barrier and do not hinder the oxidation of the metal or the alloy.

2.4.2 Fundamentals of oxidation of metals

The reaction of a metal (M) and oxygen gas (O_2) could be simply described through the following chemical equation:

$$aM_{(s)} + \left(\frac{b}{2}\right)O_{2(g)} = M_aO_{b(s)} \qquad (2.1)$$

Although this seems to be one of the simplest chemical reactions, the reaction path and the oxidation behaviour of the metals and alloys are usually dependent on many factors and

therefore the oxidation mechanisms are complex [24]. The driving force for oxidation and oxide scale formation is the free energy change associated with the formation of the oxide from the reactants. The oxide would form only if the ambient oxygen pressure is larger than the dissociation pressure of the oxide in equilibrium state with the metal. This is illustrated with Eq. 2.2 [24] for the chemical reaction 2.1 and the expression $\Delta G^{\circ}(M_aO_b)$ represents the standard free energy change for the reaction of oxidation at certain temperature.

$$pO_2 \geq \exp\left\{-\frac{2\Delta G^{\circ}(M_aO_b)}{bRT}\right\} \qquad (2.2)$$

The standard free energies of oxide formation as a function of temperature and the corresponding dissociation pressures of oxides for some important metal oxides are summarized in the form of Ellingham/Richardson diagrams (see Figure 2.15) [24]. These diagrams can be used as qualitative measure for the stability of the oxides at different temperatures and oxygen partial pressures. The most stable oxides have larger negative values for ΔG° and from the diagram shown in Figure 2.15 the stability of the oxides is increasing going down from Cu_2O to CaO.

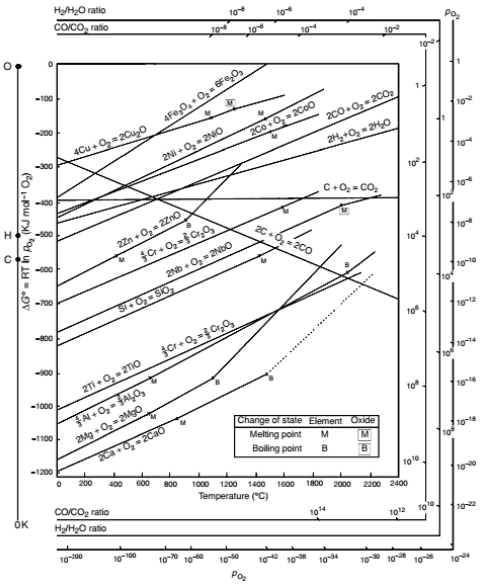

Figure 2.15 *Ellingham/Richardson diagram for some important oxides in high temperature oxidation [24]*

One of the limitations of the Ellingham/Richardson diagrams is that they do not provide any information of the oxidation kinetics. Studying the reaction rates of oxidation and the kinetics is important, because they are the basis for elucidation of the oxidation mechanism. Reaction rates and the corresponding rate equations for oxidation of metals are dependent on a number of factors such as temperature, oxygen pressure, time of the reaction, surface preparation and pretreatment of the metal. The following rate laws are commonly encountered in oxidation of metals: logarithmic, parabolic and linear [24–28].

Logarithmic law

This oxidation law is obeyed by a large number of metals at temperatures below 300–400 °C. Initially the reaction rate is very fast and then drops to low or negligible rates. Usually oxidation at low temperatures is described by the logarithmic rate equations, including the direct and the inverse logarithmic rate equations [24]:

$$\text{Direct: } x = k_{\log} \log(t + t_0) + A \qquad (2.3)$$

$$\text{Inverse: } \frac{1}{x} = B - k_{il} \log t \qquad (2.4)$$

where x normally refers to the thickness of the oxide scale, the amount of oxygen consumed per unit surface area of the metal or the amount of metal transformed to oxide. The t represents time of the oxidation process, $k_{\log}$ and k_{il} denote the rate constants and A and B are constants.

Parabolic law

At elevated temperatures most of the metals follows parabolic oxidation behaviour with respect to time. As for the logarithmic oxidation initially the rate is very rapid and then slows down, but in parabolic type of oxidation the rate is continuously increasing during the oxidation process. The parabolic rate law can be described by the following equations [24]:

$$\text{Differential: } \frac{dx}{dt} = \frac{k_p^{'}}{x} \qquad (2.5)$$

$$\text{Integrated: } x^2 = 2k_p^{'}t + C = k_p t + C \qquad (2.6)$$

where $k_p^{'}$ and k_p represent the parabolic rate constants and C is the integration constant. The parabolic oxidation signifies that uniform diffusion of one or both reactants through the oxide scale is the rate determining process [27].

Linear law

The linear law of oxidation may be described by the following rate equations [24]:

$$\frac{dx}{dt} = k_l t \qquad (2.7)$$

$$x = k_l t + C \qquad (2.8)$$

where k_l represents the linear rate constant and C the integration constant. In contrast to the parabolic and logarithmic laws, the linear rate of oxidation is constant with time and thus is independent of the amount of gas or metal [28].

However, as mentioned before, the oxidation of metals is a complex process and seldom obeys only one oxidation law. Metal oxidation normally follows a combination of the rate

laws described above [25]. Oxidation studies indicate that in many metals the oxidation occurs by two simultaneous mechanisms, where one is dominating at initial time and the other after prolonged time of oxidation [24]. One example of combining rate laws is the cubic rate that comprises a combination of logarithmic and parabolic rate. This type of rate has usually been found at low temperatures [26]. At high temperatures a combination of parabolic and linear rate usually was encountered [26]. This type of rate commonly is referred to as para–linear rate and includes parabolic rate law at initial time of the oxidation that changes to linear after prolonged oxidation times. It is considered that the combination of rates and the complex oxidation behaviour of metals and alloys are mainly due to fast changes of the nature of the oxide scales with respect to the oxidation time [24]. Figure 2.16 shows an illustration of the different oxidation rate laws and their variation with respect to oxidation time.

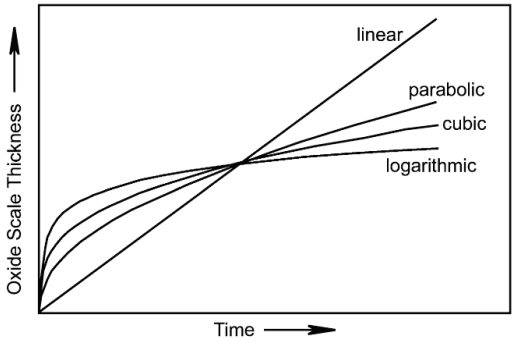

Figure 2.16 *Schematic representation of variation of oxide thickness with respect of oxidation time for different oxidation laws [24]*

The classic method to study oxidation rates and behaviour of metals is the thermogravimetry, which involves monitoring of the mass change of a heated metal with defined surface area with respect time. This mass change is usually manifested as weight gain per surface area of the metal with respect to oxidation time. The mass change is due to the formation of an oxide scale and diffusion of oxygen into the bulk metal. Monitoring the weight gain per surface area vs. time of a metal during oxidation at elevated temperature would result in one of the curves presented in Figure 2.16. These curves can be analytically treated with the following mathematical equation that compiles all the oxidation laws presented above [24,39]:

$$\left(\frac{\Delta W}{A}\right)^{n} = k_n \cdot t \qquad (2.9)$$

where, ΔW is the weight gain, A is the surface area, k_n is the rate constant, t is the exposure time and n is the reaction index. At a constant temperature, the weight gain per surface area is linear if $n = 1$, parabolic if $n = 2$ and cubic if $n = 3$ [24]. The reaction indices (n) could be estimated by regression analysis of a log–log plot of weight gain per surface area vs. time. This type of approach was used in **Paper II** to obtain the reaction indices of the oxidation of Ti–6242 alloy.

The temperature dependence of the reaction constant k can be described with the Arrhenius law [24]:

$$k = k_0 \cdot \exp\left(-\frac{Q}{RT}\right) \qquad (2.10)$$

where k_0 is the temperature independent pre–exponential factor, Q is the activation energy, R is the universal gas constant and T the absolute temperature. Arrhenius plot of the log k values versus $1/T$ enables comparison of the oxidation resistance of different metals and alloys over broad temperature range and allows computation of the activation energy for the oxidation reaction.

2.4.3 Oxide growth mechanisms

As discussed previously the oxidation of metals involves formation of an oxide scale that uniformly covers the metal surface. This process could be described through the following steps [3]:

- Oxygen adsorption
- Oxide nucleation
- Lateral growth of the oxide
- Formation of compact oxide scale

Oxygen adsorption is the initial step of the oxidation process and involves attachment of oxygen on the metal surface through chemisorption or physical adsorption (see Figure 2.17 a) [24]. The main difference between the two types of adsorption is in the bonding of the gas molecules and the metal surface. In physical adsorption gases are bound to the metal surface through week van der Waals forces, whereas in chemisorption stable chemical bonds are formed. Physical adsorption proceeds immediately once the gas molecules impinge on the metal surface and do not require any activation energy. In contrary, chemisorption may proceed slowly and involve activation energy. However, if the metal surface is clean then the chemisorption is very rapid and proceeds without any apparent activation energy. Once the oxygen molecules are adsorbed they dissociate and start being adsorbed as atoms. When the metal surface is saturated with adsorbed oxygen atoms oxide nuclei are formed that grow laterally (see Figure 2.17 b and c). The lateral growth of the nuclei results in formation of a compact oxide scale that covers the surface of the metal (see Figure 2.17 d).

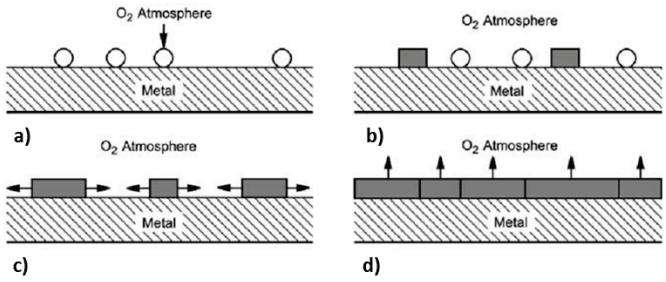

Figure 2.17 *Schematic illustrations of the four steps of oxide scale formation and growth, a) oxygen adsorption, b) formation of oxide nuclei, c) lateral growth of the oxide and d) formation of a compact oxide scale [3]*

Once the thin and compact oxide scale is formed further growth of the oxide scale is mainly controlled by mass transport though the scale itself. Since metal oxides are compounds with ionic nature the mass transport includes transport of electrons and ionic species (i.e. cations and anions) through the oxide scale (see Figure 2.18). The ability of the oxide scale to transport charged species makes them behave as semiconductors [29]. Another important characteristic of the metal oxides is that they have large numbers of imperfections, which substantially contribute to the mass transport. The most common imperfections in metal oxide lattices are metal ions located at the interstitial positions, non–metal ion vacancies, metal ion vacancies and non–metal ions located in the interstitial positions [30]. Based on conductivity of the metal oxides and the type of imperfections present, the oxides are classified into *n* and *p*–type oxides. In general, the *n*–type oxides grow inwards, whereas the *p*–type oxides grow outwards with respect to the metal/oxide interface. For example, during oxidation of titanium the forming product is an *n*–type anion defective TiO_2 through which oxygen ions diffuse and react further with the titanium metal [31]. The reaction front is the metal/oxide interface and the oxide scale grows inwards.

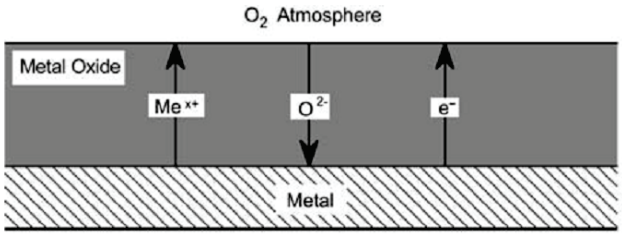

Figure 2.18 *Schematic representation of mass transport across the oxide scale (electrons, cations and anions) [3]*

Moreover, except from the ionic nature and the conductivity of the oxide scale also other mechanisms can contribute to the mass transport and affect the growth rate of the oxide scale. At low temperatures, the mass transport is affected significantly by grain boundary diffusion due to its lower activation energy, whereas at high temperatures the mass transport is affected by lattice diffusion. Also occurrence of a porous structure and cracks i.e. the physical morphology of the oxide scale could contribute to the mass transport and the growth rate.

2.4.4 Oxidation of titanium alloys

Titanium has high affinity to react with oxygen when exposed to oxidizing environments. The reaction between titanium and oxygen at room temperature results in the formation of a thin and passive TiO_2 layer that provides protection of the metal surface from further oxidation and corrosion in various corrosive environments. However, at elevated temperatures the TiO_2 layer loses its protectiveness and allows oxygen to be dissolved into the titanium bulk metal. The solubility of oxygen in α–titanium is about 30 at. % showing very small variations with temperature, whereas the solubility in β–titanium increases with temperature and at 1700 °C reaches maximum solubility about 8 at. %. Figure 2.19 shows the Ti–O phase diagram, from where it can be seen that many stable titanium oxides such as Ti_2O, TiO, Ti_2O_3 and Ti_3O_5, Ti_nO_{2n-1} ($4 < n < 38$) and TiO_2 can be formed. However, for oxidation at temperatures below 1000 °C and at near–atmospheric pressures only the Ti_2O rutile type modification has been detected in the oxide scales [24].

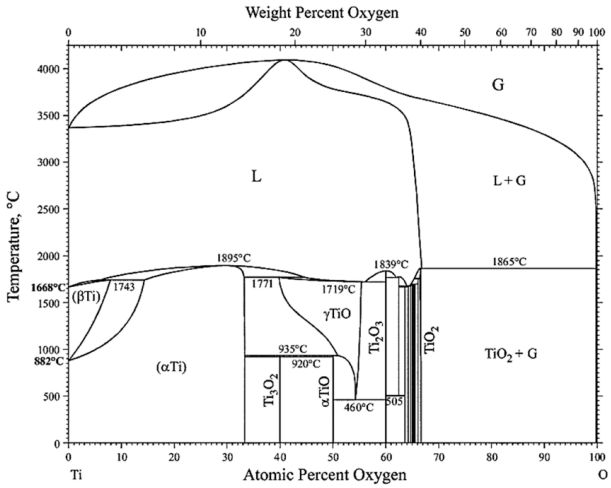

Figure 2.19 *Ti–O phase diagram [32]*

The oxidation of CP–titanium in different types of environments at wide temperature ranges have been extensively investigated by many authors [33–38]. The most notable studies of oxidation on titanium in oxygen at atmospheric pressures and broad temperature range have been performed by Kofstad et al. [24,33,34]. In these studies different oxidation behaviour of titanium was reported mainly dependent on the oxidation temperature and time (see Figure 2.20). It was shown that at temperatures below 400 °C the oxidation rate of titanium follows logarithmic law, in the temperature range 400–600 °C cubic law and in the temperature range 600–700 °C parabolic behaviour. However, after prolonged oxidation times they have observed a change of the parabolic rate to approximately a linear rate. Moreover, at temperatures higher than 900 °C, the observed oxidation rate was linear, followed with slower rates after longer times. The logarithmic oxidation resulted mainly in formation of a thin oxide scale, whereas the cubic and the parabolic rates were associated with oxide scale formation and oxygen diffusion into the titanium metal forming brittle and hard oxygen enriched layer. The linear rate of oxidation was considered to be a result of cracking and porosity of the oxide scale due to the stresses in the oxide and the oxygen enriched layer [33].

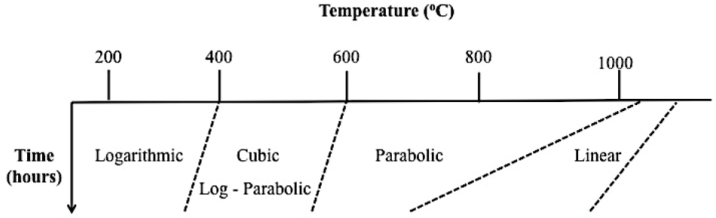

Figure 2.20 *Schematic diagram of the rate equations observed in the oxidation of titanium [34]*

For titanium alloys more complex oxidation behavior than in commercial pure titanium was found. The complex oxidation comes as a result of presence of β–phase in the alloys, the effect of the alloying elements, but also due to differences in the microstructure. Many

scientists have investigated the oxidation of different titanium alloys and in the following section a short summary with main focus on Ti–6Al–4V, Ti–6Al–2Sn–4Zr–2Mo and some other important aerospace titanium alloys will be given.

The oxidation of Ti–6Al–4V alloy has been investigated in different oxidizing conditions at different temperatures and times by many scientists [38–45]. Frangini et al. [39] have studied the oxidation behavior of Ti–6Al–4V alloy in the temperature range of 600–700 °C in air for times up to 300 hours. They reported that the oxidation kinetics in this temperature range follows mainly parabolic behavior, but changing to linear behaviour at 700 °C after 50 hours exposure time. Similar observation was reported by Guleryuz and Cimenoglu [43] and in the present work (**Paper III**). The reason for the change in oxidation behaviour from parabolic to linear is considered to be due to the changes in the morphology of the formed oxide scale. At lower temperatures the formed oxide scale is dense and compact, whereas at higher temperatures it becomes porous and spalls off which leads to an increase of the oxidation rate (**see Paper III**). Another observed physical characteristic of the oxide scales is the multi–layered structure consisting of TiO_2 and Al_2O_3 layers. The formation of a multi–layered structure in an oxide scale at temperatures 650–850 °C was presented in the work of Du et al. [40]. In their study they showed that the formation of multi–layers in the oxide scale is temperature and time dependent phenomena and the number of the Al_2O_3 layers increases with increasing either the oxidation temperature or the reaction time. The same behaviour of the oxide scale and formation of multi–layered structured was also noticed in the present study after isothermal heat treatment at 700 °C (**see Paper III**). Moreover, Du et al. [40] have presented a mechanism of formation of the multi–layered oxide scale structure that involves the activity of titanium and aluminum regarding oxygen and the oxygen partial pressure present in the oxide scale. Once the TiO_2 is formed the alloy is separated from its environment by the oxide scale and the partial oxygen pressure in the oxide moving from the gas/oxide interface towards the oxide/metal interface is decreasing to a value close to that of the dissociation pressure of TiO_2. At such low oxygen partial pressures the minimum activities required to form Al_2O_3 at different elevated temperatures are high and therefore unlikely to form Al_2O_3 at the oxide/metal interface. In contrast the oxygen partial pressure at the gas/oxide interface is relatively high which allows formation of Al_2O_3 layer on top of the already formed TiO_2 oxide scale. This indicates that oxygen is diffusing inward to the oxide/metal interface, reacting to form TiO_2 increasing the thickness of the TiO_2, whereas aluminum diffuses outward towards the gas/oxide interface where it reacts with oxygen and forms an outer layer of Al_2O_3. Once the double oxide layer of TiO_2 and Al_2O_3 is formed the consequent grow of the oxide scale causes cracks at the oxide/metal interface when some critical thickness of the oxide scale is reached. Additionally, the cracking is a result of the different thermal expansion coefficients of the oxide scale and the metal substrate that initially would start at the edges and expand progressively through the entire surface of the oxide. The detachment of the oxide scale from the metal substrate would increase the oxygen partial pressure close to the oxide/metal interface that would produce conditions favorable for formation of the second TiO_2 layer. As the oxidation continues, these processes will repeat resulting in formation of multi–layered structure of TiO_2 and Al_2O_3 layers of the oxide scale in Ti–6Al–4V (see Figure 4 c in **Paper III**). The oxidation mechanism of formation of multi–layered oxide scale in Ti–6Al–4V is schematically shown in Figure 2.21.

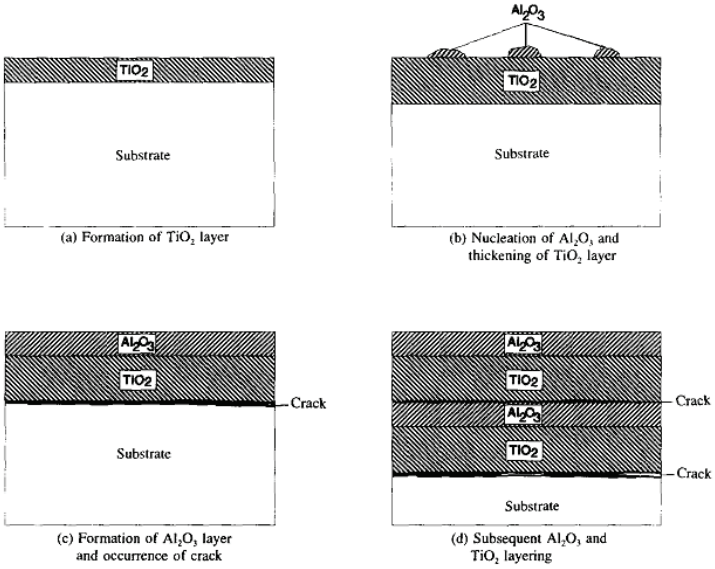

Figure 2.21 *Schematic illustration of the formation of multi–layered structure of the oxide in Ti–6Al–4V by Du et al. [40]*

However, not only the multi–layered structure of the oxide scale is responsible for changes in the oxidation kinetics. The work of Pitt and Ramulu [41] showed that the microstructure also has an influence on the oxidation kinetics. They were investigating the effect of coarse and fine microstructures in Ti–6Al–4V on the oxidation kinetics and showed that the fine microstructure exhibit faster oxidation kinetics as compared with a coarser microstructure.

There are fewer reports in the literature on the oxidation of Ti–6Al–2Sn–4Zr–2Mo alloy in air at elevated temperatures [46–49] compared to Ti–6Al–4V. One of the most notable studies on Ti–6Al–2Sn–4Zr–2Mo is the work of Shenoy et al. [47], were they presented the oxidation behaviour of Ti–6Al–2Sn–4Zr–2Mo alloy in the temperature range of 593–760 °C. Similar as for Ti–6Al–4V they observed parabolic oxidation behaviour up to 650 °C, which changed with more pronounced slope at higher temperatures deviating from parabolic behaviour after particular time intervals. The change in the oxidation behaviour at higher temperatures the authors associated to the formation of porous oxide scales. Similar observation in changes of the parabolic oxidation kinetics and formation of porous oxide scale at 700 °C for times longer than 200 hours was also made in the present study (**Paper II**). The estimated reaction index (n = 1.28) in the present work (**Paper II**) revealed that the oxidation changes from parabolic to linear after 300 hour exposure time at 700 °C. Additionally, formation of porous oxide scales was observed (see Figure 4 c in **Paper II** and Figure 4 d in **Paper III**). In the present study (**Paper III**) the formation of the porosity in the oxide scale at 700 °C and oxidation time longer than 300 hours was correlated to the possible formation of volatile MoO_3 that evaporate readily from the oxide scale. However, at 500 °C during the first 200 hours cubic oxidation was observed that changes to parabolic for longer exposure time,

whereas at 593 °C parabolic oxidation behaviour up to 500 hours exposure time was observed without any changes.

Other high temperature titanium alloys used in aerospace applications such as TIMET 834 (Ti–5.8Al–4Sn–3.5Zr–0.5Mo–0.7Nb–0.35Si–0.06C) [50–52] and Ti60 (Ti–5.8Al–4.0Sn–3.5Zr–0.4Mo–0.4Nb–1.0Ta–0.4Si–0.06C) [19] have also been studied. The oxidation behaviour of these alloys is similar to the Ti–6Al–2Sn–4Zr–2Mo alloy, with the exception that no significant change in the oxidation kinetics occurs at higher temperatures and/or longer exposure times. One notable difference between Ti–6Al–2Sn–4Zr–2Mo and TIMET 834 alloy is that in TIMET 834 presence of Ti_3AlN phase in the formed oxide scale was found [50–52].

2.5 Diffusion

In this section the fundamentals of solid–state diffusion and summary of the oxygen diffusion in titanium and its alloys are presented.

2.5.1 Fundamentals of solid–state diffusion

Solid–state diffusion covers studying the movement and transport of atoms in solid phases. The atoms movement usually takes place through imperfections present in the crystal lattices of the solid materials i.e. metals [53,68]. Vacancies and interstitial sites are the two types of imperfections in the crystal lattices through which the atom transport could occur. This type of diffusion is commonly known as lattice or volume diffusion. However, the movement and transport of the atoms can also occur through line and surface defects of solids such as grain boundaries and dislocations. If such transport of the atoms takes place then the type of diffusion is called short–circuit diffusion. This type of diffusion has lower activation energy and it is faster than the lattice diffusion.

Two diffusion mechanisms for lattice diffusion are known: vacancy and interstitial diffusion mechanism. The diffusion takes place through vacancy mechanism when an atom or normal lattice position moves to an adjacent vacant lattice site or vacancy. On the other hand, the interstitial diffusion mechanism involves transport of atoms from one interstitial position to another in the crystal lattice. Schematic representation of this two lattice diffusion mechanisms is shown in Figure 2.22. The interstitial diffusion mechanism is typical for diffusion of atoms with small atomic radius such as hydrogen, carbon, nitrogen and oxygen [54]. The small atomic radius of these elements allows them to be easily suited and move in the free interstitial positions of different types of crystal lattices. In most of the metal alloys the interstitial diffusion goes much faster since the interstitial atoms are smaller and thus more mobile.

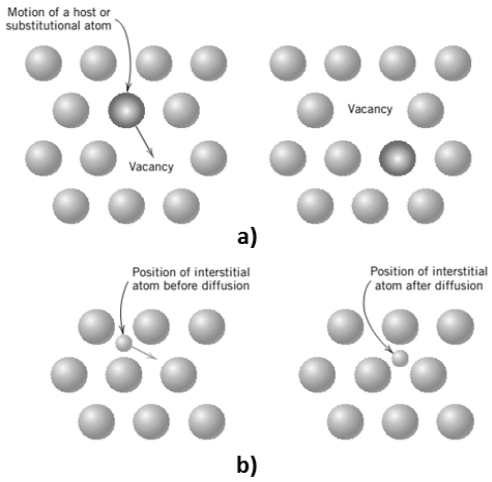

Figure 2.22 *Schematic representations of a) vacancy diffusion and b) interstitial diffusion [54]*

The rate of movement of the atoms can be described through the diffusion flux (J), which is defined as the number of diffusing atoms (N) through a cross–sectional area (perpendicular to the flux of atoms) of the solid per time. Mathematically this can be represented as [55]:

$$J = \frac{N}{A \cdot t} \qquad (2.11)$$

or in differential form:

$$J = \frac{1}{A}\frac{dN}{dt} \qquad (2.12)$$

where A is the area across which the diffusion is taking place and t is the time during which the movement of the atoms is taking place.

The driving force for diffusion is the diffusion flux or the existence of a concentration gradient. Two types of diffusion are known based on the change of the diffusion flux with time. If the diffusion flux does not change with time, then steady–state diffusion exists. The steady–state diffusion in one direction (x) can mathematically be described with Fick's first law [55]:

$$J = -D\frac{dC}{dx} \qquad (2.13)$$

where D is the constant of proportionality termed as diffusion coefficient and it has units of square meters per second and C is the concentration. The negative sign indicates that the direction of the diffusion is opposite to the concentration gradient i.e. from high to low concentration.

A more realistic type of diffusion is the nonsteady–state diffusion in which the diffusion flux and the concentration gradient varies with time (see Figure 2.23). In such conditions Eq. 2.13 is not valid. Instead Fick's second law for diffusion may be applied [55]:

$$\frac{\partial C}{\partial t} = \frac{\partial}{\partial x}\left(D\frac{\partial C}{\partial x} \right) \qquad (2.14)$$

and, if the diffusion coefficient is independent of the composition then Eq. 2.14 is simplified as [55]:

$$\frac{\partial C}{\partial t} = D\frac{\partial^2 C}{\partial x^2} \qquad (2.15)$$

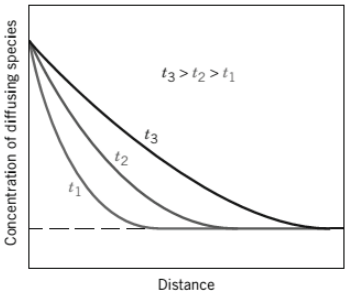

Figure 2.23 *Schematic representation of nonsteady–state diffusion; variation of the concentration gradient into the bulk metal with time [54]*

Solutions for Eq. 2.15 are possible when physically meaningful boundary conditions are specified. One solution with practical importance for diffusion of gas phase in solids with semi–infinite thickness and constant surface concentration C_s of the gas is [55]:

$$\frac{C_x - C_0}{C_s - C_0} = 1 - erf\left(\frac{x}{2\sqrt{Dt}} \right) \qquad (2.16)$$

where C_x is the concentration of the diffused atoms at distance x after time t, C_0 is the initial concentration in the bulk of the metal at time t_0 and the expression $erf(x/2\sqrt{Dt})$ is the Gaussian error function, which values can be extracted from mathematical tables for different $x/2\sqrt{Dt}$ values. The following boundary conditions are applied to obtain Eq. 2.16:

- For $t = 0$, $C = C_0$, at $0 \le x \le \infty$
- For $t > 0$, $C = C_s$ at $x = 0$ and $C = C_0$ at $x = \infty$

The Eq. 2.16 shows that C_x is a function of the dimensionless parameter $x/2\sqrt{Dt}$ and it can be estimated at any time and position if the parameters, C_0, C_s and D are known.

Moreover, if it is desired to achieve a specific C_x concentration then the left and the right side of Eq. 2.16 becomes constant. This results in the following expression [55]:

$$\frac{x^2}{Dt} = \text{constant} \qquad (2.17)$$

Eq. 2.17 is considered as a simplified approximate solution for Fick's second law of diffusion. The Eq. 2.17 was applied in the present study (**Paper I, II and III**) to estimate the diffusion coefficients for oxygen diffusion in Ti–64 and Ti–6242 alloys.

The diffusion coefficient D represents a measure of the rate at which the atoms diffuse and is a function of temperature. The temperature dependence of the diffusion coefficient can be described with the Arrhenius law [55]:

$$D = D_0 \exp\left(-\frac{Q}{RT}\right) \qquad (2.18)$$

where D_0 is the temperature independent pre–exponential factor, Q is the activation energy, R is the universal gas constant and T the absolute temperature. Arrhenius plot of the D values versus $1/T$ allows estimation of the activation energy for the diffusion process.

2.5.2 Diffusion in titanium alloys

Knowledge of the diffusivity of various elements in titanium is of metallurgical and technological importance. Many of the production processes, such as heat treatments are diffusion dependent. On the other hand, as mentioned before, some of the application conditions of titanium and its alloys confront with diffusion of oxygen into titanium, which has detrimental effect on the mechanical properties. The oxygen atoms diffuse in α–titanium through interstitial diffusion mechanism and preferably occupy the free octahedral interstitial positions in the HCP crystal lattice of titanium. However, a recent theoretical study showed that the hexahedral and crowdion interstitial positions are also available for the oxygen atoms to be situated in [56]. Moreover, the authors also showed that all three interstitial positions in HCP crystal lattice of titanium cooperate and form a network where the oxygen atoms could move. The oxygen diffusion rate in titanium and different titanium alloys has been investigated by many authors. Liu and Welsch [57] have published a comprehensive review of the diffusivities of oxygen in α and β–titanium. They presented that the differences in the pre–exponential factors D_0 and the value of the activation energies Q are due to the different methods used for obtaining the concentration gradient of diffused oxygen and the technique used to measure the concentration gradient. In Table 2.4 values for pre–exponential factors D_0 and activation energies Q obtained for diffusion of oxygen in α and β–titanium and for the alloys studied in the present work are listed.

Table 2.4 *Pre–exponential constants and activation energies for diffusion of oxygen in α and β–titanium [57]*

	Temperature (°C)	D_0 (m2/s)	Q (kJ/mol)	Method	Reference
α-titanium					
Ti	700–850	5.08×10^{-7}	140	conc. grad., MG[1]&MH[2]	58
Ti	450–550	4.97×10^{-11}	102	conc. grad., AES[3]	59
Ti–6242	538–816	6.2×10^{-5}	203	oxid.	46
Ti	700–950	4.5×10^{-5}	201	oxid.	60
Ti	650–875	4.08×10^{-5}	197	oxid.	61
Ti	250–900	4.5×10^{-5}	200±30	oxid.	62
β-titanium					
Ti	1127–1347	8.3×10^{-6}	131±8.4	conc. grad.	63
Ti	900–1150	3.14	288	conc. grad.	58
Ti	950–1150	6.3×10^{-5}	155	conc. grad., XSA[4]	64
Ti	1335–1575	2×10^{-6}	115±17	conc. grad.	65
Ti	932–1142	3.30×10^{-2}	246	oxid.	66
Alloys					
Ti–64	500–700	6.31×10^{-3}	215	conc. grad., MG	Paper III
Ti–6242	500–700	6.54×10^{-7}	153	conc. grad., MG	Paper III

[1]MG–Metallography, [2]MH–Microhardenss, [3]AES–Auger electron spectroscopy, [4]XSA–X–ray structure analysis

A recent study by Tiley et al. [67] showed that the lath orientation in the lamellar microstructure of the Ti–6242S alloy also has effect on the oxygen diffusion rate. The authors suggested that the β–phase and the α/β interfaces between the neighbouring α–laths have contribution for the deeper oxygen ingress in the alloy due to the faster diffusion rate in comparison with the α–phase. Similar behaviour has been observed in the present study (**Paper III**) for the heat treatment performed at 500 °C for the two tested alloys. In Ti–6242 it was observed slightly thicker alpha–case layer than in Ti–64 and it is believed that this is due to the higher number of α/β interfaces in the microstructure of Ti–6242 that enhance the oxygen diffusion rate in this alloy at 500 °C.

The oxygen diffusion rate into the bulk can be determined using different methods. One of the simplest and most conventional methods to measure the oxygen diffusive layer thickness is the microhardness method, since the increase of oxygen concentration in the metal corresponds to an increase of the hardness [68]. In **Paper I**, an increase of the average hardness in the alpha–case layer in comparison with the bulk hardness of the investigated alloys, Ti–6242 and Ti–64 was observed. In the present study the oxygen diffusive layer was measured using metallographic technique (**Paper I, II and III**) that involves a two–step etching procedure. The diffusion rates and the activation energies for Ti–64 and Ti–6242, presented in Table 2.5, were estimated using the measured oxygen diffusive layer thicknesses. The oxygen diffusive layer thickness was also measured using Electron Probe Micro Analyser (EPMA). EPMA is a non–destructive method complementary to the more conventional techniques that can probe oxygen in thin layers and thereby providing the oxygen concentration gradient. Good agreement was found between the metallographic and the EPMA technique in evaluating the alpha–case thickness developed in the alloys used in the present study (see **Paper II and III**). Therefore, it can be said that the metallographic evaluation of the thickness of the oxygen diffusive layer is a reliable method.

2.6 Alpha–case formation in titanium alloys

As mentioned previously titanium oxidizes easily when exposed to elevated temperature and oxygen containing environments. The overall oxidation reaction includes oxide formation and inward oxygen diffusion in the titanium. The oxygen diffusion results with formation of an oxygen enriched layer beneath the oxide scale, commonly known as alpha–case layer. The diffusion of oxygen is possible due to the high solubility of oxygen in α–titanium and the stabilizing effect by the oxygen of the HCP crystal structure of α–titanium. Alpha–case is defined as a continuous, hard and brittle layer that significantly reduces several important mechanical properties of titanium alloys.

The simultaneous oxide scale and alpha–case formation can be described by the Wagner's model [69]. Figure 2.24 shows schematically the oxygen concentration profile in oxidized titanium.

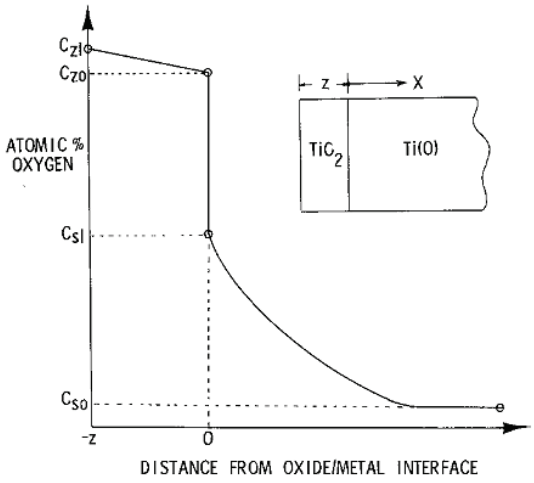

Figure 2.24 *Schematic representation of the oxygen concentration profile of oxidized titanium according to Wagner's model [37]*

As shown in Figure 2.24 the oxygen concentration profile is composed of two individual concentration profiles, one for the oxide (TiO_2) and the other one for the oxygen diffusion layer i.e. alpha–case layer. Both profiles have specific thicknesses, TiO_2 has thickness z, whereas the alpha–case layer has thickness x. The alpha–case layer has large oxygen solubility range starting with the highest oxygen concentration at the point C_{sl}, i.e. the oxide/metal interface and ending at distance C_{so} where the oxygen content reaches the oxygen bulk concentration present in the base metal. In contrast, the solubility of oxygen in the oxide scale is limited and it can be considered to be linear. It can be seen that the oxygen concentration present in the metal gradually decreases. The oxygen concentration at the oxide/metal interface (C_{sl}) is dependent on the exposure temperature and time and it can reach a maximum value of 14.3 wt. %, which is the maximum solid solubility of oxygen in α–titanium. Similar oxygen concentration profiles were obtained from the microhardness testing (**Paper I and II**) and the EPMA analysis in the present study (**Paper II and III**) for Ti–64 and Ti–6242 alloy after heat treatment. Unfortunately, the values obtained from the EPMA

measurements in the present study are not the absolute oxygen concentrations present in the investigated alloys, so they had to be normalised as described in **Paper II**. The lack of absolute concentration values from the EPMA measurements is due to the difficulties in quantifying the oxygen concentrations during the measurement.

Moreover, not only the oxygen content was probed with the EPMA measurements in the alloys investigated. The main alloying elements in the alloys were also probed and their concentration profiles were analysed. The analysis of the main alloying element concentration profiles (**Paper III**) revealed that in the Ti–64 alloy after heat treatment at 700 °C for 500 hours, large changes in the concentration distributions of vanadium and iron occur.

2.7 Prevention and removal of alpha–case in titanium alloys

Because alpha–case has detrimental effect on important mechanical properties of titanium alloys, actions to prevent its formation or if already existing, measures to machine away alpha–case are necessary. By performing any elevated temperature heat treatment in vacuum atmosphere, alpha–case formation can be limited or avoided. In some cases high temperature coatings like ceramics [1,3,70–72] are used to prevent oxygen to enter into the base material. However, if alpha–case has already formed, the conventional method for taking care of the alpha–case layer in aerospace industry is by removal using a process known as chemical milling or pickling [1,3,4]. The chemical milling process includes treatment of the aerospace engine component in chemical baths i.e. removal of the alpha–case by using chemical agents. Mixture of HF and HNO_3 acids in aqueous solution are used. The acid concentration and the bath temperature are controlling the rate of removal. HF dissolves the oxide scale and the titanium metal, whereas HNO_3 serves as oxidizing agent and repassivate the surface of the titanium. The metal dissolution is exothermic and therefore continuous cooling of the bath is required. If the removal rate is very high then gas is forming on the metal surface, which can cause uneven removal. Moreover, good control of the acids ratio in the chemical bath is required, because of the possibility of formation of high quantity of hydrogen that can be absorbed by titanium. Hydrogen uptake during the chemical milling process can be harmful and therefore must be avoided.

CHAPTER 3

MATERIALS AND EXPERIMENTAL METHODS

In this chapter the investigated alloys, the test methods used for sample examination and the experimental techniques used in the present thesis are described.

3.1 Materials

Ti–6Al–2Sn–4Zr–2Mo (Ti–6242) and Ti–6Al–4V (Ti–64) alloys were investigated.

3.1.1 Ti–6Al–2Sn–4Zr–2Mo

Ti–6Al–2Sn–4Zr–2Mo (Ti–6242) is a near–α alloy, solution and precipitation heat–treated. The alloy was obtained in forged condition according to AMS 4979 G [73]. This alloy is characterized with high strength, toughness and good creep resistance up to 538 °C. It finds application in airframe and jet engine components. Ti–6242 alloy used in this study had a bimodal microstructure consisting of equiaxed and/or elongated primary alpha in a transformed beta matrix (see Figure 2.12 a). The chemical composition of the alloy investigated in the present work in wt. % is listed in Table 3.1.

Table 3.1 *Chemical composition in wt. % of Ti–6242*

Element	Al	Zr	Mo	Sn	Si	O	Fe	C	N	H	Y	Ti
min	5.50	3.60	1.80	1.80	0.06	—	—	—	—	—	—	Bal.
max	6.50	4.40	2.20	2.20	0.10	0.15	0.10	0.05	0.05	0.0125	0.005	Bal.

3.1.2 Ti–6Al–4V

Ti–6Al–4V (Ti–64) is an α+β alloy in the present work received in plate form according AMS 4911 L [74]. This alloy shows a good combination of strength, corrosion resistance and fabrication ability. In aerospace it is used mainly for manufacturing of aircraft structural and engine components where the temperature does not exceed 300–350 °C. In the present study the Ti–64 alloy had equiaxed microstructure with primary alpha grains and elongated alpha needles in transformed beta matrix (see Figure 2.12 b). The chemical composition of the alloy investigated in the current work is presented in Table 3.2.

Table 3.2 *Chemical composition in wt. % of Ti–64*

Element	Al	V	Fe	O	C	N	H	Y	Ti
min	5.50	3.50	—	—	—	—	—	—	Bal.
max	6.75	4.50	0.3	0.20	0.08	0.05	0.015	0.005	Bal.

3.2 Methods of sample examination

A three step procedure was used to characterise the oxide scale and the alpha–case development: preparation of test samples prior to heat treatment; heat treatment; and finally processing of the samples for evaluation of alpha–case thickness using light optical microscopy (OM).

Pre heat treatment preparation comprised cutting of the samples into a square plate shape with dimensions 10 x 10 x 5 mm (Figure 3.1), manual polishing and cleaning. Two test

samples for each heating time were cut using a Struers Secotom–10 cutting machine. After cutting, all samples were manually polished using silicon carbide polishing paper up to 2500P grit size (8.4 ± 0.5 μm). Prior to heat treatment the samples were immersed in technical acetone and cleaned in an ultrasonic bath for 15 min.

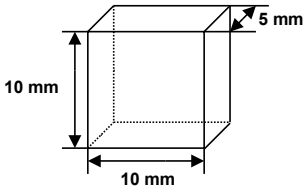

Figure 3.1 *Geometry of test samples*

Heat treatments were carried out in a NABERtherm model N11/R and NABERtherm tube model furnace in air at atmospheric pressure. Test samples were placed onto Al_2O_3 crucibles in a vertical position and introduced into the furnaces. A thermocouple positioned at a specific location inside the furnace was used to follow the actual temperature during testing. Every 24 hours the temperature of the furnace was checked. Ti–6242 and Ti–64 were isothermally held at 500, 593 and 700 °C for time up to 500 hours. Additionally, thermal gravimetric analysis (TGA) measurements were performed at 593 °C for time of 200 hours for both alloys using a NETZSH STA 446C instrument. All test samples were scaled using analytical microbalance with an accuracy of ± 0.0001 g, before and after each heat treatment to follow the change in weight.

The determination of the alpha–case thickness required preparation of the test samples in several steps. All test samples were cut in half parallel to the face placed on the crucible and then cleaned in acetone for 15 minutes in an ultrasonic bath. Cleaned samples were mounted in bakelite using BUEHLER Simplimet model 1000 mounting machine. After mounting, samples were polished to ~ 0.05 μm with colloidal silica using a semiautomatic BUEHLER Phoenix 4000 polishing machine. Polished test samples were etched using a standard etching procedure for titanium alloys, which comprises two steps. First, swabbing the polished sample surface with Kroll's reagent (a mixture of 1–2 ml 40 ± 45 % HF, 2–3 ml 68 ± 45 % HNO_3 in 100 ml distilled water), which gave low microstructural contrast, followed by etching in Weck's reagent (3 g NH_4HF_2 in 100 ml distilled water) for 10 s, ceasing when bubbles started to appear.

3.3 Experimental techniques

In this section the experimental techniques used to investigate the oxide scale and the alpha–case layer are described.

3.3.1 Light optical microscopy (OM)

The alpha–case layer was evidenced after the two step etching procedure as a continuous bright layer using a Nikon Eclipse optical microscope model MA200 (see Figure 3.2). From the optical micrographs of all samples the alpha–case thickness was estimated in both alloys.

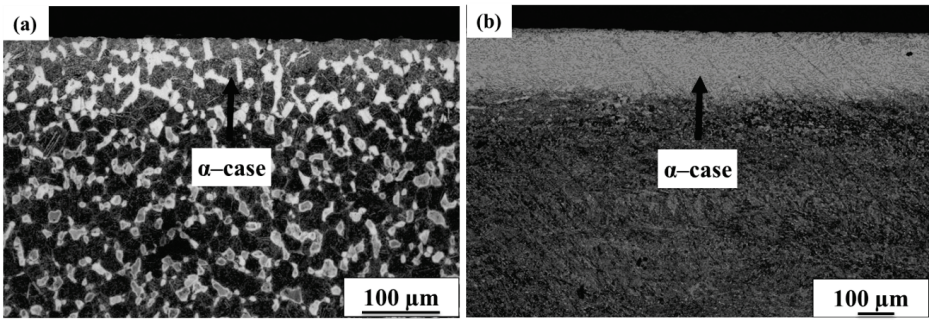

Figure 3.2 *Optical micrographs of alpha–case layer along entire periphery of cross–sectioned samples of a) Ti–6Al–2Sn–4Zr–2Mo and b) Ti–6Al–4V*

3.3.2 Scanning electron microscopy

The oxide scales and the alpha–case layer in both alloys were evaluated by using scanning electron microscope (SEM) model JEOL JSM–6460LV and high–resolution field emission scanning electron microscope (FE–SEM) model MERLIN from Carl Zeiss. The micrographs were obtained using secondary (SE) and back scattered electrons (BSE) mode, accelerate voltage of 3–25 kV, probe current of 1nA for FE–SEM and 84 µA for JEOL SEM.

3.3.3 X–ray Diffraction

An X–ray Diffractometer (XRD), model PANalytical Empyrean equipped with a PIXcel3D detector was used to record the XRD pattern of the oxide scales in both alloys. The X–ray tube was an Empyrean Cu LFF HR and scans were performed with 0.026° step size and in the 2–theta range of 20°–80°.

3.3.4 Electron Probe Micro Analyzer

JEOL JXA–8500F Electron Probe Micro Analyzer (EPMA) situated at the Norwegian University of Science and Technology was used to evaluate the concentration profiles of oxygen and the alloying elements along the alpha–case layer. Accelerating voltage of 10 keV and probe current 20 nA was used for the measurements. Line scans, with lengths between 100–400 µm, across the thickness of the alpha–case layer in point mode with step width between the points in the range of 0.5–1 µm were performed. The concentration of the measured elements was quantified by overlapping the intensities of the characteristic peaks from the alloying elements and standards with known concentration. The following standards were used: titanium nitride (TiN) for measuring titanium (Ti) and nitrogen (N) concentrations, pure aluminum (Al), pure tin (Sn), pure zirconium (Zr), pure molybdenum (Mo), pure vanadium (V) for measuring Al, Sn, Zr, Mo, V concentrations and quartz (SiO_2) for measuring O concentration. The obtained intensity peaks later were subjected to ZAF (Z–atomic weight, A–adsorption coefficient and F–fluorescence) correction [75].

CHAPTER 4

SUMMARY OF APPENDED PAPERS

4.1 Paper I

Study of alpha–case depth in Ti–6Al–2Sn–4Zr–2Mo and Ti–6Al–4V

Raghuveer Gaddam, Birhan Sefer, Robert Pederson and Marta–Lena Antti

In **Paper I**, the alpha–case depth formed in Ti–6Al–2Sn–4Zr–2Mo (Ti–6242) and Ti–6Al–4V (Ti–64) alloys was evaluated after isothermal heat treatment in ambient air and times up to 500 hours. The selected temperatures were 500 and 593 °C for Ti–6242 and 593 and 700 °C for Ti–64, respectively. Moreover, the isothermal oxidation behaviour was studied for both alloys using thermal gravimetric analysis (TGA) in dry air at 593 °C for times up to 200 hours. In addition, the alpha–case depth was measured and compared for the two alloys. The analysis of the TGA curves for Ti–6242 and Ti–64 showed consequent increase of the weight gain per surface area with respect to the exposure time which approximately followed parabolic behaviour in both alloys. From the TGA curves a higher weight gain per surface area for Ti 64 than for Ti–6242 was observed. It is believed that the higher weight gain is due to the formation of thicker oxide scale in Ti–64 (~ 5 μm) in comparison with Ti–6242 (< 1 μm). The alpha–case depths of all the samples and for both alloys were measured optically after using a two–step etching procedure, where the alpha–case appeared as bright continuous layer next to the edge of the samples (see **Paper I**, Figure 3). An approximately parabolic behaviour of the alpha–case growth with respect to the exposure time at all tested temperatures in the two alloys was found. Similar maximum values for the depth of the alpha–case layers (~ 30 μm) formed after the heat treatment performed at 593 °C for 500 hours were observed in both alloys. This indicated that there is not any significant influence of the differences in the chemical composition and the microstructure of the two alloys on the alpha–case depth at 593 °C. Additionally, the heat treatment at 500 °C for Ti–6242 and at 700 °C for Ti–64 resulted in formation of 10 μm and 200 μm alpha–case depths after 500 hours exposure time. Moreover, in this paper the hardness of the alpha–case layer was measured and compared with the bulk hardness. It was found that the hardness in the alpha–case layer for both alloys is higher compared with the bulk hardness of the alloys. Additionally, the hardness profile of the Ti–64 sample heat–treated at 700 °C for 500 hours showed that the hardness is gradually decreasing from the surface into the bulk of the alloy to a depth of ~ 250 μm.

Author's contribution: The author performed the isothermal heat treatment experiments for Ti–6Al–4V alloy, wrote the experimental section of the paper and presented the paper at the conference.

4.2 Paper II

Oxidation and alpha–case formation in Ti–6Al–2Sn–4Zr–2Mo

Raghuveer Gaddam, Birhan Sefer, Robert Pederson and Marta–Lena Antti

In **Paper II**, the oxidation and the alpha–case layer formed in Ti–6242 alloy after isothermal heat treatments in air at 500, 593 and 700 °C for times up to 500 hours were investigated. It was found that the weight gain is increasing with increase of temperature and time. Analysis of the weight gain per surface area curves at all three tested temperatures has been performed. The estimated reaction indices for the weight gain per surface area curves showed changes in the oxidation kinetics. At 500 °C for times up to 200 hours a cubic behaviour of the oxidation was found, which for prolonged times changed to parabolic. For the heat treatment carried out at 593 °C parabolic oxidation kinetics was found without any changes for times up to 500 hours. Finally, at 700 °C the oxidation followed parabolic behaviour for times up to 200 hours, which for longer times changed to linear. The activation energy for the parabolic oxidation in the temperature range of 500–700 °C was estimated to 157 kJ/mol. SEM on the oxide scales formed after 500 hour exposure at all three tested temperatures showed two types of morphologies of the oxide scale, i.e. dense and porous. At 500 °C the formed oxide scales were compact and dense with thicknesses less than 1 μm, whereas at 593 and 700 °C higher thickness and porosity of the oxide scales were observed. The highest porosity of the oxide scale was found in the sample heat–treated at 700 °C for 500 hours. It is believed that the formation of porous structure of the oxide scale at 700 °C for times longer than 200 hours is the main reason for the observed change in the oxidation kinetics from parabolic to linear behaviour. The alpha–case thickness was measured optically for all samples and a parabolic relationship with respect to time at all three tested temperatures was found. Additionally, the activation energy for oxygen diffusion was estimated to 153 kJ/mol. The Electron Probe Micro Analyzer (EPMA) was used to obtain the normalised oxygen concentration profiles in the Ti–6242 from which the alpha–case thickness was evaluated. Values for the alpha–case thicknesses measured optically and evaluated from the normalised EPMA oxygen concentration profiles were compared. Good agreement between the values obtained from both techniques was found, except for the samples heat–treated at 700 °C for times longer than 200 hours. The normalised EPMA oxygen profiles for these samples indicated about 50 μm higher alpha–case thicknesses in comparison to the ones measured optically. On the other hand, the microhardness profile of the sample heat–treated at 700 °C for 500 hours showed good agreement and similar alpha–case thickness as the corresponding normalised EPMA oxygen concentration profile.

Author's contribution: The author performed the optical evaluation of the alpha–case thickness and the microhardness measurements for 700 °C heat–treated samples, analysed all the experimental data and wrote the paper along with the first author and with suggestions from the other co–authors.

4.3 Paper III

Characterization of the oxide scale and alpha–case layer in Ti–6Al–4V and Ti–6Al–2Sn–4Zr–2Mo in the temperature range 500–700 °C

Birhan Sefer, Raghuveer Gaddam, Robert Pederson, Antonio Mateo and Marta–Lena Antti

In **Paper III**, the oxide scale and the alpha–case layer formed after oxidation in the temperature range 500–700 °C in Ti–64 and Ti–6242 were studied by means of metallographic and microscopic techniques. Faster and more complex oxidation was noted in Ti–64 compared with Ti–6242. It is believed that the different oxidation behaviour of the alloys is a result of the differences in the chemical composition and microstructure of the investigated alloys. Multi–layered structure of the oxide scale in Ti–64 was observed after heat treatment at 700 °C for 500 hours, which was absent in Ti–6242. The thicknesses of the alpha–case layers were measured metallographically in both alloys. The diffusion coefficients and the activation energies for the diffusion of oxygen into the alloys were estimated from the measured alpha–case thicknesses to be 215 kJ/mol and 153 kJ/mol for Ti–64 and Ti–6242, respectively. Based on the experimentally evaluated D_0 and Q values the alpha–case thickness values were estimated for all temperatures and times in both alloys. The estimated alpha–case thickness values were compared with the corresponding optically measured values for the alpha–case thickness and good agreement between them was found, except for the heat treatments carried out at 700 °C after 200 and 300 hours in Ti–64 and Ti–6242, respectively. The oxygen concentration profiles in both alloys were obtained by the EPMA measurements and the alpha–case thickness was estimated from the profiles. Alpha–case thicknesses evaluated metallographically and from the EPMA oxygen profiles were compared and a good agreement between the techniques in determination of the alpha–case layer boundary was found, except at 700 °C for 300 hours heat treatment in Ti–6242. The EPMA concentration profiles of the main α and β alloying elements in both alloys for the heat treatment at 700 °C for 500 hours were analysed. It was found that vanadium and iron accumulate in the β phases, forming solid solution of β–titanium with vanadium and iron. This accumulation led to coarsening of the microstructure and increase of the α–phase volume fraction in Ti–64 alloy.

Author's contribution: The author performed the isothermal heat treatment experiments for Ti–6Al–4V alloy, analysed the experimental data and wrote the paper with suggestions from the co–authors.

CHAPTER 5

CONCLUSIONS AND FUTURE WORK

5.1 Conclusions

Based on the results and the observations presented in **Papers I, II** and **III** the following conclusions can be made with respect to oxidation and alpha–case phenomena in Ti–6242 and Ti–64 alloys after isothermal heat treatment at 500, 593 and 700 °C for times up to 500 hours.

Oxidation

- The isothermal heat treatment for both alloys at all three temperatures and times resulted in simultaneous formation of oxide scale and oxygen enriched layer beneath the scale, known as alpha–case.
- Faster oxidation, higher weight gain and thicker oxide scales were observed in Ti–64 compared with Ti–6242 at all three tested temperatures and time up to 500 hours.
- The oxidation of Ti–6242 followed approximately parabolic relationship with time at all three tested temperatures and the activation energy for parabolic oxidation was estimated to 157 kJ/mol.
- The heat treatment at 700 °C for 500 hours resulted in porous structure of the oxide scales in the two alloys, but with different morphology. In Ti–64 alloy a multi–layered oxide scale was observed, whereas in Ti–6242 such morphology was not present.

Alpha–case

- The alpha–case formation kinetics was a function of temperature and time and it followed mainly parabolic growth behavior in both alloys at all tested temperatures for times up to 500 hours.
- The heat treatment at 593 °C for up to 500 hours resulted in formation of similar alpha–case thicknesses in both alloys. This indicated that at this temperature the differences in chemical composition and microstructure of the two alloys did not influence the alpha–case formation.
- Highest microhardness values were observed at the sample surface in the alpha–case layers of the two alloys, gradually decreasing until reaching the bulk hardness of the alloys.
- The evaluation of the alpha–case thickness using optical microscope and EPMA showed similar values for all tested temperatures and times, except for the samples heat–treated at 700 °C in the time interval 300–500 hours.
- The activation energy for oxygen diffusion was estimated to 215 kJ/mol and 153 kJ/mol for Ti–64 and Ti–6242, respectively.
- For Ti–64 samples heat–treated at 700 °C for 500 hours there was a coarsening of the microstructure and formation of solid solution between β–phase and vanadium and iron.
- The heat treatment at 700 °C for 500 hours in Ti–6242 and Ti–64 resulted in an increase of the alpha phase volume fraction in the alloys.

5.2 Future work

The work performed in the present thesis contributed to some extent in better understanding of the oxidation and the alpha–case formation phenomena in Ti–6242 and Ti–64 alloys exposed to ambient air at elevated temperatures in the range 500–700 °C. However, there are still some points that need to be studied more in detail and therefore further research is required.

One industrial interest is to develop a universal oxidation model for prediction of the alpha–case layer thickness that would be useable for different titanium alloys. Such a model would result in minimizing the costs for removal of the alpha–case either by machining or by chemical milling. Therefore, further chemical analysis of the alpha-case layer and determination of the absolute oxygen concentration are required. One of the ways to determine the absolute oxygen content in the alpha–case layer is by conducting secondary ion mass spectrometry (SIMS) analysis. SIMS analysis of the alpha–case layer is in progress and hopefully the results obtained from the analysis would provide information for the absolute oxygen content in the alloys.

Moreover, in **Paper III** an increase of the volume fraction of the α–phase in Ti–64 alloy was observed, but this increase was not quantified. One of the future plans is to quantify the increase of the α–phase volume fraction after heat treatment by using image analysis techniques.

In addition, research focused on investigating the influence of alpha–case on the mechanical properties of titanium alloys is planned to be performed. In particular the main interest is to investigate the effect of the alpha–case layer on the low cycle fatigue (LCF) strength of the Ti–64 and Ti–6242 alloys.

Another issue of these alloys that is planned to be addressed in the future is the pitting corrosion. Pitting corrosion occurs during removal of the alpha–case layer using chemical milling, which is performed in mixtures of strong acids. The presence of pits has detrimental effect on the mechanical properties of these alloys especially under dynamic loading conditions. They act as initiation sites for cracking and lead to faster crack growth and failure of the titanium alloy components. Therefore, one of the future plans is to investigate the pitting corrosion of these two alloys and its effect on the LCF properties.

CHAPTER 6

REFERENCES

[1] G. Lutjering and J. C. Williams, *Titanium*, Berlin: Springer–Verlag, **2007.**

[2] R. R. Boyer, *An Overview of the Use of Titanium in the Aerospace Industry*, Materials Science and Engineering A 213, **1996**, 103–114.

[3] C. Leyens and M. Peters, *Titanium and Titanium Alloys*, Weinheim: Wiley, **2003.**

[4] J. M. Donachie, *Titanium, A Technical Guide*, ASM International, Metals Park, OH **2000.**

[5] M. Peters, J. Kumpfert, C. H. Ward and C. Leyens, *Titanium Alloys for Aerospace Applications*, Advanced Engineering Materials, 5, 6, **2003**, 419–427.

[6] T. B. Massalski, Binary alloy phase diagrams Vol 1–3, Materials Park, Ohio, ASM International, **1990.**

[7] F.C. Campbell, *Manufacturing Technology for Aerospace Structural Materials*, Elsevier, **2006.**

[8] W. L. Finlay and J. A. Snyder, *Effects of three interstitial solutes (Nitrogen, Oxygen and Carbon) on the mechanical properties of high–purity alpha titanium*, Journal of Metals 188, **1950,** 227–286.

[9] H. R. Ogden and R. I. Jaffe, *The effects of carbon, oxygen and nitrogen on the mechanical properties of titanium and titanium alloys*, report no. 20, **1955.**

[10] A. I. Kahveci and G. E. Welsch, *Effect of oxygen on the hardness and alpha/beta phase ratio of Ti–6Al–4V alloy*, Scripta Metallurgica 20, **1986,** 1287–1290.

[11] C. E. Shamblen and T. K. Redden, *Air contamination and embrittlement in titanium alloys*, in: R. I. Jaffe and N. E. Promisel (Eds.), The Science Technology and Application of Titanium, Pergamon Press, Oxford, United Kingdom, **1968,** 199–208.

[12] J. Ruppen, P. Bhowalm D. Eylon and A. J. McEvily, *On the process of subsurface fatigue crack initiation in Ti–6Al–4V*, in: (J. T. Fong, Ed.), Fatigue mechanisms, Proceedings of and ASTM–NBS–NSF symposium, Kansas city, **1979,** ASTM–STP American Society for Testing and Materials, 47–68.

[13] R. N. Shenoy, J. Unnam and R. K. Clark, *Oxidation and embrittlement of Ti–6Al–2Sn–4Zr–2Mo alloy*, Oxidation of Metals 26, **1986,** 105–124.

[14] Z. Liu and G. Welsch, *Effects of oxygen and heat treatment on the mechanical properties of alpha and beta titanium alloys*, Metallurgical Transactions 19A, **1988,** 527–542.

[15] L. Bendersky and A. Rosen, *The effect of exposure on fracture of Ti–6Al–4V alloy*, Engineering Fracture Mechanics 13, **1980,** 111–118.

[16] H. Dong and X. Y. Li, *Oxygen boost diffusion for the deep–case hardening of titanium alloys*, Materials Science and Engineering A280, **2000,** 303–310.

[17] A. Majorell, S. Srivatsa and R. C. Picu, *Mechanical behaviour of Ti–6Al–4V at high and moderate temperatures – Part I: Experimental results*, Materials Science and Engineering A326, **2002,** 297–305.

[18] A. R. Ebrahimi, F. Zarei and R. A. Khosroshahi, *Effect of thermal oxidation process on fatigue behaviour of Ti–6Al–2V alloy*, Surface and Coatings Technology 203, **2008,** 199–203.

[19] W. Jia, W. Zeng, X. Zhang, Y. Zhou, J. Liu and Q. Wang, *Oxidation behaviour and effect of oxidation on tensile properties of Ti60 alloy*, Journal of Materials Science 46, **2011,** 1351–1358.
[20] A. L. Pilchak, W. J. Porter and R. John, *Room temperature fracture processes of a near–α titanium alloy following elevated temperature exposure*, Journal of Materials Science 47, **2012,** 7235–7253.
[21] H. Fukai, H. Iizumi, K. Minakawa and C. Ouchi, *The effect of the oxygen–enriched surface layer on mechanical properties of α+β type titanium alloys*, ISIJ International 45, **2005,** 133–141.
[22] R. Dobeson, N. Petrazoller, M. Dragusch and S. McDonald, *Effect of thermal exposure on the room temperature tensile properties of grade 2 titanium*, Materials Science and Engineering A528, **2011,** 3925–3929.
[23] C. Leyens, M. Peters, D. Weinem and W. A. Kaysser, *Influence of long–term annealing on tensile properties and fracture of near–α titanium alloy Ti–6Al–2.75Sn–4Zr–0.4Mo–0.45Si*, Metallurgical and Materials Transactions 27A, **1996,** 1709–1717.
[24] P. Kofstad, *High Temperature Corrosion*, Elsevier, **1988.**
[25] O. Kubaschewski and B. E. Hopkins, *Oxidation of Metals and Alloys*, Butterworths, London, **1962.**
[26] K. Hauffe, *Oxidation of Metals*, Plenum, New York, **1966.**
[27] A. T. Fromhold, Jr., *Theory of Metal Oxidation*, Vol. I, *Fundamentals*, North–Holland, Amsterdam, **1976.**
[28] U. R. Evans, *The Corrosion and Oxidation of Metals*, Edward Arnold, London, **1960.**
[29] P. Kofstad, *Nonstoichiometry, diffusion and electric conductivity in binary metal oxides*, Malaba Florida, R. E. Krieger Publishing Company, **1983.**
[30] P. Kofstad, *Defects and Transport Properties of Metals Oxides*, Oxidation of Metals 44, **1995,** 3–27.
[31] M. H. Kim, S. B. Baek, U. Paik, S. Nam and J. D. Byun, *Electrical conductivity and Oxygen Diffusion in Nonstoichiometric* TiO_{2-x}, Journal of the Korean Physical Society 32, **1998,** 1127–1130.
[32] H. Okamoto, *O–Ti (Oxygen–Titanium)*, Journal of Phase Equilibria and Diffusion 32, **2011,** 473–474.
[33] P. Kofstad, K. Hauffe and H, Kjöllesdal, *Investigation on the oxidation mechanism of titanium*, Acta Chemica Scandinavica 12, **1958,** 239–266.
[34] P. Kofstad, *High Temperature Oxidation of Metals*, Wiley, New York, **1966.**
[35] J. Stringer, *The oxidation of titanium in oxygen at high temperatures*, Acta Metallugica 8, **1960,** 758–766.
[36] J. E. Lopes Gomes and A. M. Huntz, *Correlation between the oxidation mechanism of titanium under a pure oxygen atmosphere, morphology of the oxide scale and diffusional phenomena,* Oxidation of Metals 14, **1980,** 249–261.
[37] J. Unnam, R. N. Shenoy and R. K. Clark, *Oxidation of commercial purity titanium,* Oxidation of Metals 26, **1986,** 249–261.
[38] H. L. Du, P. K. Datta, D. B. Lewis and J. S. Burnel–Gray, *High–temperature corrosion* of Ti and *Ti–6Al–4V alloy*, Oxidation of Metals 45, **1996,** 507–527.
[39] S. Frangini and A. Mignone, *Various aspects of the air oxidation behaviour of Ti6Al4V alloy at temperatures in the range 600–700 °C*, Journal of Materials Science 29, **1994,** 714–720.
[40] H. L. Du, P. K. Datta, D. B. Lewis and J.S. Burnel–Gray, *Air oxidation behaviour of Ti–6Al–4V alloy between 650 and 850 °C*, Corrosion Science 63, **1994,** 631–642.

[41] F. Pitt and M. Ramulu, *Influence of grain size and microstructure on oxidation rates in titanium alloy Ti–6Al–4V under superplastic forming conditions*, Journal of Materials Engineering and performance 13, **2004,** 727–734.
[42] M. N. Mungole, N, Singh and G. N. Mathur, *Oxidation behaviour of Ti6Al4V titanium alloy in oxygen*, Materials Science and Technology 18, **2002,** 111–114.
[43] H. Guleryuz and H. Cimenoglu, *Oxidation of Ti–6Al–4V alloy,* Journal of Alloys and Compounds 472*,* **2009,** 241–246.
[44] D. Poquillon, C. Armand and J. Huez, *Oxidation and oxygen diffusion in Ti–6Al–4V alloy: Improving measurements during Sims analysis by rotating the sample*, Oxidation of metals 79, **2013,** 249–259.
[45] S. Zeng, A. Zhao, H. Jiang, X. Fan, X. Duan and X. Yan, *Cyclic oxidation behaviour of the in Ti–6Al–4V alloy*, Oxidation of metals 81, **2014,** 467–476.
[46] C. E. Shamblen and T.K. Redden, *Air contamination and embrittlement of titanium alloys*, The Science, Technology and Application of Titanium (Pergamon Press, Oxford, United Kingdom), **1968,** 199–208.
[47] R. N. Senoy, J. Unnam and R. K. Clark, *Oxidation and embrittlement of Ti–6Al–2Sn–4Zr–2Mo alloy*, Oxidation of Metals 26, **1986,** 105–124.
[48] P. W. M. Peters, J. Hemptenmacher and C. Todd, *Oxidation and stress enhanced oxidation of Ti–6–2–4–2*, Titan–2003, Science and Technology IV, Weinheim, Wiley–VCH, **2004,** 2067–2074.
[49] K. S. McReynolds and S. Tamirisakandala, *A study on alpha–case depth in Ti–6Al–2Sn–4Zr–2Mo*, Metallurgical and Materials Transactions 42A, **2011,** 1732–1736.
[50] R. W. Evans, R. J Hull. and B. Wilshire, *The effects of alpha–case formation on the creep fracture properties of the high–temperature titanium alloy IMI834*, Journal of Materials Processing Technology 56, **1996,** 492–501.
[51] I. Gurrapa, *On the mechanism of degradation of titanium alloy IMI 834 in an oxidizing atmosphere at elevated temperatures*, Corrosion Prevention and Control, **2002,** 79–84.
[52] K. V. Sai Srinadh and V. Singh, *Oxidation behaviour of the near α–titanium alloy IMI 834,* Bulletin of Materials Science 27, **2004,** 347–354.
[53] P. Shewmon, *Diffusion in Solids*, Warrendale, Pa., Minerals, Metals and Materials Society cop., 2nd Ed., **1989.**
[54] W. D. Callister, *Materials Science and Engineering an Introduction*, Wiley, New York, **2007.**
[55] J. Crank, *The mathematics of diffusion*, Oxford Clarendon Press, 2nd Ed., **1979.**
[56] H. H. Wu and D. R. Trinkle, *Direct diffusion through interpenetrating networks: oxygen in titanium*, Physical Review Letters 107, **2011,** 1–4.
[57] Z. Liu and G. Welsh, *Literature survey on diffusivities of oxygen, aluminum and vanadium in alpha titanium, beta titanium and in rutile*, Metallurgical and Materials Transactions A 19, **1988,** 1121–1125.
[58] W. P. Roe, H. R. Palmer and W. R. Opie, *Diffusion of oxygen in alpha and beta titanium*, Transactions of the ASM 52, **1960,** 194–200.
[59] T. N. Wittberg, J. D. Wolf, R. G. Keil and P. S. Wang, *Low–temperature oxygen diffusion in alpha titanium characterized by Auger sputter profiling*, Journal of Vacuum Science and Technology A1, **1983,** 475–478.
[60] D. David, E. A. Garcia, G. Beranger, J. P. Bars, E. Etchessahar and J. Debuigne, *Comparative study of insertion and diffusion of oxygen and nitrogen in alpha–titanium*, Titanium ’80 Science and Technology, Proceedings of the 4th international conference on titanium, H. Kimura and O. Izumi, eds., TMS–AIME, **1980,** 537–547.

[61] M. Dechamps and P. Lehr, *On the oxidation of α titanium in an oxygen atmosphere: the role of oxidized layer and mechanism of oxidation*, Journal of Less–Common Metals 56, **1977**, 193–207.

[62] D. David, G. Beranger and E. A. Garcia, *A study of the diffusion of oxygen in α – titanium oxidized in the temperature range 460–700 °C*, Journal of the Electrochemical Society 130, **1982,** 1426–1426.

[63] F. Claisse and H. P. Koenig, Thermal and forced diffusion of oxygen in β–titanium, Acta Metallurgica 4, **1956,** 650–654.

[64] L. F. Sokiryanskii, D. V. Ignatov, A. Ya. Shinyaev, I. V. Bogolyubova, V. V. Latsh and M. S. Model, Titanovye Splavy Nov. Tekh., Mater. Nauch.–Tekh. Soveshch., 1966 (pub. 1968), 201–210 (Ed. N. P. Sazhin, Izd. "Nauka": Moscow, USSR), from Chemical Abstracts, **1969,** vol. 71, no. 8, 83986r.

[65] O. N. Carlson, F. S. Schmidt and R. R. Lichtenberg, *Investigation of reported anomalies in the electrotransport of interstitial solutes in titanium and iron*, Metallurgical Transactions 6A, **1975,** 725–731.

[66] C. J. Rosa, *Oxygen diffusion in alpha and beta titanium in the temperature range 932 to 1142 °C*, Metallurgical Transactions 1, **1970,** 2517–2522.

[67] J. Tiley, J. Shaffer, A. Shiveley, A. Pilchack and A. Salem, *The effect of lath orientations on oxygen ingress in titanium alloys*, Metallurgical and Materials Transactions 45A, **2014,** 1041–1048.

[68] Aerospace Series–Test methods–Titanium and titanium alloys–Part 009–Determination of surface contamination (SS–EN 2003–009:2007), **2007,** Swedish Standards Institute.

[69] C. Wagner, *Diffusion in Solids, Liquids, Gases*, W. Jost, Ed. Academic Press, New York, **1952**.

[70] S. Fujishiro and D. Eylon, *Improved high temperature mechanical properties of titanium alloys by platinum ion plating*, **1978,** Thin Solid Films 54, 309–315.

[71] C. Leyens, M. Peters and W. A. Kaysser, *Intermetallic Ti-Al coatings for protection of titanium alloys: oxidation and mechanical behavior*, **1997,** Surface and Coatings Technology 94–95, 34–40.

[72] I. Gurrappa and A. K. Gogia, *Development of oxidation resistant coatings for titanium alloys*, **2001,** Materials Science and Technology 17, 581–587.

[73] AMS 4976 G, **2008,** Titanium alloy, forgings 6.0Al–2.0Sn–4.0Zr–2.0Mo solution and precipitation heat–treated (SAE–AMS/MAM).

[74] AMS 4911 L, **2008,** Titanium alloy, sheet, strip and plate 6Al–4V annealed (SAE–AMS/MAM).

[75] J. Goldstein, D. E. Newbury, D. C. Joy, C. E. Lyman, P. Echlin, E. Lifshin, L. Sawyer and J. R. Michael, *Scanning Electron Microscopy and X-ray Microanalysis*, Springer, **2003.**

Paper I

IOP Conf. Series: Materials Science and Engineering **48** (2013) 012002 doi:10.1088/1757-899X/48/1/012002

Study of alpha-case depth in Ti-6Al-2Sn-4Zr-2Mo and Ti-6Al-4V

R Gaddam[1], B Sefer[1], R Pederson[1,2] and M-L Antti[1]
[1]Division of Materials Science, Luleå University of Technology, S-97187 Luleå, Sweden
[2]Research Centre, GKN Aerospace Engine Systems, S-46181 Trollhättan, Sweden

E-mail: raghuveer.gaddam@ltu.se

Abstract. At temperatures exceeding 480°C titanium alloys generally oxidises and forms a hard and brittle layer enriched with oxygen, which is called alpha case. This layer has negative effects on several mechanical properties and lowers the tensile ductility and the fatigue resistance. Therefore any alpha-case formed on titanium alloys during various manufacturing processes, such as heat treatment procedures, must be removed before the final part is mounted in an engine. In addition, long time exposure at elevated temperatures during operation of an engine could possibly also lead to formation of alpha-case on actual parts, therefore knowledge and understanding of the alpha-case formation and its effect on mechanical properties is important. Factors that contribute for growth of alpha-case are: presence of oxygen, exposure time, temperature and pressure. In the present study, isothermal oxidation experiments in air were performed on forged Ti-6Al-2Sn-4Zr-2Mo at 500°C and 593°C up to 500 hours. Similar studies were also performed on Ti-6Al-4V plate at 593°C and 700°C. Alpha-case depth for both alloys was quantified using metallography techniques and compared.

1. Introduction

The titanium alloys, Ti–6Al–2Sn–4Zr–2Mo (Ti-6242) and Ti-6Al-4V (Ti-64) are widely used for components in aeroengines because of their excellent combination of weight and strength [1-3]. The maximum service temperature for these alloys is limited to 450°C for Ti-6242 and 350°C for Ti-64 [2,3]. It is partly because of degradation of mechanical properties above these respective temperatures as at elevated temperatures (above 480°C), titanium alloys oxidises in oxygen containing environments; this results in simultaneous formation of an oxide (TiO_2) scale on the surface and an oxygen-rich layer beneath the scale, commonly referred to as alpha-case (α-case). Alpha-case is a continuous, hard, and brittle layer with higher oxygen content [1,2]. It forms because of higher solid solubility of oxygen in α-titanium (i.e.14.5 wt.% [4]) and higher affinity of titanium to absorb oxygen, which instantaneously reacts and stabilise the α phase. This brittle alpha-case degrades the mechanical properties such as tensile ductility and fatigue strength [5-10]. Therefore it is necessary to remove any alpha-case formed on parts manufactured from titanium alloys if they are subjected to high loads and/or dynamic loading conditions.

Environmental and economical requirements on future aero engines set higher demands on the efficiency and thereby pressure ratio. The increased pressure leads to higher temperatures, which could make it necessary to replace titanium alloys with nickel based super alloys in the front end of the engine. Unfortunately this increases the weight of the engine and leads to an increase of fuel consumption and is therefore undesirable. However, there is a possibility to increase the maximum working temperature of the currently used Ti-6242 alloy in compressor parts by developing a better understanding on how different mechanical properties and physical phenomena such as oxidation mechanisms are affected in the high temperature regimes. And since some aeroengine parts consists of a combination of both Ti-64 and Ti-6242. Hence both of these alloys are investigated in the current study. The objective of present study was to investigate the effect of heat treatment conditions on the

depth of alpha-case in two common aerospace grade titanium alloys; Ti-6242 and Ti-64. The heat treatment conditions investigated include the temperatures and times in ambient air that are of interest for heat treatment during manufacturing and for application in an aeroengine for both of these alloys.

2. Materials and Methods

The materials investigated are Ti-6242 and Ti-64 with the chemical compositions shown in table 1. Ti-6242 is a near- α alloy that has been solution and precipitation heat treated; and was obtained in forged condition according to AMS 4976G [11]. It consists of a bi-modal microstructure with primary α and transformed β (see figure 1(a)). Ti-64 is a α+β titanium alloy that has been obtained in plate form according to AMS 4911L [12], which consists of a microstructure with equiaxed primary α and elongated α in transformed β (see figure 1(b)).

Table 1. Chemical composition (wt.%) of the materials investigated.

Material	Al	Sn	Zr	Mo	N	O	C	H	Fe	Si	V	Ti
Ti-6242	6.5	2.2	4.4	2.2	0.05	0.15	0.05	0.05	0.1	0.1	-	Bal.
Ti-64	6.75	-	-	-	0.05	0.20	0.08	0.015	0.3	-	4.5	Bal.

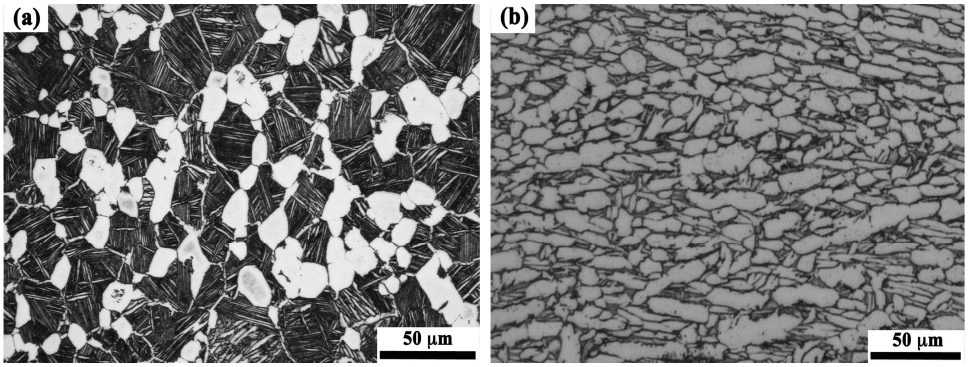

Figure 1. Optical micrographs showing the microstructure of as received materials, (a) forged Ti-6242 and (b) Ti-64 plate. In micrographs light or grey areas is α phase and dark areas is β.

2.1. Heat treatment

The samples for heat treatments were cut using electric discharged machining (EDM) from the as received material in dimensions of 10 x 5 x 10 mm. Totally 64 samples were cut out, where two samples were used for each exposure time and temperature. All the sample surfaces were metallographically polished to remove the recast layer. Thereafter, the polished samples were ultrasonically cleaned in technical acetone for approximately 15 min and rinsed with ethanol. The cleaned samples were heat treated in ambient air using a Nabertherm box furnace (N11/R) and a Nabertherm tube furnace (RHTC 80-450/15) at atmospheric pressure. The temperature inside the furnace is calibrated using a reference sample with a thermocouple welded to it and positioned at the locations inside the furnace where the samples are placed. The temperature inside the furnace was about ± 5ºC of the desired temperature**.** The samples were placed onto an Al_2O_3 plate or crucible and then introduced into the furnaces at the desired temperature and isothermally held for selected exposure times as shown in table 2. All samples were weighed using a microbalance with an accuracy of ± 0.0001 g before and after each heat treatment. In addition, heat treatments were also performed on Ti-6242 and Ti-64 samples, with a cross section of 17 x 2.5 x 10 mm, in dry air (i.e. technical air)

using a simultaneous thermal analysis instrument (STA 449C from Netschz Gmbh). The samples were isothermally held at 593°C for 200 hours.

Table 2. Heat treatment conditions.

Material	Temperature (ºC)	Exposure times (hour)
Ti-6242 forged	500	
	593	5, 10, 50, 100, 200, 300, 400 and 500
Ti-64 plate	593	
	700	

2.2. Alpha-case evaluation

Heat treated samples were cut into half, parallel to the face that is placed on the crucible (10 x 5 mm^2), thereafter ultrasonically cleaned in technical acetone for 15 min and rinsed with ethanol. Cleaned samples were mounted in bakelite using BUEHLER Simplimet model 1000 mounting machine and then metallographically prepared, which involves grinding and polishing the surface up to 0.05 μm with colloidal silica using a semiautomatic BUEHLER Phoenix 4000 polishing machine. The polished samples were etched in two steps to observe the alpha-case: first, swabbing the sample surface with Kroll's reagent (a mixture of 1-3 ml HF, 2-3 ml HNO_3 and distilled water) and second, immersing in Weck's reagent (1-3 g NH_4HF_2 and distilled water) for approximately 10 sec. Alpha-case layer was observed using a Nikon Eclipse optical microscope (model MA200) and the depth of alpha-case layer was quantitatively measured using NIS elements software. Totally 60 individual measurements of alpha-case depth on each sample were made along the entire perimeter at approximately 500 μm spacing on two samples of Ti-6242 and Ti-64 at each temperature and time combination, and the average values of alpha-case depth is then reported. The hardness measurements related to the alpha-case at the surface was obtained by applying a load of 100 g using MXT- α microhardness tester from Matsuzawa with a Vickers indenter (indent size is approximately 20 – 25 μm).

3. Results and Discussion

3.1. Weight gain

Figure 2(a) presents the amount of weight gain (ΔW) per surface area (A) for Ti-6242 and Ti-64 when isothermally held at 593°C for 200 hours in dry air. It is calculated by dividing the weight gain values of the samples, measured using STA 449C, with their total surface areas. The unit is (mg/cm^2). From figure 2(a) it can be seen that the ($\Delta W/A$) increased with time and approximately followed a parabolic relationship for both the alloys. Similar behaviour for both the alloys was observed on samples that were isothermally held in a laboratory furnace at 593°C for up to 500 hours in ambient air, where the weight gain is calculated by weighing before and after the heat treatment. It was noted that in Ti-6242 samples held at 500°C for up to 500 hours the weight gain followed approximately a parabolic relationship, while deviating from parabolic below 100 hours. In contrast, Ti-64 samples held at 700°C showed deviation from parabolic relationship beyond 200 hours. The observation of weight gain in both the alloys is obtained by fitting and performing regression analysis of the weight gain data using the following equation [13]:

$$(\Delta W/A) = Kt^{1/n} \quad (1)$$

where K is the rate constant and n is the reaction index. At a constant temperature, the weight gain is assumed to be linear if n=1, parabolic if n=2. The weight gain in the Ti-6242 alloy at the tested temperatures is consistent with other investigators [8, 14]. On the other hand, the Ti-64 alloy that was

held at 700°C for up to 500 hours, indicated a transition from parabolic to linear weight gain at about 200 hours. This confirms with the results found by others [15-17]. In figure 2(a) it can be seen that weight gain is much higher in Ti-64 compared to Ti-6242 at the constant temperature and time. This could be due to the thicker oxide layer (≈ 5 μm) in Ti-64 than in Ti-6242 (< 1 μm), see figure 2(b) and figure 2(c).

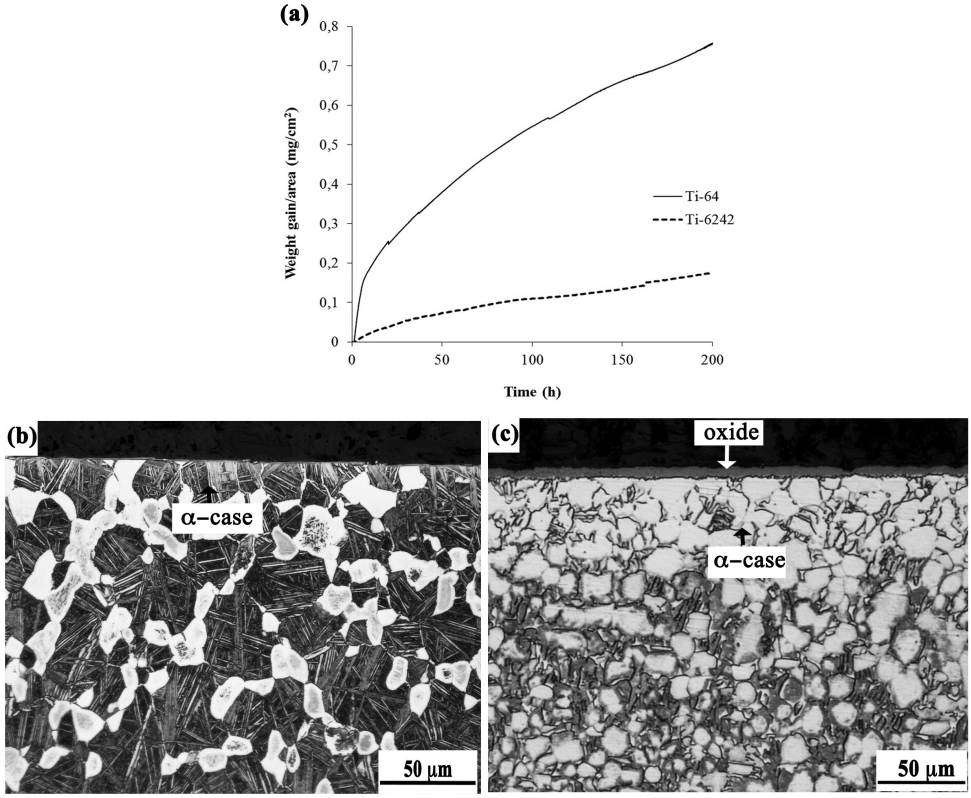

Figure. 2 (a) Plot showing the weight gain per unit area (mg/cm^2) in Ti-6242 and Ti-64 held at 593°C for 200 hours in dry air, (b,c) optical micrographs of Ti-6242 and Ti-64, showing the oxide layer and alpha case.

3.2. Alpha-case evaluation

Figure 3 shows the representative optical micrographs of alpha-case (white layer) in Ti-6242 and Ti-64 after long exposure time (500 hours) at 593°C. It can be seen that alpha-case is formed beneath the surface simultaneously with the oxide (see Figure 3(b)). Figure 4 shows the plot of alpha-case depth versus exposure time for Ti-6242 and Ti-64 at the tested temperatures. Here, alpha-case is measured quantitatively using the optical micrographs. From figure 4, it can be seen that depth of alpha-case is increased with temperature and time in both the alloys and mainly follows a parabolic relationship at the selected heat treatment conditions. The maximum depth of alpha-case formed in Ti-6242 is approximately 30 μm when exposed at 593°C for 500 hours, and 10 μm at 500°C after 500 hours (see figure 4). The depth of alpha-case in Ti-64 when exposed to 593°C for 500 hours was about 30 μm. In addition, it is observed that a thick alpha-case layer of approximately 200 μm is formed in Ti-64 when exposed at 700°C for 500 hours.

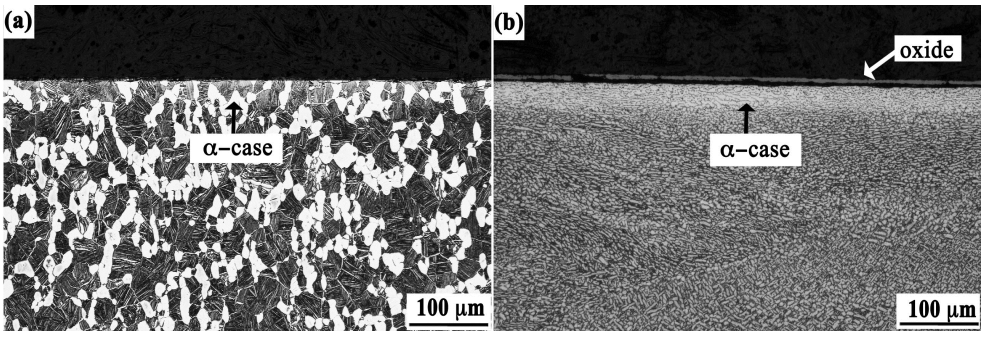

Figure 3. Optical micrographs showing alpha-case (white layer) in (a) Ti-6242 and (b) Ti-64 heated at 593°C up to 500 hours.

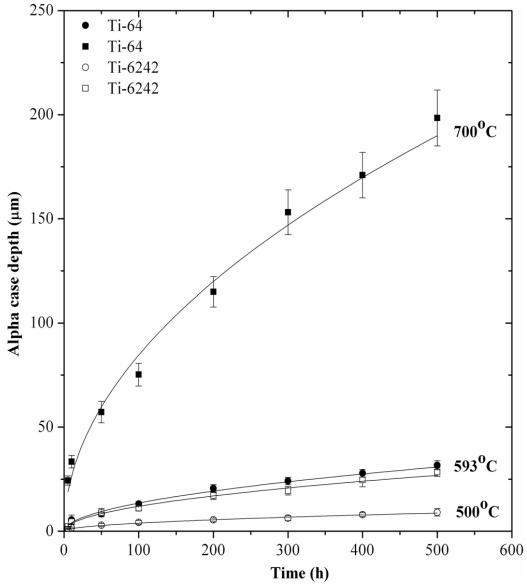

Figure 4. Variation of alpha-case depth in Ti-6242 and Ti-64 as a function of time at different temperatures. Empty data points correspond to Ti-6242 and filled data points are for Ti-64.

From figure 4, it can be seen that the growth of alpha-case in both Ti-6242 and Ti-64 alloys exposed at 593°C for 500 hours follows a parabolic relationship, which can be related to the bulk diffusion. The approximate solution that describe Fick's second law of diffusion is given by $x=\sqrt{(Dt)}$, where x is alpha-case depth, D is the diffusion coefficient (m^2/s), and t is exposure time. Figure 5 shows a log-log plot of alpha-case depth versus exposure time. It shows a linear relationship with R-values 0.995. The exponents from the linear fits are nearly equal to 0.5. Hence, the values for D are calculated from the slope obtained from the best-fit lines. The D calculated here is found to be in the order of 10^{-16} m^2/s for Ti-6242 and Ti-64. From the present study, it can be seen that there is no significant change in the depth of alpha-case and the diffusion of oxygen in Ti-6242 and Ti-64 when

exposed at 593°C up to 500 hours. This shows that there might be no substantial influence of the difference in chemical composition and the microstructure between the two alloys on alpha-case depth. Similar observations were also noted for both the alloys when exposed at 704°C for 24 hours in air [18].

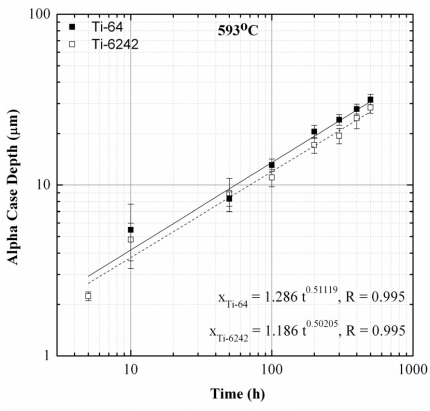

Figure 5. Plot showing the alpha-case depth vs exposure time for Ti-6242 (empty boxes) and Ti-64 (filled boxes) at 593°C up to 500 hours (log- log scale).

Alpha-case is commonly referred to a region enriched with oxygen. It is known that oxygen stabilizes the α phase and increases the strength of titanium by solid solution strengthening [2-3]. Therefore the alpha-case layer is harder than the bulk. Table 3 shows the results obtained from the microhardness measurements on Ti-6242 that are isothermally treated at 593°C; Ti-64 at 593 and 700°C for up to 500 hours. It was found that the hardness values in the alpha-case are higher in magnitude than in the bulk. Figure 6 shows the variation of hardness on the sample held at 700°C for 500 hours from the surface to the bulk. It can be seen that hardness values are gradually decreasing from the surface into the material to approximately 250 µm. From optical measurements on the samples held at 700°C for 500 hours, the depth of alpha-case is approximately measured to be 200 µm (see figure 4 and figure 6). The hardness values decrease with decreasing oxygen content. The difference in depth of alpha-case measured in optical microscope (OM) and indicated by the plateau in the hardness measurements suggests that there are uncertainties in identifying the border between the alpha-case layer and the bulk material in optical microscope after etching.

Table 3. Average hardness values (HV) for Ti-6242 and Ti-64 exposed at different temperatures.

	Ti-6242	Ti-64	
	593°C	593°C	700°C
Alpha case	511 ± 40	412 ± 37	630 ± 34
Bulk	362 ± 23	332 ± 10	300 ± 2.88

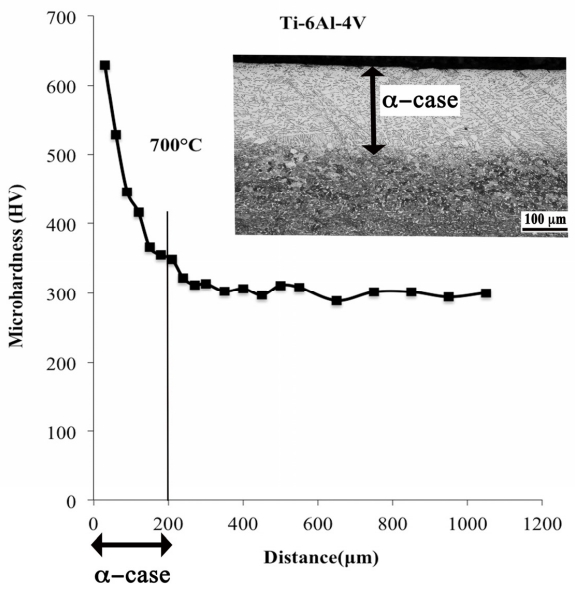

Figure 6. Variation of hardness from the surface to the bulk of the Ti-64 sample exposed to 700°C for 500 hours. An optical micrograph of the corresponding sample showing the alpha-case is also included (the white layer in the micrograph).

4. Conclusions

In the present work, isothermal heat treatments were performed on the Ti-6242 and Ti-64 titanium alloys in ambient air and at atmospheric pressure in order to study the depth of alpha-case. The conclusions are as follows:

1. Alpha-case depth in both alloys increases with temperature and time. Alpha-case growth mainly follows a parabolic relationship at 500 and 593°C in Ti-6242, and at 593°C and 700°C in Ti-64.

2. At 593°C after 500 hours Ti-6242 and Ti-64 have similar values of alpha-case depth (≈ 30 μm).

3. The alpha-case depth in Ti-6242 is 10 μm after 500 hours at 500°C.

4. The alpha-case depth in Ti-64 is 200 μm after 500 hours at 700°C.

5. The microhardness is higher in the alpha-case and decreases into the bulk.

6. A thicker oxide layer forms on Ti-64 then on Ti-6242 when isothermally held at 593°C for 200 hours. This results in a higher weight gain/area for the Ti-64 alloy. The weight gain followed a parabolic relationship.

5. References

[1] Lutjering G and Williams J C 2007 *Titanium* 2nd ed (Berlin, Springer-Verlag)
[2] Leyens C and Peters M 2003 *Titanium and titanium alloys* (Wiley VCH Verlag GmbH, Weinheim) 187
[3] Boyer R R 1996 *Mater. Sci. Eng.* A **213(1-2)** 103
[4] Murray J L and Wriedt H A 1990 Binary alloy phase diagrams Massalski T B ed. (ASM International, Materials Park, Ohio) 2924
[5] Shamblen C E and Redden T K 1968 *Proc. of The Science, Technology, and Application of Titanium*, Jaffee R I and Promisel N E eds, (Pergamon Press, Oxford, United Kingdom) 199
[6] Ruppen J A and McEvily A J 1979 *Fatigue Engg. Mater. Struct.* **2** 63
[7] Bendersky L and Rosen A 1980 *Engg. Fract. Mech.* **13** 111
[8] Shenoy R N, Unnam J and Clark R K 1986 *Oxid. Met.* **26** 105
[9] Fukai H, Iizumi H, Minakawa K-N and Ouchi C 2005 *ISIJ Inter*. **45(1)** 133
[10] Chan K S, Koike M, Johnson B W and Okabe T 2008 *Metall. Mater. Trans.* **39A** 171
[11] AMS 4976 G 2008 Titanium alloy, forgings 6.0Al-2.0Sn-4.0Zr-2.0Mo solution and precipitation heat treated (SAE-AMS/MAM)
[12] AMS 4911 L 2008 Titanium alloy, sheet, strip, and plate 6Al-4V annealed (SAE-AMS/MAM)
[13] Kofstad P 1988 *High temperature corrosion* (Elseiver Applied Science, Essex)
[14] McReynolds K S and Tamirisakandala S 2011 *Metall. Mater. Trans.* A **42A** 1732
[15] Guleryuz H and Cimenoglu H 2009 *J. Alloys Compd.* **472** 241
[16] Frangini S, Mignone A and De Riccardis F 1994 *J. Mater. Sci.* **29** 714
[17] Du H L, Datta P K, Lewis D B and Burnell Gray J S 1994 *Corros. Sci.* **36(4)** 631
[18] Unnam J, Shenoy R N and Clark R K 1984 Effect of alloy chemistry and exposure conditions on the oxidation of titanium Report No. NASA TM-86295 (NASA Technical Memorandum)

Acknowledgments
The authors kindly acknowledge Graduate School of Space Technology and National Aviation Engineering Research Programme (NFFP) for funding the present work through research collaboration with GKN Aerospace Engine Systems, Sweden. We would also like to acknowledge Francois Mattera for assisting in the experiments.

Paper II

Oxidation and alpha–case formation in Ti–6Al–2Sn–4Zr–2Mo alloy

Raghuveer Gaddam[a1*], Birhan Sefer[a], Robert Pederson[a,b], Marta–Lena Antti[a]

[a]Division of Materials Science, Luleå University of Technology, S–97187 Luleå, Sweden

[b]Research and Technology Centre, GKN Aerospace Engine Systems, S–46181 Trollhättan, Sweden

[1] Present Address: AB Sandvik Materials Technology, 8311 11, Sandviken, Sweden

[*]Corresponding author: raghuveer.gaddam@ltu.se, raghuveergaddam@gmail.com,

Mobile: +46(0)722038582

Abstract

Isothermal heat treatments in ambient air were performed on wrought Ti–6Al–2Sn–4Zr–2Mo (Ti–6242) material at 500, 593 and 700 °C for times up to 500 hours. In presence of oxygen at elevated temperatures simultaneous reactions occurred in Ti–6242 alloy, which resulted in formation of an oxide scale and a layer with higher oxygen concentration (termed as alpha–case). Total weight gain analysis showed that there was a transition in oxidation kinetics. At 500 °C, the oxidation kinetics obeyed cubic relationship up to 200 hours and thereafter changed to parabolic at prolonged exposure times. At 593 °C, it followed parabolic relationship. After heat treatment at 700 °C, the oxidation obeyed parabolic relationship up to 200 hours and thereafter changed to linear at prolonged exposure times. The observed transition is believed to be due to the differences observed in the oxide scale. The activation energy for parabolic oxidation was estimated to be 157 kJ/mol. In addition, alpha–case layer was evaluated using optical microscope, electron probe micro analyser and microhardness tester. The thickness of the alpha–case layer was found to be a function of temperature and time, increasing proportionally and following parabolic relationship. The activation energy for formation of alpha–case layer was estimated to be 153 kJ/mol.

Keywords: Titanium alloy, Oxidation, Oxygen Diffusion, Optical Metallography, SEM, EPMA, Alpha–case.

1. Introduction

Oxidation of titanium and its alloys proceeds as two simultaneous reactions: 1) formation of a thin (5 – 10 nm) n–type oxide scale (TiO_2) on the surface and 2) inward diffusion of oxygen into the bulk metal [1,2]. During the first stage of oxidation the oxide scale is protective, whereas after prolonged oxidation time it loses its protective nature and favours higher diffusion of

oxygen through the oxide [2,3]. Additionally, it is known that oxygen has high solid solubility in α–titanium (about 14.5 wt. %) [4]. Therefore, exposure of titanium and its alloys at elevated temperatures above 480 °C to any oxygen containing environment results in simultaneous formation of an oxide (TiO_2) scale and an oxygen enriched layer beneath the scale commonly referred to as alpha–case (α–case). Oxygen, being an α–stabilising element increases the amount of alpha phase [4]. In addition, it also increases the strength of titanium via solid solution hardening [5]. Alpha–case is defined as a continuous, hard and brittle layer formed because of the inward diffusion of oxygen [1,2]. It is formed during elevated temperature processing such as: casting, heat treatments and thermo–mechanical treatments [6–8]. Additionally, prolonged exposure of titanium and its alloys at elevated temperatures i.e. during service could also lead to the formation of alpha–case [1,2]. It is well known that the presence of alpha–case results in reduction of important mechanical properties such as: ductility, fracture toughness and fatigue life [7,9–18]. Therefore, in aerospace applications alpha–case is removed by machining and chemical milling processes [1,2,19], or avoided by using high temperature coatings [1,2,19–24]. The necessity of using these additional processes is one of the reasons for higher manufacturing cost of titanium and its alloys.

The environmental restrictions and economic requirements of future aero engines set higher demands on the efficiency. One way of improving the efficiency is to increase the pressure in the engines. However, by increasing the pressure, the temperature also increases. For titanium parts in jet engines that are used today, exposed to their maximum allowed temperatures (especially if close to the temperatures where alpha–case formation starts) an additional temperature increase could become a serious issue with regard to formation of brittle alpha–case layer. The time that a jet engine spends at maximum temperature during a normal flight is relatively short, but if each such short time is added together the time at the maximum temperature becomes significant, when considering the fact that the jet engines run many thousands of flight hours during their total life. If a small amount of oxygen diffuses a short distance into the titanium alloy component during each such maximum envelope, the accumulative effect of this could eventually lead to formation of critical amount of oxygen to form alpha–case. In order to be able to increase the maximum working temperature of the titanium alloys in jet engines it is important to increase the understanding of the physical phenomena such as oxidation mechanisms, alpha–case formation and its effect on mechanical properties. Many studies have been performed on evaluating the detrimental effect of alpha–case layer on the mechanical properties of titanium alloys [9–18]. However, there is scarcity in the understanding of oxidation mechanisms and formation of alpha–case in high temperature titanium alloys especially for prolonged exposure times that are relevant for service. The most notable studies were by Shamblen et al. [9], Shenoy et al. [12] and McReynolds et al. [25] on Ti–6242 alloy; Leyens et al. [13] on Ti–6Al–2.75Sn–4Zr–0.4Mo–0,45Si (Timetal 1100); Evans et al. [14] and Gurappa [26] on Ti–5.8Al–4Sn–3.5Zr–0.5Mo–0.7Nb–0.35Si–0.06C (Timetal 834); and Jia et al. [27] on Ti–5.8Al–4Sn–3.5Zr–0.4Mo–0.4Nb–1Ta–0.4Si–0.06C (Ti60). In these studies, the thickness of the alpha–case layer was either measured directly using optical microscope (OM) or indirectly by estimating the change in microhardness values from the surface to the bulk, which is a standardised method in the aerospace industry for evaluation of oxygen contamination in titanium alloys [28]. In addition to these methods, electron probe micro analyser (EPMA) is an advanced instrumental technique, which could be used as a complementary method to the more conventional methods in evaluation of the alpha–case thickness. EPMA could probe the gradient of oxygen in very thin layers. It is

shown that EPMA is a reliable method, with capabilities of identifying light elements including oxygen and simultaneously providing the distribution of other alloying elements within the alpha–case layer [15,17,25,29].

The objective of this study was to investigate the effect of temperature and time on the oxidation kinetics and alpha–case formation in wrought Ti–6242 alloy. The selected heat treatment conditions were of interest from manufacturing and application point of view. In addition, EPMA was used on selected samples to characterise the alpha–case layer, estimate the oxygen concentration profiles and compare the thickness of alpha–case layer with those measured by metallographic studies.

2. Experimental methods

The investigated alloy was a commercially available Ti–6242 forging, received in solution and aged condition according to the standard AMS 4976G [30]. Table 1 shows the chemical composition in weight percent.

Table 1. Chemical composition of the Ti–6Al–2Sn–4Zr–2Mo alloy (wt. %) in as received condition.

Al	Sn	Zr	Mo	N	O	C	H	Fe	Si	Y	Ti
6.14	2.02	4.06	1.97	0.003	0.14	0.008	0.0049	0.02	0.08	<0.0004	Bal.

The as–received material has a bimodal microstructure consisting of 65 vol. % transformed β with grain size of about 25 μm and 35 vol. % primary α, with grain size about 18 μm (see Fig. 1(a)). Additionally, the transformed β has a microstructure with α and β lamellas (see Fig. 1(b)).

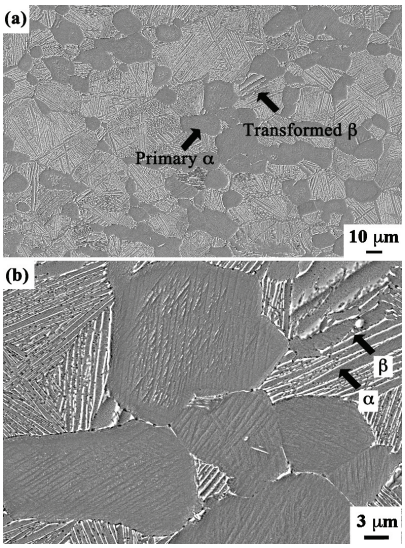

Fig. 1. Microstructure of as–received Ti–6242 alloy.

In total 48 samples with the dimension 10 x 5 x 10 mm were cut using electric discharge machining (EDM) followed by grinding and polishing to remove the recast layer derived from the EDM process. The samples were ultrasonically cleaned in acetone, rinsed with ethanol and dried in hot air. After cleaning, the samples were isothermally heat–treated at 500, 593 and 700 °C up to 500 hours in ambient air. The heat treatments were performed using Nabertherm box furnace (N11/R) and Nabertherm tube furnace (RHTC 80–450/15). After heat treatments the samples were cooled in air. All samples were weighed before and after each heat treatment using analytical microbalance Sartorius Analytic with an accuracy of ± 0.0001 g.

The heat–treated samples were cross–sectioned followed by cleaning in acetone, rinsing with ethanol and drying in hot air. Further, the samples were grinded and polished with colloidal silica using a semiautomatic BUEHLER Phoenix 4000 to achieve a surface roughness of ~ 0.05 µm. The polished sample surfaces were chemically treated by using a two–step etching procedure that reveals the alpha–case layer. The first step involves swabbing the sample surface with Kroll's reagent and the second immersing in Weck's reagent (1 – 3 g NH_4HF_2 in 100 ml distilled water). The thickness of the alpha–case layer was estimated using a Nikon Eclipse OM (model MA200). In total 40 measurements of the alpha–case thickness was conducted on each sample and the measurements were done along the entire perimeter with approximately 500 µm spacing. In addition, the alpha–case layer was characterised using Jeol JXA–8500F Electron Probe Micro Analyser (EPMA), with an accelerating voltage of 10 keV and beam current 20 nA probe. The EPMA measurements were performed using 100 – 300 points from the edge to the bulk with a step width of approximately 0.5–2 µm.

Scanning electron microscope (FEG–SEM, Merlin© from Zeiss) was used to characterise the oxide scale on the samples. Accelerating voltage of 3 kV, probe current of 1 nA and secondary/back–scattered electrons were used. The hardness measurements were performed using MXT–α Vickers microhardness tester from Matsuzawa with a load of 100 g.

3. Results and discussion

3.1.Weight gain analysis

Fig. 2 shows the weight gain per surface area $(\Delta W/A)$ for samples heat–treated at 500, 593 and 700 °C in ambient air up to 500 hours. The weight gain per surface area (mg/cm^2) was estimated by dividing the weight difference of the samples (ΔW) (measured before and after each heat treatment) with their total surface area (A). It can be seen that the $(\Delta W/A)$ ratio is increasing with increasing time and temperature.

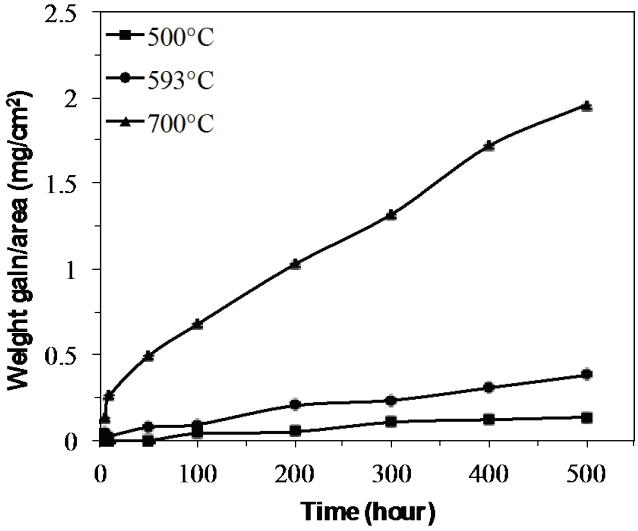

Fig. 2. Weight gain per surface area ($\Delta W/A$) as a function of time for different temperatures.

To analyse the oxidation kinetics, the weight gain per surface area shown in Fig. 2 was fitted using the following power law equation [31,32]:

$$\left(\frac{\Delta W}{A}\right)^n = k_n \cdot t \qquad (1)$$

where k_n is the rate constant, t is the exposure time and n is the reaction index. At a constant temperature, the weight gain per surface area is linear if $n = 1$, parabolic if $n = 2$ and cubic if $n = 3$. The n values are obtained by regression analysis of the log–log plots of weight gain per surface area vs. time from Fig. 2. Table 2 shows the values of the reaction index determined for the oxidation kinetics in Ti–6242 alloy at the investigated temperatures.

Table 2. Rate constants showing the oxidation kinetics in Ti–6242 alloy at tested temperatures.

Temperature (°C)	Time (hours)	*n*
500	5–200	2.96
	300–500	2.08
593	5–500	1.84
700	5–200	1.94
	300–500	1.28

The results show that at 500 °C oxidation kinetics follows cubic relationship up to 200 hours, where for prolonged exposure times (i.e. >200 hours) it obeys parabolic relationship. At 593 °C, oxidation kinetics follows parabolic relationship for all tested times. At 700 °C, oxidation

kinetics follows parabolic relationship up to 200 hours, thereafter it tend to follow linear relationship at prolonged exposure times above 200 hours.

It has been suggested that a transition in the oxidation rate could occur for prolonged exposure times at certain temperatures in titanium and its alloys [31]. Such type of transition has been noted for pure titanium [3,33], Ti–64 alloy [32,34], Timetal 834 alloy [35] and Ti60 alloy [27]. In the present study, the oxidation mostly followed parabolic relationship at the tested temperatures within the time intervals. This is in agreement with the observations made by McReynolds and Tamriskandala [25] for the same alloy when heat–treated at 538–649 °C up to 500 hours. However, in the present study it was noted that there is a transition from parabolic to linear relationship at 700 °C when heat–treated for more than 200 hours.

The parabolic rate constants were estimated in the parabolic regions (see Table 2) by fitting the data shown in Fig. 2 using the following equation [36]:

$$\left(\frac{\Delta W}{A}\right) = \sqrt{k_p \cdot t} + C \qquad (2)$$

where k_p is the parabolic rate constant in $g^2cm^{-4}s^{-1}$ and C is a constant. By plotting $\left(\frac{\Delta W}{A}\right)$ vs $\sqrt{t}$, a straight line is obtained where the slope is equal to k_p. The k_p values along with the C values for all three temperatures are listed in Table 3.

Table 3. Parabolic rate constants for the oxidation of Ti-6242 alloy.

Temperature (°C)	k_p ($g^2cm^{-4}s^{-1}$)
500	$9.34 \cdot 10^{-15}$
593	$7.84 \cdot 10^{-14}$
700	$1.41 \cdot 10^{-12}$

The temperature dependence of k_p was estimated by Arrhenius equation [29]:

$$k = k_0 \cdot \exp\left(-\frac{Q_{ox}}{RT}\right) \qquad (3)$$

where k_o is the frequency factor, Q_{ox} is the activation energy for parabolic oxidation, R is the universal gas constant (8.3143 J/(mol K)) and T is the reaction temperature (K). The Q_{ox} value was estimated to 157 kJ/mol, by plotting the logarithmic values of the rate constant vs. $1/T$, where the slope of the best–fit line is equal to $-Q_{ox}/2.303R$. The activation energy for oxidation reported in this study is similar to the value 151 kJ/mol reported by Shenoy et al. [12].

3.2. Evaluation of alpha–case layer and oxide scale

3.2.1. Optical microscopy

Fig. 3(a) and 3(b) show micrographs of alpha–case for the samples exposed at 700 °C for 500 hours with lower and higher magnification, respectively. After appropriate etching the alpha–case layer appears as a continuous white layer at the surface of the sample, which is observed

along the entire periphery of the cross–section of the sample. Fig. 3(c) shows the oxide scale in higher magnification. X–ray diffraction analysis on the oxide scale for the samples heat–treated at all three temperatures showed formation of rutile (TiO_2) type of oxide [37]. However, energy dispersive spectroscopy analysis showed that the oxide scale also contained elements such as Al, Zr, Sn along with the Ti and O.

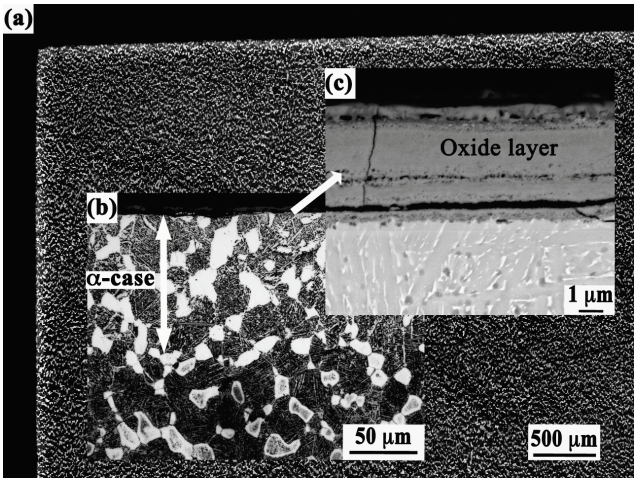

Fig. 3. Micrographs showing (a–b) the alpha–case layer and (c) the oxide scale on the sample heat–treated at 700 °C for 500 hours.

It is known that an increase in weight after oxidation in titanium alloys is because of simultaneous formation of oxide scale and diffusion of oxygen into the bulk (i.e. formation of alpha–case) [12,27,33,34]. Therefore, analysis of the oxide scale has been performed from its physical perspective i.e. thickness, adherence and porosity. Fig. 4 shows SEM micrographs of the oxide scales formed at 500, 593 and 700 °C after 500 hours exposure time.

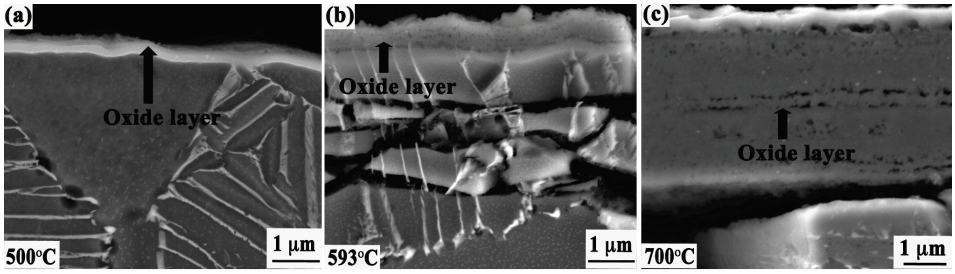

Fig. 4. SEM micrographs showing the oxide scale after 500 hours exposure time (a) 500 °C, (b) 593 °C and (c) 700 °C.

It can be seen that the thickness of the oxide scale increases with temperature and exposure time, ranging from 500 nm to 5 μm. The adherence of the oxide to the metal substrate for the samples

heat–treated at 500 and 593 °C was not affected by increased exposure time (see Fig. 4(a), and 4(b)). In contrast, the oxide scales on the samples heat–treated at 700 °C showed poor adherence to the metal substrate after 500 hours (Fig. 3(c) and Fig. 4(c)). This can be said because spallation was noted in the samples heat–treated at 700 °C at and above 200 hours exposure time. Whereas, this behaviour was not noted in the samples heat–treated at 500 and 593 °C. Coddet et al. [38] observed similar adherence behaviour for commercially pure titanium in the temperature range of 500–700 °C and suggested that the adhesion strength of the oxide scale is relatively high for temperatures below 650 °C, while at 700 °C the oxide adhesion strength decrease significantly. In addition, in the present study it has been noted that there were two types of appearances of the oxide scale i.e. dense and porous. The oxide scale formed on the samples heat–treated at 500 °C was compact and dense, while the oxide scale formed at 593 and 700 °C was porous (see Fig. 4(a), 4(b) and 4(c)). After 500 hours at 700 °C, the thickest and most porous oxide scale was observed (see Fig. 3(c) and Fig. 4(c)). It is thus assumed that spallation of the oxide layer along with increased porosity in the oxide scale could lead to the transition in oxidation kinetics (i.e. parabolic to linear) at 700 °C above 200 hours (see Fig. 2). This could be possible as spallation of the oxide lead to higher rate of interaction between the oxygen and the bulk metal. Cracking beneath the oxide layer has been noted (Fig. 4(b) and 4(c)) and is most likely occurring during polishing because of the hard and brittle alpha–case layer.

Fig. 5 shows representative micrographs of the alpha–case layers formed at 500, 593 and 700 °C after 50 and 500 hours exposure time. Using the optical micrographs, the average thickness of the alpha–case layer was measured and plotted as a function of square root of time for different temperatures (see Fig. 6). It can be seen that the thickness of the alpha–case increased with increasing temperature and time. The maximum measured thickness of the alpha–case layer was about 9, 28 and 108 μm after 500 hours exposure at 500, 593 and 700 °C, respectively.

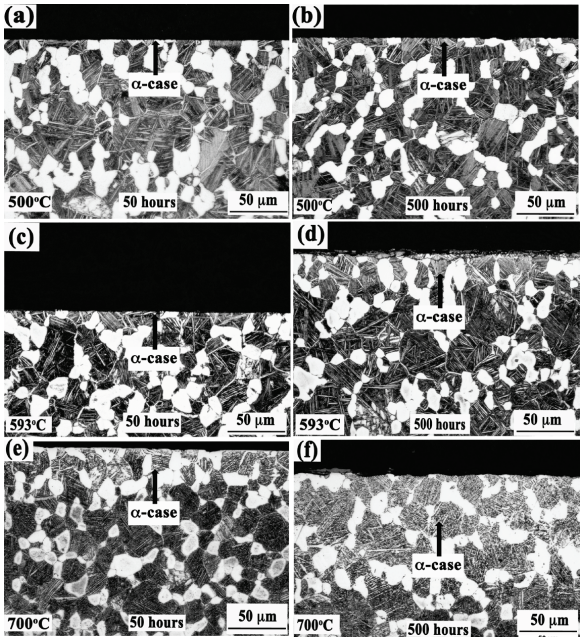

Fig. 5. Optical micrographs showing the alpha–case (bright layer) after 50 and 500 hours at 500, 593 and 700 °C.

It is well known from literature [39] that diffusion follows a parabolic relationship. Therefore it can be assumed that the diffusion of oxygen from the oxide scale to the bulk while forming the alpha–case layer follows a parabolic relationship.

To estimate the diffusion of oxygen the approximate solution of Fick's second law was used [39]:

$$x = \sqrt{Dt} \qquad (4)$$

where x is the alpha–case thickness, D is the diffusion coefficient and t is the exposure time. In Fig. 6 the alpha–case thickness values are plotted versus square root of the heat treatment time. The D values were estimated by linear regression of the data in Fig. 6 (see Table 4).

Table 4. Coefficients for diffusion of oxygen in Ti–6242 alloy at tested temperatures.

Temperature (°C)	D (m^2s^{-1})
500	$3.78 \cdot 10^{-17}$
593	$4.17 \cdot 10^{-16}$
700	$4.87 \cdot 10^{-15}$

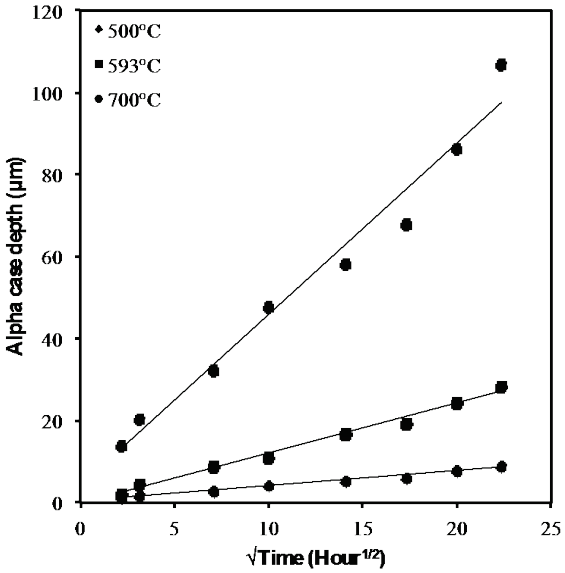

Fig. 6. Alpha–case thickness measured optically as a function of time for different temperatures.

The temperature dependence of D can be estimated by using the Arrhenius type of equation:

$$D = D_0 \exp\left(-\frac{Q_{diffusion}}{RT}\right) \qquad (5)$$

where D_0 is the pre–exponent factor, $Q_{diffusion}$ is the activation energy for diffusion of oxygen in alpha–case layer, R is the universal gas constant (8.3143 J/(mol K)) and T is the temperature (K). The activation energy can be estimated by plotting log D vs. $1/T$ in which the slope of the best fit line is equal to $-Q_{diffusion}/2.303R$. The $Q_{diffusion}$ value was estimated to be 153 kJ/mol, which is in reasonable agreement to the values reported by Shamblen et al. [9] (203 kJ/mol) and Shenoy et al. [12] (167 kJ/mol) for the same alloy. The reported values in the present study are also close to the ones reported for Ti–834 (160 kJ/mol) [14] and Ti–1100 (188 kJ/mol) [13]. In addition, the value is close to the activation energy for interstitial diffusion of oxygen in alpha–titanium (200 kJ/mol) in the temperature range of 250–900 °C [40], which suggests that the alpha–case formed is due to inward diffusion of oxygen in alpha–phase. However, in a study McReynolds et al. [25] reported that $Q_{diffusion}$ = 242 kJ/mol for Ti–6242, which is slightly different from the $Q_{diffusion}$ reported in the present study. The reason for this discrepancy is probably related to differences in microstructure and sensitivity of the etchant used to estimate the alpha–case thickness by OM.

3.2.2. EPMA analysis

Fig. 7(a) shows a SEM micrograph of the area where the EPMA was performed (dark dotted line). The element composition profiles obtained from EPMA in the alpha–case layer are shown

in Fig. 7(b). The fluctuations in some of the element compositions are considered to be due to different concentration of alloying elements in different microstructural constituents.

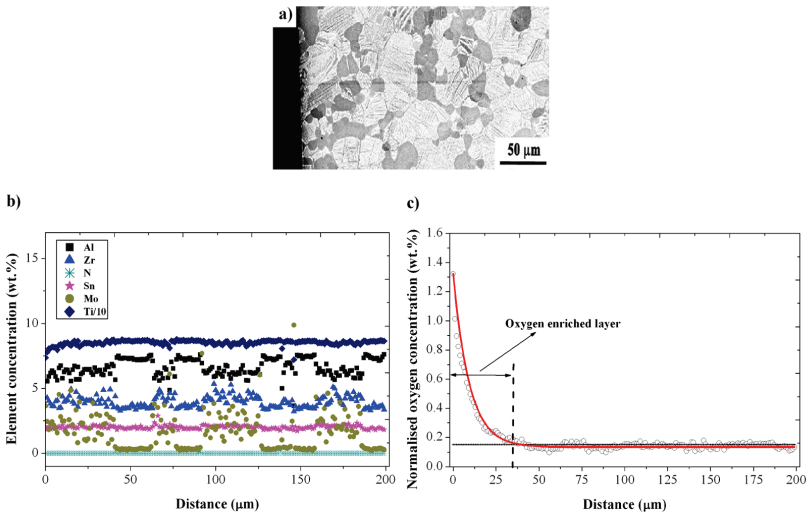

Fig. 7. (a) SEM micrograph with EPMA line area, (b) element concentration profiles and (c) normalised oxygen concentration profile along the thickness of alpha–case for the sample exposed for 500 hours at 593 °C.

It is known that oxygen and nitrogen dissolve in alpha phase of titanium alloys and that they are strong α–stabilisers [1,2]. Both elements have solid solution strengthening effect and have been accounted as main contributors for alpha–case formation [1,19]. From Fig. 7(c) it can be seen that there is a gradient of oxygen in the alpha–case layer. The oxygen concentration is highest at the surface and gradually decreases moving towards the bulk. The amount of nitrogen was below the detection limit of the EPMA instrument, therefore it was not detected.

Fig. 7(c) shows the normalised oxygen concentration profile in wt. % (normalised with respect to the known bulk oxygen concentration i.e. 0.14 wt. %) with respect to the distance (µm) for the sample exposed at 593 °C for 500 hours. The oxygen concentrations (wt. %) measured by EPMA were normalised to the bulk oxygen concentration (wt. %) using the following expression:

$$O_{wt.\%}^{(normalised)} = O_{wt.\%}^{(measured)} \cdot F \qquad (6)$$

where $O_{wt.\%}^{(measured)}$ is the weight percentage of oxygen concentration and $F = \frac{O_{wt.\%}^{(bulk)}}{O_{wt.\%}^{(average)}}$. F represents a quotient from the weight percentage of oxygen concentration in the non–heat–treated sample ($O_{wt.\%}^{(bulk)} = 0.14$) and the average weight percentage of oxygen concentration measured in the bulk for each heat–treated sample ($O_{wt.\%}^{(average)}$). It is important to note that the presented normalised oxygen concentration values are not the absolute oxygen concentration values diffused into the substrate, as there are some difficulties in quantifying the oxygen content

using EPMA. However, these values, showing the distribution of oxygen along the thickness of the samples, can still be used to estimate the alpha–case thickness (i.e. layer enriched with oxygen). For example, the alpha–case thickness for the heat–treated sample at 593 °C for 500 hours is estimated as the depth where the oxygen concentration exceeds 0.14 wt. %, i.e. around 35 µm, see Fig. 7(c).

Fig. 8 shows the normalised oxygen concentration as a function of distance for the samples heat–treated at 500 °C, 593 °C and 700 °C for 50 and 500 hours, respectively. It can be seen that the oxygen concentrations decrease with increasing distance from the surface eventually becoming constant when reaching the bulk (~ 0.14 wt. %). The distance where the oxygen concentration reaches the bulk concentration is defined as the boundary for alpha–case layer.

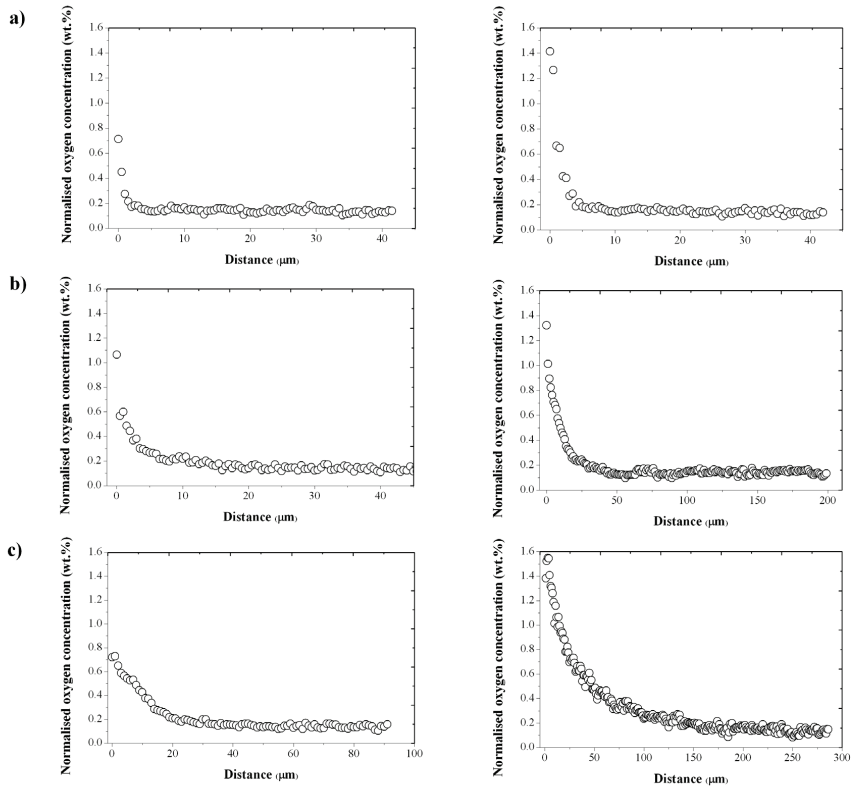

Fig. 8. Normalised oxygen concentration profiles measured by EPMA at (a) 500 °C, (b) 593 °C and (c) 700 °C after 50 and 500 hours.

The oxygen concentration was exponentially decreasing with respect to the distance. Hence, the following modified Arrhenius equation was used to analyse the data:

$$O_{wt.\%\,(x)}^{(normalised)} = O_{wt.\%}^{(bulk)} + O_{wt.\%}^{(surface)} exp(-Ax) \qquad (7)$$

where $O_{wt.\%\,(x)}^{(normalised)}$ is the normalised concentration of oxygen at a certain thickness x, $O_{wt.\%}^{(bulk)} = 0.14$ wt. % is the concentration of oxygen in the non–heat–treated sample, $O_{wt.\%}^{(surface)}$ is the concentration of oxygen at the surface and A is a constant.

The boundary of the alpha–case layer (i.e. oxygen enriched layer) was determined by regression analysis on the normalised oxygen concentration vs. distance data using Eq. (7). The intersection of the fitted lines with the bulk concentration (0.14 wt. %) is assumed to be the boundary of the alpha–case layer (see Fig. 7(c)). The estimated alpha–case thicknesses are given in Table 5.

Table 5. Comparison of the alpha–case thickness values measured using OM and EPMA.

	OM Alpha–case thickness (µm)			EPMA Oxygen enriched layer thickness (µm)		
Time (hour)	**5**	**50**	**500**	**5**	**50**	**500**
Temperature (°C)						
500	1.5 ± 0.2	2.9 ± 0.7	9 ± 1.8	2 ± 1	4 ± 1	9 ± 1
593	2.2 ± 0.3	8.9 ± 1.9	28.4 ± 2	5 ± 1	12 ± 2	35 ± 2
700	14.5 ± 1.5	32.5 ± 1.6	107.2 ± 4.2	17 ± 2	33 ± 4	157 ± 2

3.3. Comparison between alpha–case thickness measured by OM, EPMA and microhardness

Table 5 shows the alpha–case thickness measured by OM and EPMA on the samples heat–treated at 500, 593 and 700 °C for 5, 50 and 500 hours. In Table 5, it can be seen that the alpha–case thickness estimated by the two techniques are comparable for all tested temperatures and times, except for the samples heat–treated at 700 °C for 500 hours. Similar observation was also noted on the samples heat–treated at 700 °C for 300 and 400 hours. In these samples the alpha–case thickness values estimated by EPMA were approximately 50 µm higher than when measured with OM.

Microhardness testing of the samples heat–treated at 593 and 700 °C for 500 hours has been performed as another way to estimate the alpha–case thickness. Oxygen increases the hardness by solid solution strengthening [5] and Rosa et al. [41] suggested that the hardness values are directly proportional to the oxygen concentration present in titanium and its alloys. Fig. 9 shows the alpha–case thicknesses measured using OM, EPMA and microhardness for the sample heat–treated at 700 °C for 500 hours.

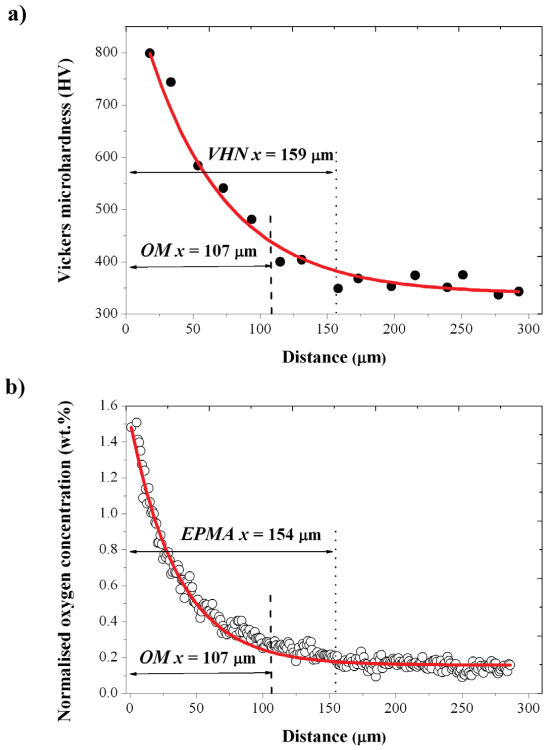

Fig. 9. (a) Microhardness profiles and (b) oxygen concentration profile of the sample heat–treated at 700 °C for 500 hours. The alpha–case thickness estimated by OM is also included in (a) and (b).

From Fig. 9(a), it can be seen that the hardness gradually decreases from the surface towards the bulk, where it becomes constant ($HV_{(bulk)}^{Ti-6242} = 362 \pm 23$). The distance at which the microhardness becomes constant indicates the alpha–case layer boundary. In Fig. 9(a) and 9(b) it can be seen that the alpha–case thickness measured using OM was lower ($OMx = 107 \pm 9\,\mu m$) in comparison to those thicknesses obtained by EPMA concentration profiles and the microhardness testing [($EPMAx = 154 \pm 9\,\mu m$) and ($VHNx = 159\,\mu m$)]. Additionally, it can also be seen that the distance where the hardness is becoming constant is similar to the distance where the oxygen concentration is reaching the bulk concentration.

The microhardness and the EPMA oxygen concentration profiles revealed that the optical evaluation of the alpha–case thickness is accurate for all investigated time/temperature combinations except for the samples heat–treated at 700 °C in the time interval 300–500 hours where there is a deviation from parabolic relationship. The physical explanation for this deviation is not yet clear and further investigation intends to give a reason for this difference.

4. Conclusions

Isothermal heat treatments at 500, 593 and 700 °C for times up to 500 hours were performed on Ti–6242 alloy in ambient air. The conclusions from the present study are as follows:

1. Exposure of the alloy at all tested temperatures resulted in formation of an oxide scale and an alpha–case layer, i.e. a layer enriched with oxygen.
2. Weight gain analysis showed that oxidation mainly follows parabolic relationship, but a change in the oxidation kinetics at certain time intervals was observed at 500 and 700 °C.
3. The activation energy for parabolic oxidation was estimated to be 157 kJ/mol.
4. The activation energy for formation of alpha–case was estimated to be 153 kJ/mol.
5. Evaluation of alpha–case thicknesses with OM, EPMA and microhardness measurements gave similar results for all tested time/temperature combinations, except for the samples heat–treated at 700 °C in the time interval 300–500 hours. OM evaluation underestimated the alpha–case thickness.

Acknowledgments

The authors kindly acknowledge the Graduate School of Space Technology, Joint European Doctoral Programme in Materials Science and Engineering Programme (DocMASE) and Aeronautical Research Engineering Programme (NFFP) for financial support. The authors would like to acknowledge GKN Aerospace Engine Systems Sweden for its support during the research work and Francois Mattera for assisting in performing the heat treatments. We would like to acknowledge Morten Raanes at Norwegian University of Science and Technology, Norway for performing the EPMA measurements and for fruitful discussions in evaluating the results. The authors are grateful to Professor Ragnar Tegman for the discussions of the results.

References

[1] G. Lütjering and J.C. Williams, Titanium, 2nd Edition, in: B. Derby (Ed.), Engineering Materials and Processes, Berlin, Springer, 2007.
[2] C. Leyens, M. Peters, Titanium and Titanium Alloys: Fundamentals and Applications, Weinheim, Wiley–VCH, Weinheim, 2003.
[3] P. Kofstad, J. Less–Common Met. 12 (1967) 449–464.
[4] J.L. Murray, H.A. Wriedt, Binary Alloy Phase Diagrams, Vol. 2, ASM International, Materials Park, Ohio, 1990.
[5] W.R. Tyson, Scr. Met. 3 (12) (1969) 917–921.
[6] S.Y Sung, Y.J Kim, Mater. Sci. Eng. A 405 (2005) 173–177.
[7] K.S. Chan, M. Koike, B.W. Johnson, T. Okabe, Metall. Mater. Trans. A 39 (2008) 171–180.
[8] D. Jordan, Heat Treating Prog. 8 (2008) 45–47.
[9] C.E. Shamblen and T.K. Redden, Air contamination and embrittlement in titanium alloys, in: R.I. Jaffee and N.E. Promisel (Eds.), The Science, Technology and Application of Titanium, Pergamon Press, Oxford, United Kingdom, 1968, pp. 199–208.

[10] J. Ruppen, P. Bhowal, D. Eylon, A.J. McEvily, On the process of subsurface fatigue crack initiation in Ti–6Al–4V, in: J.T. Fong (Ed.), Fatigue mechanisms: Proceedings of an ASTM–NBS–NSF symposium, Kansas city, May 1978, ASTM–STP 675 American Society for Testing and Materials, 1979, pp.47–68.
[11] L. Bendersky, A. Rosen, Eng. Fract. Mech. 13 (1980) 111–118.
[12] R.N. Shenoy, J. Unnam, R.K. Clark, Oxid. Met. 26 (1986) 105–124.
[13] C. Leyens, M. Peters, D. Weinem, W.A. Kaysser, Metall. Mater. Trans. A 27 (1996) 1709–1717.
[14] R.W. Evans, R.J. Hull, B. Wilshire, J. Mater. Process. Tech. 56 (1996) 492–501.
[15] H. Fukai, H. Iizumi, K. Minakawa, C. Ouchi, ISIJ Int. 45 (2005) 133–141.
[16] R. Dobeson, N. Petrazoller, M. Dargusch, S. McDonald, Mater. Sci. Eng. A 528 (2011) 3925–3929.
[17] A.L. Pilchak, W.J. Porter, R. John, J. Mater. Sci. 47 (2012) 7235–7253.
[18] R. Gaddam, M.L. Antti, R. Pederson, Mater. Sci. Eng. A 599 (2014) 51–56.
[19] M.J. Donachie, Titanium – A Technical Guide, 2nd Edition, ASM International, 2000.
[20] S. Fujishiro, D. Eylon, Thin Solid Films 54 (1978) 309–315.
[21] R.K. Clark, J. Unnam, K.E. Wiedemann, Oxid. Met. 29 (1988) 255–269.
[22] C. Leyens, M. Peters, W.A. Kaysser, Surf. Coat. Tech. 94–95 (1997) 34–40.
[23] I. Gurrappa, A.K. Gogia, Mater. Sci. Technol. 17 (2001) 581–587.
[24] J.K. Sahu, D.K. Das, T.K. Nandy, D. Mandal, V. Rajinikanth, J. Swaminathan, A.K. Ray, Mater. Sci. Eng. A 530 (2011) 664–668.
[25] K.S. McReynolds, S. Tamirisakandala, Metall. Mater. Trans. A 42 (2011) 1732–1736.
[26] I. Gurrappa, J. Alloys Compd. 389 (2005) 190–197.
[27] W. Jia, W. Zeng, X. Zhang, Y. Zhou, J. Liu, Q. Wang, J. Mater. Sci. 46 (2011) 1351–1358.
[28] Aerospace series–Test methods–Titanium and titanium alloys–Part 009–Determination of surface contamination (SS–EN 2003–009:2007), Swedish Standards Institute, 2007.
[29] R. H. Olsen, Metallography 3 (1970) 183–195.
[30] AMS 4976 G, Titanium alloy, forgings 6.0Al–2.0Sn–4.0Zr–2.0Mo solution and precipitation heat treated (SAE–AMS/MAM), 2008.
[31] P. Kofstad, High Temperature Corrosion, Springer, 1988.
[32] S. Frangini, A. Mignone, F. De Riccardis, J. Mater. Sci. 29 (1994) 714–720.
[33] J. Unnam, R. N. Shenoy, R. K. Clark, Oxid. Met. 26 (3/4) (1986) 231–252.
[34] H. Guleryuz, H. Cimenoglu, J. Alloy Compd. 472 (2009) 241–246.
[35] K.V.S. Srinadh, V. Singh, Bull. Mater. Sci. 27(4) (2004) 347–354.
[36] B. Pieraggi, Oxid. Met. 27 (3/4) (1987) 177–185.
[37] B. Sefer, R. Gaddam, R. Pederson, A. Mateo, M.L. Antti, To be submitted.
[38] C. Coddet, A.M. Craze, G. Beranger, J. Mater. Sci. 22 (1987) 2969–2974.
[39] H. Mehrer, Diffusion in Solid Metals and Alloys, Volume 26, Group III: Cryst. Solid State Phys. Springer Verlag Berlin, Heidelberg, New York, 1990, pp. 2–7.
[40] Z. Liu, G. Welsch, Metall. Trans. A, 19A (1988) 1121–1125.
[41] C.J. Rosa, Metall. Mater. Trans. A 1 (1970) 2517–2522.

Paper III

Characterization of the oxide scale and alpha–case layer in Ti–6Al–4V and Ti–6Al–2Sn–4Zr–2Mo in the temperature range 500–700 °C

Birhan Sefer[1,3*], Raghuveer Gaddam[1], Robert Pederson[1,2], Antonio Mateo[3], Marta–Lena Antti[1]

[1]Division of Materials Science, Luleå University of Technology, S–97187 Luleå, Sweden

[2]Research and Technology Centre, GKN Aerospace Engine Systems, S–46181 Trollhättan, Sweden

[3]Department of Materials Science, Universitat Politècnica de Catalunya, Av. Diagonal 647, Barcelona, Spain

* Corresponding author: birhan.sefer@ltu.se, Ph: +46(0)920 492358

Abstract

Isothermal heat treatments of Ti–6Al–4V (Ti–64) and Ti–6Al–2Sn–4Zr–2Mo (Ti–6242) alloys in air at 500, 593 and 700 ºC for times up to 500 hours have been performed. The oxide scale and alpha–case layer formed were characterized for both alloys by means of metallographic and microscopy techniques. Faster oxidation in Ti–64 than in Ti–6242 at all tested temperatures was observed. The oxide scale in the two alloys consisted of rutile TiO_2 along with Al_2O_3 layers closest to the air/oxide interface. A multi–layered structure of the oxide scale in Ti–64 was observed, but not in Ti–6242. The thickness of the alpha–case layer was found to be a function of temperature and time, obeying parabolic behaviour in both alloys. The activation energy for oxygen diffusion was calculated to be 215 kJ/mol and 153 kJ/mol, for Ti–64 and Ti–6242, respectively. Electron probe micro analyser (EPMA) showed a gradual decrease of the oxygen concentration from the oxide/metal interface moving to the center of the samples in the two alloys. The oxygen concentration profiles were used to estimate the alpha–case thicknesses in both alloys and they showed good agreement with the optically measured values for all temperatures and times, except at 700 ºC for 500 hours in Ti–6242.

Keywords: Titanium alloys, Oxidation, Oxygen diffusion, Microscopy, Oxide scale, Alpha–case, XRD, SEM, EPMA.

1. Introduction

Ti–6Al–4V (Ti–64) and Ti–6Al–2Sn–4Zr–2Mo (Ti–6242) are commercially available titanium (Ti) alloys. Both alloys are commonly used for manufacturing components in aero engines because of their high strength and low density [1–4]. However, a common drawback of these alloys is their limited maximum service temperature, which is about 300 and 450 ºC, for Ti–64 and Ti–6242, respectively [5]. This limitation is due to the reduction of the mechanical properties of the alloys when they are exposed to elevated temperatures (> 500 ºC) in oxygen containing environments. In such conditions, the alloys rapidly oxidize. The overall oxidation reaction includes two processes running simultaneously: 1) formation of an

oxide scale (TiO_2) and 2) diffusion of oxygen into the bulk metal [6,7]. The process of oxygen diffusion into the bulk metal is accountable for the formation of an oxygen enriched layer beneath the oxide scale called alpha–case layer [1,2,4]. The alpha–case layer is a continuous, hard and brittle layer that has detrimental effect on several important mechanical properties of the titanium alloys such as ductility, fracture toughness and fatigue life [6,8–13]. Alpha–case is developed during manufacturing processes of Ti alloys such as casting, heat treatments and thermo–mechanical treatments [8,14,15], but it might also develop while the aero engine operate at elevated temperatures and oxygen environments [1,2,4]. Therefore, in aerospace applications the formation of alpha–case is either prevented by using high temperature coatings [16–18] or is removed by machining or chemical milling [1,2,4]. Concepts of future engines indicate higher maximum working temperature in compressor sections where titanium alloys are normally used. Even though the exposure time at peak temperature is short during one flight, there is an apparent risk of accumulation of excess oxygen after a large number of flights.

Numerous reports can be found in the literature that are focused on studying the oxidation behaviour of different Ti alloys in air at elevated temperatures [6,7,9,19–28]. In all of these studies the oxide scale and the alpha–case layer were analysed and characterized by using metallographic techniques. One of the conventional methods used for evaluating the alpha–case layer thickness is measuring the hardness along the cross–section of the samples because the increase of oxygen content in Ti alloys is proportional to the increase of the hardness [29]. However, the alpha–case layer thickness might also be evaluated by using electron probe micro analyser (EPMA), which serves as a complementary method to the more conventional ones. EPMA provides identification of the light elements such as oxygen and simultaneously follows the distribution of other alloying elements within the alpha–case layer [11,25]. Despite that many Ti alloys have been studied there is still lack of understanding of the oxidation mechanisms and their relation to the formation of the oxide scale and the alpha–case layer. Moreover, there were not found any comparative studies in the literature on the oxide scale and the alpha–case formation in Ti–64 and Ti–6242 alloys. It is believed that such comparative study would provide better understanding of the oxidation mechanisms and the formation of oxide scale and alpha–case layer in various titanium alloys.

The objective of the present study was to investigate, characterize and compare the oxide scale and the alpha–case layer formed in Ti–64 and Ti–6242 after isothermal heat treatment in air at elevated temperatures.

2. Materials and methods

The investigated materials were commercially available Ti–6Al–4V (Ti–64) and Ti–6Al–2Sn–4Zr–2Mo (Ti–6242). The chemical compositions in weight percentage for each alloy in as–received condition are shown in Table 1.

Table 1. Chemical composition in wt. % of Ti–6Al–4V and Ti–6Al–2Sn–4Zr–2Mo.

	Al	V	Sn	Zr	Mo	N	O	C	H	Fe	Si	Y	Ti
Ti–64	6.75	4.5	–	–	–	0.05	0.20	0.08	0.015	0.3	–	–	Bal.
Ti–6242	6.14	–	2.02	4.06	1.97	0.003	0.14	0.008	0.0049	0.02	0.08	<0.0004	Bal.

Ti–64 is an α+β alloy obtained in plate form according to AMS 4911L [30] and consists of an equiaxed microstructure with primary α grains and elongated α needles in transformed β (Figure 1(a)). Ti–6242 is a near–α alloy, solution and precipitation heat–treated, obtained in forged condition according to AMS 4976G [31], with a bi–modal microstructure, composed

of primary α grains and transformed β, where the transformed β consists of α and β lamellas (Figure 1(b)).

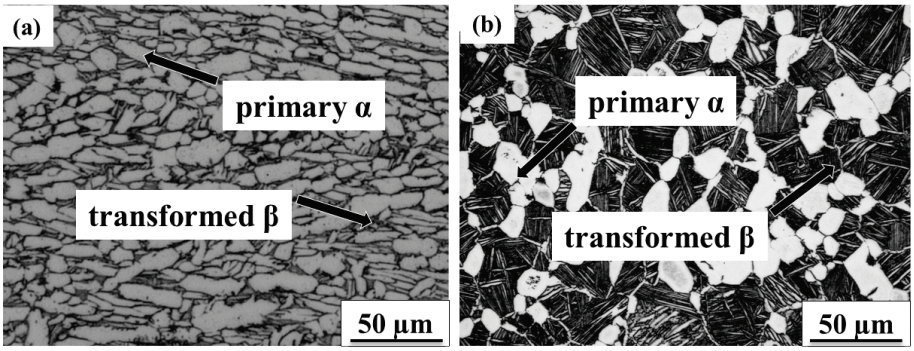

Fig. 1. Microstructure of as–received Ti–64 and Ti–6242 alloys.

Before heat treatment all samples were sectioned to dimensions of 10 x 5 x 10 mm using an Electro Discharge Machine (EDM). The cutting of the samples was followed by grinding and polishing to remove the recast layer on the sample surfaces derived from the EDM process. The samples were ultrasonically cleaned in technical acetone, rinsed with ethanol and dried in hot air. After cleaning, all the samples were isothermally heat–treated at 500, 593 and 700 ºC up to 500 hours in atmospheric air. After heat treatments, the samples were cooled in air. All samples were weighed before and after each heat treatment using an analytical microbalance with an accuracy of ± 0.0001 g.

The heat–treated samples were cross–sectioned, followed by cleaning in acetone, rinsing with ethanol and dried in hot air. Further, the samples were grinded and polished with colloidal silica to achieve a surface roughness of ~ 0.05 µm. The polished sample surfaces were chemically treated by using a two–step etching procedure that reveals the alpha–case layer. The first step involves swabbing the sample surface with Kroll's reagent and the second step immersing in Weck's reagent (1–3 g NH_4HF_2 in 100 ml distilled water). The alpha–case layer was estimated by using an optical microscope. At least 60 measurements of the alpha–case thickness were conducted in each sample, along the entire perimeter with approximately 500 µm spacing. In addition, the alpha–case layer was characterised using Electron Probe Micro Analyser (EPMA), with an accelerating voltage of 10 keV and beam current 20 nA probe. The EPMA measurements were performed using 50–300 points from the edge to the bulk with a step width of approximately 0.5–1 µm.

Scanning electron microscopes (SEM), JEOL JSM–6460LV and MERLIN from Carl Zeiss were used to characterise the oxide scale on the samples. Accelerating voltage of 3–25 kV and probe current of 1 nA–84 µA were used. Secondary and back–scattered electrons were used.

An X–ray diffractometer (XRD), model PANalytical Empyrean equipped with a PIXcel3D detector was used to record the XRD pattern of the oxide scale. The X–ray tube was an Empyrean Cu LFF HR and scans were performed with 0.026° step size and in the 2–theta range of 20°–80°.

3. Results and Discussion

3.1 Weight gain analysis

Figure 2 shows the weight gain per surface area for Ti–64 and Ti–6242 alloys after isothermal heat treatment in air at 500, 593 and 700 °C up to 500 hours. The weight gain per surface area (mg/cm^2) was computed by dividing the weight difference of the samples (ΔW) (before and after heat treatment) with the total surface area of the samples (A).

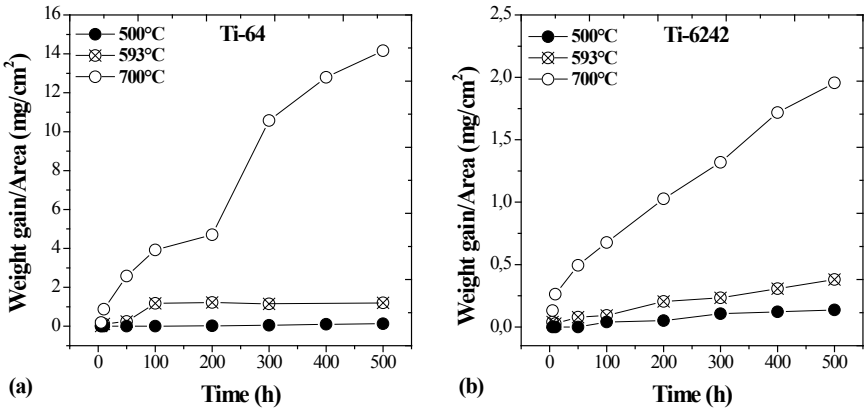

Fig. 2. Weight gain per surface area *vs.* time for (a) Ti–64 and (b) Ti–6242 at 500 °C, 593 °C and 700 °C up to 500 hours (note the differences in scales).

From Figure 2 it can be seen that at 500 ºC both alloys did not experience significant weight gain compared with the weight gain obtained from the heat treatments at 593 and 700 ºC. At 593 and 700 °C, the measured weight gain was higher in Ti–64 than in Ti–6242. This result indicates that at these temperatures Ti–64 is oxidizing faster than Ti–6242. Note that the weight gain at 593 °C for Ti–64 increased until 100 hours and thereafter remained unaffected even for the longest exposure time. In contrast, at 593 and 700 °C Ti–6242 experienced continuous increase of the weight gain with respect to exposure time. Similar to Ti–6242, Ti–64 at 700 °C showed continuous increase of the weight gain, but only for exposure times up to 200 hours. For exposure times longer than 200 hours the initial weight gain behaviour was changed. Similar change of the weight gain in Ti–64 alloy at 700 °C after prolonged exposure times has been reported by Frangini et al. [20] and Guleryuz and Cimenoglu [24].

3.2 Oxide scale analysis

Figure 3 shows representative XRD patterns of the oxide scale formed in Ti–64 and Ti–6242 after heat treatment at 700 °C for 500 hours. The analysis of the XRD patterns revealed that the oxide scales in both alloys mainly consist of rutile type of TiO_2. Additionally, peaks for α and β– titanium phase have been identified in the XRD pattern of the oxide scale in Ti–6242, which is due to the penetration of the X–rays beyond the oxide scale through the metal substrate, which in this alloy was thin (< 5 μm). These results are in good agreement with those reported in the literature for different titanium alloys [26,32–34].

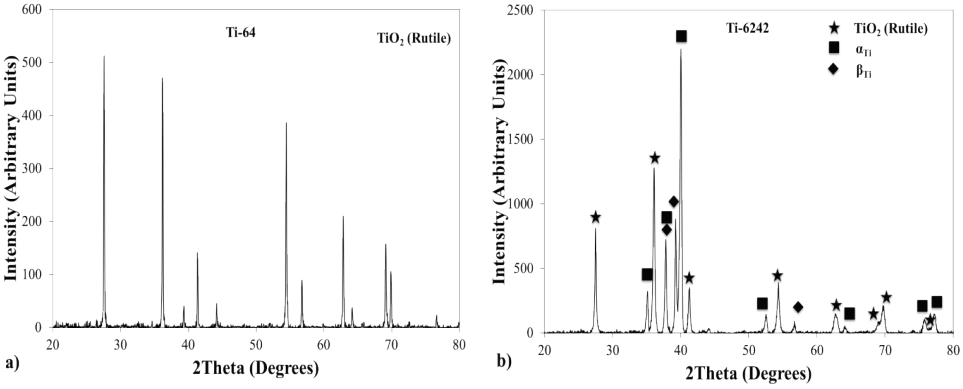

Fig. 3. XRD patterns of the oxide scales in (a) Ti–64 and (b) Ti–6242 alloy formed after heat treatment at 700°C for 500 hours.

Figure 4 presents SEM micrographs of the oxide scales of Ti–64 and Ti–6242 formed after heat treatments at 700 °C for 5 and 500 hours, respectively. From Figure 4, it can be seen that the oxide scale exhibited two types of morphologies (i.e. dense and porous), which are dependent on heating temperature and exposure time. Larger thickness of the oxide scales in Ti–64 than in Ti–6242 was observed, at all tested temperatures and times. This observation confirms the faster oxidation kinetics in Ti–64 than in Ti–6242 alloy (see Figure 2). For the two alloys heat treated at 500 °C, adherent and uniform scales with dense nature and thicknesses less than 1 μm were observed even after 500 hours exposure time. Similar morphology of the oxide scales was observed in both alloys for the heat treatments performed at 593 °C and for all the exposure times. However, the heat treatment for both alloys at 700 °C resulted in formation of dense and uniform oxide scales only in the samples heat–treated until 100 hours, whereas for prolonged exposure times porous oxide scales were observed (see Figure 4(c) and (d)). The porous morphology of the oxide scales allows an increase of the oxygen partial pressure close to the oxide/metal interface, which further facilitates the oxidation kinetics [19]. It is believed that the porous morphology of the oxide scale is the reason for the observed change in the weight gain in Ti–64 heat–treated at 700 °C and after 200 hours exposure time (see Figure 2(a)).

At 700 °C spallation of the oxide scale was observed for Ti–64 and Ti–6242, after 50 and 200 hours exposure times, respectively. The spallation at earlier time interval for Ti–64 alloy indicates that this alloy is less oxidation resistant at higher temperatures than Ti–6242. Also, it is important to note that spallation was more severe in Ti–64 than in Ti–6242. The oxide scale on Ti–64 spalled off from the metal substrate after air cooling as thin and brittle flakes with maximum average thickness of about 120 μm for the longest exposure time. Such flaking of the oxide scales was not observed in Ti–6242, where the spallation manifested more like a loss of small particles from the metal substrate. The more severe spallation of the oxide scale in Ti–64 is considered to be due to thermal stresses formed during cooling and the mismatch of the thermal expansion coefficients between the oxide scale ($\alpha(TiO_2) = 8.2 \cdot 10^{-6}\ K^{-1}$) and the alloy ($\alpha$(Ti–64) = $10–12 \cdot 10^{-6}\ K^{-1}$), which is not the case for Ti–6242 (α(Ti–6242) = $8.1 \cdot 10^{-6}\ K^{-1}$).

SEM–EDS mapping on the oxides scale shown in Figure 4 revealed multi–layered structure in Ti–64 consisting mainly of TiO_2 and Al_2O_3 layers arranged in ordered pattern at certain distances (see Figure 4(c)). Additionally, in the oxide scale vanadium (V) and iron (Fe) were

probed. In contrary, such morphology was absent in Ti–6242 and the oxide scale consisted mainly of TiO_2 doped with aluminium (Al), zirconium (Zr) and tin (Sn) together with a uniform layer of Al_2O_3 on top of the scale (see Figure 4(d)). It is important to note that no molybdenum (Mo) was detected in the oxide scale. This indicates that both alloys, even if exposed to the same testing conditions (temperature, time and environment), exhibit different oxidation mechanisms and kinetics. Apparently, the differences in the alloying elements in the alloys have significant impact on the oxidation mechanism and kinetics. It has been reported earlier that Al additions reduce the oxygen embrittlement in Ti–Al alloys oxidized up to 700 °C by forming alumina layer on top of the oxide scale (see Figure 4(c)) [35]. Du et al. [19] have reported that the oxidation in Ti–64 at elevated temperatures depends on: 1) the activity of titanium and aluminium and 2) the oxygen partial pressure in the oxide scale. Both are subjected to changes with respect to exposure time due to the scale porosity and cracking. Additionally, vanadium suppresses the formation of protective alumina layer on top of the oxide scale by reducing the activity of aluminium, thereby stimulating faster oxidation kinetics [36–38]. In contrary, no information was found in the literature for the effect of the alloying elements on the oxidation in Ti–6242 alloy. However, the data for the standard enthalpy of oxides formation ($\Delta_f H°$/kJ/mol) for Al, Sn, Zr and Mo oxides at 700 °C revealed that all elements are forming thermodynamically stable oxides [39]. Moreover, it is well known that Mo could form volatile oxides such as MoO_3 with melting point at 795 °C, when present as alloying element in alloys. The vapour pressure of MoO_3 at 700 °C is relatively high (4.69×10^{-4} atm.) and therefore could be expected to evaporate from the surface of the oxide scale [40]. The evaporation of the low melting oxide would cause physical defects in the oxide scale and thereby it is reasonable to associate this phenomenon to the pores formation in the Ti–6242 alloy. Additional support for the possible evaporation of molybdenum oxides from the scales and its accountability to the pore formation phenomena is that Mo was not detected with the SEM–EDS mapping in the scale of Ti–6242 alloy. Moreover, since V also has ability to form volatile oxide species i.e. V_2O_5 with melting point 674 °C [41], it is believed that V in similar manner as MoO_3 could be formed and thus be the main reason for the forming of porous structure in the Ti–64 oxide scale even though V was probed with EDS in the oxide scale.

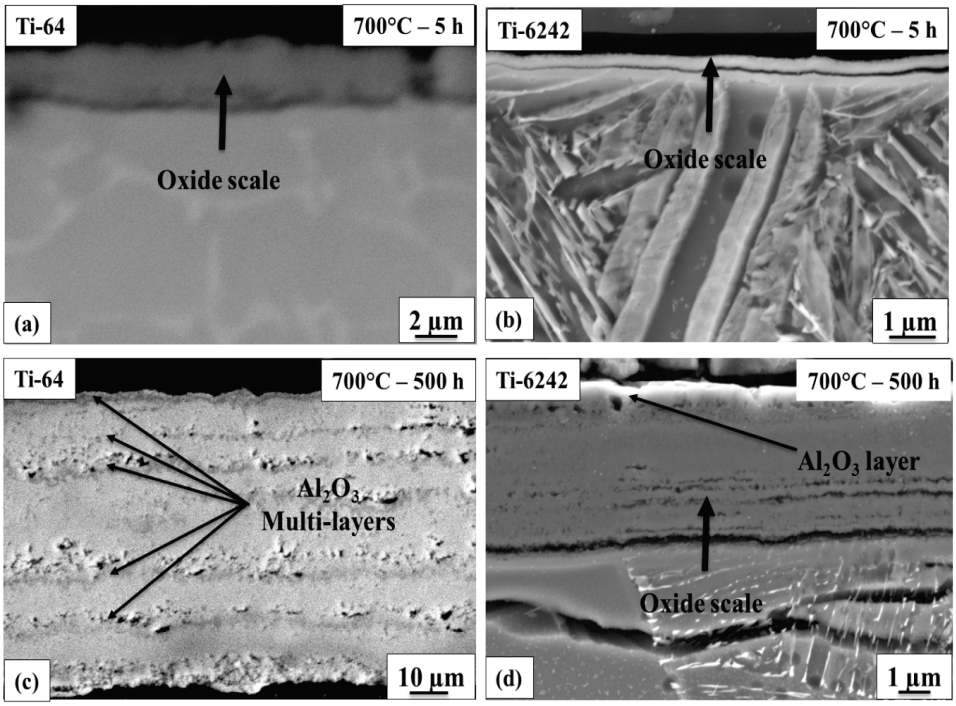

Fig. 4. Oxide scales of Ti–64 and Ti–6242 alloy after 5 and 500 hours heat treatment at 700 °C.

3.3 Alpha–case analysis

3.3.1 Light optical microscopy

Figure 5 shows representative optical micrographs of the alpha–case layers formed in Ti–64 and Ti–6242 after heat treatment at 700 ºC for 500 hours. The two–step etching procedure reveals the alpha–case layer as a continuous white layer at the edge of the sample. Such bright layer has been observed along the entire periphery of the cross–section of all samples and for both alloys. Using the optical micrographs, the average thickness of the alpha–case layer was measured. After 500 hours at 500, 593 and 700 ºC the alpha–case layer in Ti–64 was about 6.5, 32 and 198 µm, whereas for Ti–6242 about 9, 28 and 108 µm, respectively.

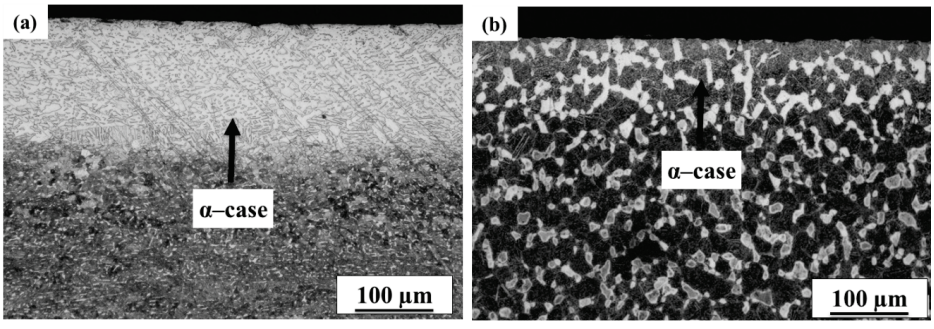

Fig. 5. Optical micrographs of alpha–case layer in (a) Ti–64 and (b) Ti–6242, after heat treatment at 700 ºC and 500 hours.

The diffusion coefficients of oxygen (D) were estimated by using Fick's second law:

$$x = \sqrt{Dt} \qquad (1)$$

where x is the alpha–case thickness, D is the diffusion coefficient and t is the exposure time. Figure 6 shows alpha–case thickness vs. square root of time plots, for Ti–64 and Ti–6242. The plots from Figure 6 were used to derive the D values from the slopes of the fitted linear regression straight lines. It can be seen that the thickness of the alpha–case layer increased with increasing temperature and time in both alloys. In Table 2 the calculated D values for the alloys at all three temperatures are listed. It is important to note that the large error bars for the alpha–case thickness in both alloys for the heat treatment at 700 ºC are due to the spallation of the oxide scales, which was not homogeneous along the periphery of the samples, inaccuracies in estimating the alpha–case thickness optically due to the microstructural differences in both alloys and the sensitivity of the used etchant to reveal the alpha–case boundary.

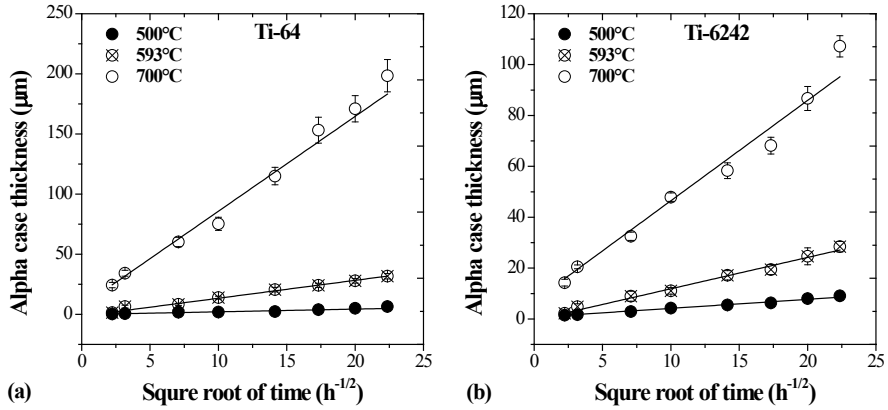

Fig. 6. Alpha–case thickness as function of time in (a) Ti–64 and (b) Ti–6242 at 500, 593 and 700 ºC.

Table 2. Diffusion coefficients for Ti–64 and Ti–6242 calculated from Eq. 1.

	Diffusion coefficient D (m^2/s)	
T (°C)	Ti–64	Ti–6242
500	$2.08 \cdot 10^{-17}$	$3.78 \cdot 10^{-17}$
593	$5.66 \cdot 10^{-16}$	$4.17 \cdot 10^{-16}$
700	$2.03 \cdot 10^{-14}$	$4.87 \cdot 10^{-15}$

The temperature dependence of D was estimated by using an Arrhenius type of equation:

$$D = D_0 \exp\left(-\frac{Q}{RT}\right) \qquad (2)$$

where D_0 is the pre–exponent factor, Q is the activation energy for diffusion of oxygen, R is the universal gas constant (8.3143 J/(mol K)) and T is the temperature (K). The activation energy has been estimated by plotting log D vs. $1/T$ (see Figure 7) in which the slope of the best fit line is equal to $-Q/2.303R$. The Q value was estimated to be 215 kJ/mol and 153 kJ/mol, for Ti–64 and Ti–6242, respectively. The reported Q values are close to those

reported for Ti–64 by Frangini et al. (200 kJ/mol) [20], Guleryuz and Cimenoglu (202 kJ/mol) [24] and for Ti–6242 by Shenoy et al. (167 kJ/mol) [6]. Additionally, the Q values presented in this study are near to the activation energy for interstitial diffusion of oxygen in α–titanium reported by Chaze and Codet (214 kJ/mol) [35] and other alloys used in aerospace industry such as TIMETAL 1100 (188 kJ/mol for bimodal and 191 kJ/mol for lamellar microstructure) by Leyens et al. [32] and IMI 834 (160 kJ/mol) by Evans et al. [11].

The Arrhenius plot shown in Figure 7 indicates that Ti–64 and Ti–6242 alloys exhibit different oxygen bulk diffusion rates at temperatures below and above 593 ºC. It is known that oxygen interstitial diffusion in the β phase of titanium proceeds at higher rates than in α phase [42]. Moreover, lattice diffusion is more favourable at higher temperatures. However, the grain boundary diffusion could not be excluded, because it is considerably faster than the lattice diffusion and it is a common diffusion mechanism at low temperatures [43].

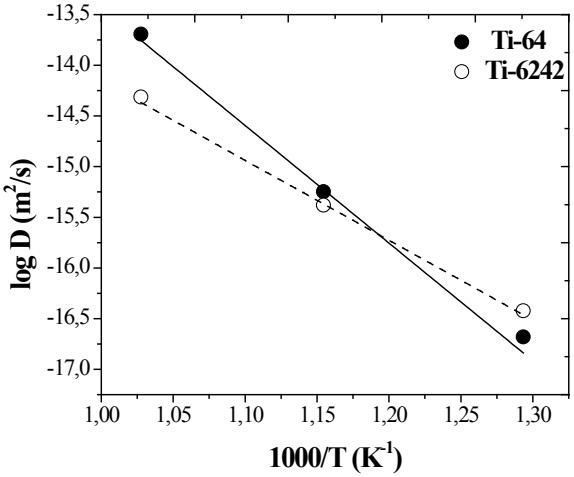

Fig. 7. Arrhenius plot of the diffusion of oxygen in Ti–64 and Ti–6242 alloy.

From the optical micrographs of as–received alloys shown in Figure 1 it can be seen that Ti–6242 alloy has higher amount of α/β interfaces per unit area than Ti–64. This implies that at low temperatures (i.e. 500 ºC) grain boundary and interstitial diffusion in the β phase are more likely than diffusion in α phase. This explains the slightly higher measured alpha–case thicknesses in Ti–6242 than in Ti–64 at 500 ºC (see Figure 8(a)). On the other hand, for higher temperatures (≥593 ºC) the lattice diffusion in α phase becomes more favourable. As shown in Figure 8 (b) the alpha–case thickness values at 593 ºC in Ti–64 start to overcome the corresponding thickness values in Ti–6242 and finally, at 700 ºC, it reaches almost twice the thickness measured in Ti–6242 alloy (see Figure 8(c)). Pitt and Ramulu [43] studied the effect of coarse and fine microstructures of Ti–64 on oxidation and diffusion rates, finding a similar behaviour of the alpha–case thickness with respect to microstructure as in the present study.

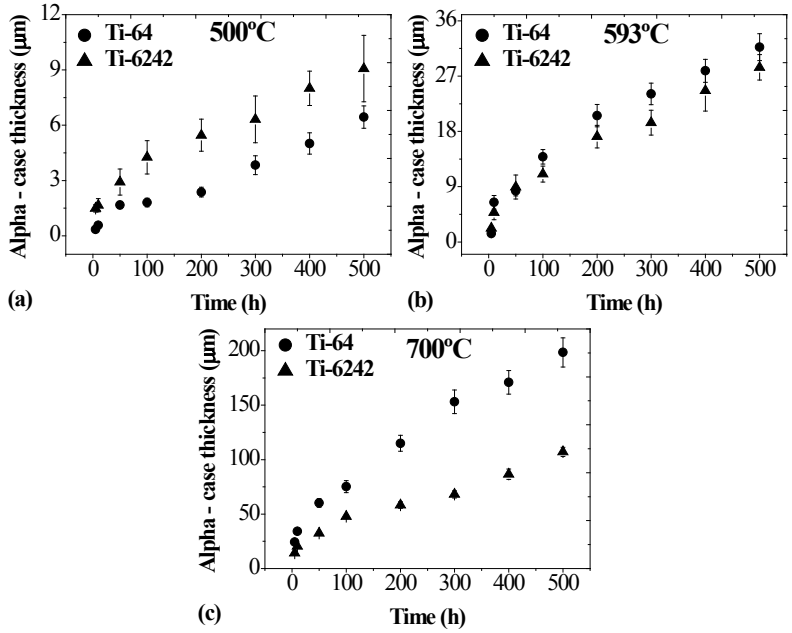

Fig. 8. Comparison of the optically measured alpha–case thickness as function of time in Ti–64 and Ti–6242 at (a) 500, (b) 593 and (c) 700 ºC.

3.3.2 EPMA analysis

Figure 9 (a) and (b) show the EPMA composition profiles of Ti–64 and Ti–6242 measured after of heat treatment at 593 ºC for 500 hours along the thickness of the alpha–case layer. The EPMA element composition profile depicts the microstructure of the alloys. As shown in Figure 9 (a) and (b) each line represent the concentration and correspond to the distribution of the elements present in the alloys. Fluctuations of the elements concentrations are considered to be due to different concentration of the alloying elements in every microstructural constituent. Oxygen and nitrogen readily dissolve in alpha phase of Ti alloys, thereby conducting its stabilization [1–3]. Additionally, both elements have solid solution strengthening effect and therefore, they are considered as main contributors for alpha–case formation [1,3]. In the present study nitrogen was not detected by the EPMA measurements, because its concentration was below the detection limit of the EMPA instrument.

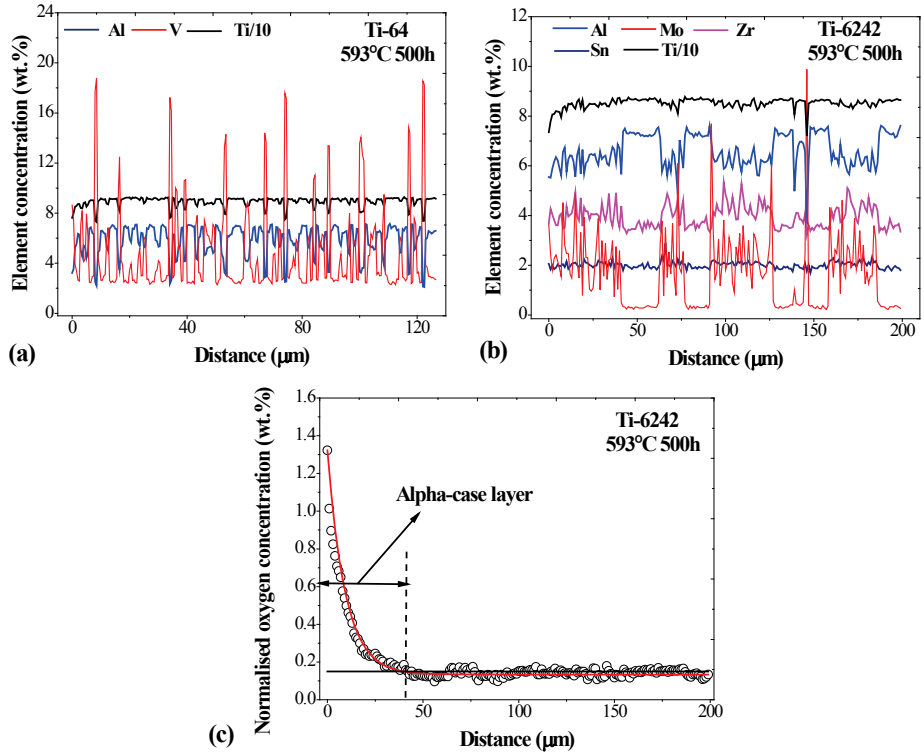

Fig. 9. Composition profiles measured with EPMA for (a) Ti–64 and (b) Ti–6242 alloy and (c) normalized oxygen concentration profile along the alpha–case layer in Ti–6242.

Figure 9 (c) shows a representative normalized oxygen concentration profile, as a function of the distance measured by the EPMA instrument after heat treatment at 593 ºC for 500 hours in Ti–6242. Oxygen concentration data were normalized with respect to the bulk oxygen concentrations, 0.2 wt. % and 0.15 wt. % for Ti–64 and Ti–6242, respectively. More extensive description about the normalization of the EPMA oxygen concentration data can be found elsewhere [44]. It can be seen that there is a gradient of oxygen in the alpha–case layer. The oxygen concentration is highest at the surface and gradually decreases moving towards the bulk, where it reaches the oxygen bulk concentration and becomes constant (see Figure 9(c)). It is important to note that the presented normalized oxygen concentration values do not correspond to the absolute oxygen concentration diffused into the substrate, as there are some difficulties in quantifying the oxygen content using EPMA. However, these normalized oxygen profiles show the distribution of oxygen along the thickness of the sample and can be used to estimate the thickness of the alpha–case layer.

Table 3 compares optically measured (OM) and EPMA estimated alpha–case thicknesses for both alloys. Good agreement between both types of quantification for both alloys and for all temperatures and times was found, except in Ti–6242 for the heat treatments performed at 700 ºC for the time interval 300–500 hours, where the EPMA oxygen concentration profiles indicated about 50 μm thicker alpha–case layer than estimated with OM. These results confirmed that the metallographic evaluation is a reliable technique for determining the

thickness of the alpha–case layer in Ti–64 and Ti–6242, with exception in Ti–6242 at 700 ºC for time intervals longer than 300 hours.

Table 3. Comparison of the alpha–case thickness values measured using OM and EPMA in Ti–64 and Ti–6242.

		Ti–64		Ti–6242	
		OM	EPMA	OM	EPMA
		Alpha–case thickness (µm)	Alpha–case thickness (µm)	Alpha–case thickness (µm)	Alpha–case thickness (µm)
T (ºC)	Time (h)				
500	5	0	0	1.5 ± 0.2	2 ± 1
	50	1.7 ± 0.2	3 ± 1	2.9 ± 0.7	4 ± 1
	500	6.5 ± 0.5	7 ± 1	9 ± 1.8	9 ± 1
593	5	1.5 ± 0.5	5 ± 2	2.2 ± 0.3	5 ± 1
	50	8.3 ± 0.8	10 ± 2	8.9 ± 1.8	12 ± 2
	500	31.7 ± 2.2	30 ± 2	28.4 ± 2	35 ± 2
700	5	24.3 ± 2.2	30 ± 2	14.5 ± 1.5	17 ± 2
	50	60.2 ± 3.9	55 ± 2	32.5 ± 1.6	33 ± 4
	500	198.5 ± 13.5	200 ± 2	107.2 ± 4.2	157 ± 2

3.4 Comparison of the estimated and optically measured alpha–case thickness values

By substituting Eq. 2 in Eq. 1 the following expression will result:

$$x = \sqrt{D_0 \exp\left(-\frac{Q}{RT}\right) \cdot t} \qquad (3)$$

where x is the alpha–case thickness, D_0 is the pre–exponent factor, Q is the activation energy for diffusion of oxygen, R is the universal gas constant (8.3143 J/(mol K)) and T is the temperature (K). Eq. 3 was applied to estimate the alpha–case thickness in Ti–64 and Ti–6242 for all three tested temperatures and times, by using D_0 and Q values obtained from the optical measured alpha–case thickness values from the present study (see Table 4).

Table 4. Pre–exponent factors D_0 and activation energies Q for Ti–64 and Ti–6242 alloys.

Pre–exponent factor D_0 (m^2/s)		Activation Energy Q (kJ/mol)	
Ti–64	Ti–6242	Ti–64	Ti–6242
$6.31 \cdot 10^{-3}$	$6.54 \cdot 10^{-7}$	215	153

Figure 10 compares the estimated alpha–case thicknesses using Eq. 3 with those measured optically for both alloys at all three tested temperatures. Good agreement between the estimated and measured values is found for heat treatments performed at 500 and 593 ºC (see Figure 10(a) and (b)) for both alloys. In contrast for the treatment performed at 700 ºC, a higher degree of inconsistency between the estimated and the measured values was observed after 200 and 300 hours in Ti–64 and Ti–6242, respectively (see Figure 10(c)). This indicates that alpha–case formation does not fully obey Arrhenius behaviour at 700 ºC and time intervals longer than 200 hours. It is assumed that the major factors to such behaviour are the morphology changes of the oxide scales with respect to time and the influence of the main alloying elements to both the oxide scale formation and oxygen diffusion into the bulk metal.

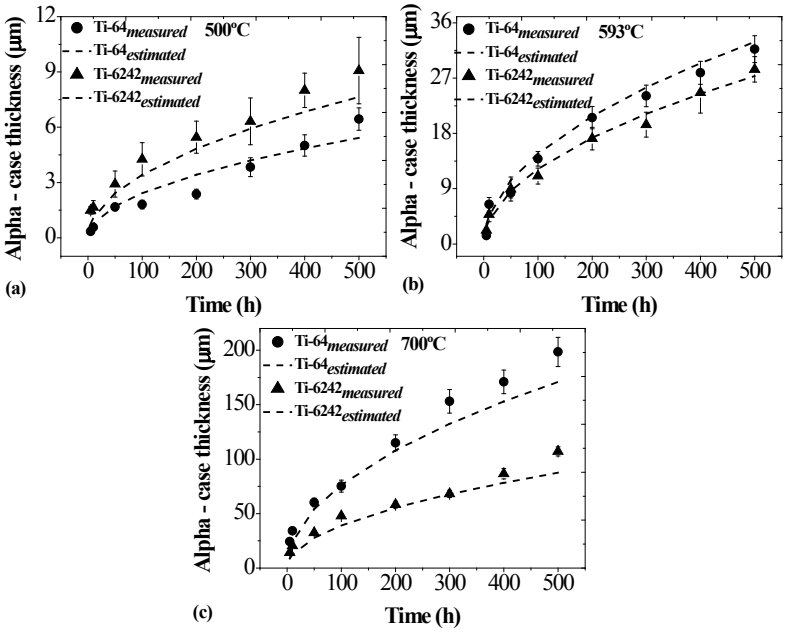

Fig. 10. Optically measured *vs*. estimated alpha–case thickness of Ti–64 and Ti–6242 alloy at (a) 500 ºC, (b) 593 ºC and (c) 700 ºC.

3.5 Analysis of the EPMA profiles of the main alloying elements in the alpha–case layer

Figure 11 shows representative optical micrographs near the sample surface of the Ti–64 and Ti–6242 samples, before and after heat treatment at 700 °C for 500 hours. Figure 11 (a) and (b) compare the microstructure before and after heat treatment of Ti–64. It can be seen that coarsening of the primary α grains in Ti–64 occurred as result of the performed heat treatment. Such coarsening of the microstructure was not observed in Ti–6242 (see Figure 11(c) and (d)). Additionally, from the optical micrographs shown in Figure 11, it can be seen that the heat treatment resulted in increase of the amount of alpha phase in both alloys. The increase of the alpha phase in the two alloys can be observed visually by comparing the optical micrographs.

From the EPMA composition profiles of Ti–64 and Ti–6242 shown in Figure 9 (see section 3.3.2), it can be seen that the concentration profiles for vanadium in Ti–64 and molybdenum in Ti–6242 varied significantly with respect to the thickness of the alpha–case layer. Vanadium and molybdenum are β–isomorphous elements, both with high solubility in β phase above the β–transus temperature. However, their solubility in α phase is limited to about 2.7 at. % for Ti–64 and 0.4 at. % for Ti–6242, respectively [46]. Guided by the fact that alpha–case formation in Ti alloys is related to phase transformation from β to α at elevated temperatures and oxygen containing environments, it is believed that the concentration profiles of the β and α stabilizing elements (V, Mo and Al) in both alloys can reveal details about the alpha–case formation mechanism in the two studied alloys.

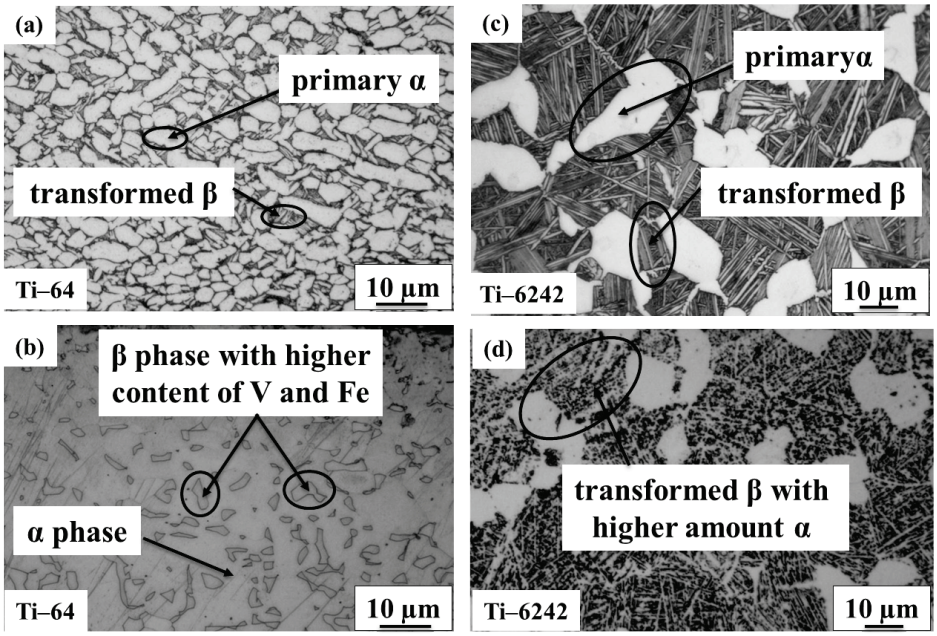

Fig. 11. Optical micrographs of (a) as–received Ti–64, (b) alpha–case layer in Ti–64 after heat treatment at 700 ºC for 500 hours, (c) as–received Ti–6242 and (d) alpha–case layer in Ti–6242 after heat treatment at 700 ºC for 500 hours.

Figure 12 compares the EPMA concentration profiles of β and α alloying elements in Ti–64 (vanadium and aluminium) and in Ti–6242 (molybdenum and aluminium) before and after heat treatment at 700 ºC for 500 hours for defined distance from the surface of the samples (90 µm). It is important to note that the EPMA measurement was performed in point (0.5 µm diameter) mode, where the spacing between each point was 0.5–1 µm. It is considered that following the distribution of the main α and β alloying elements obtained from the EPMA measurement, would give information of the size and distribution of α and β phases in the alloys before and after heat treatment. For example, when β phase is probed then increase of the concentration of β stabilizing element is observed and when α phase is probed then the concentration drops to minimum. This maximum and minimum concentration of the β stabilizing element results in peaks in the EPMA profile that represent β phase (see Figure 12 (a), designation 1), whereas each plateau between peaks depicts α phase, where the concentration of the β stabilizing elements is low (see Figure 12 (a), designation 2). Similar shape (i.e. peaks and plateaus) of the concentration profiles of α stabilizing elements were observed (see aluminium concentration profiles in Figure 12). Two parameters characterize the EPMA concentration profiles of α and β stabilizing elements: 1) height and width of the peak and 2) width of the plateau between peaks. The height of the peaks corresponds to the measured concentration of the β stabilizing element, whereas the width of the peak and the plateau corresponds to α and β phase sizes and their distribution in the alloys.

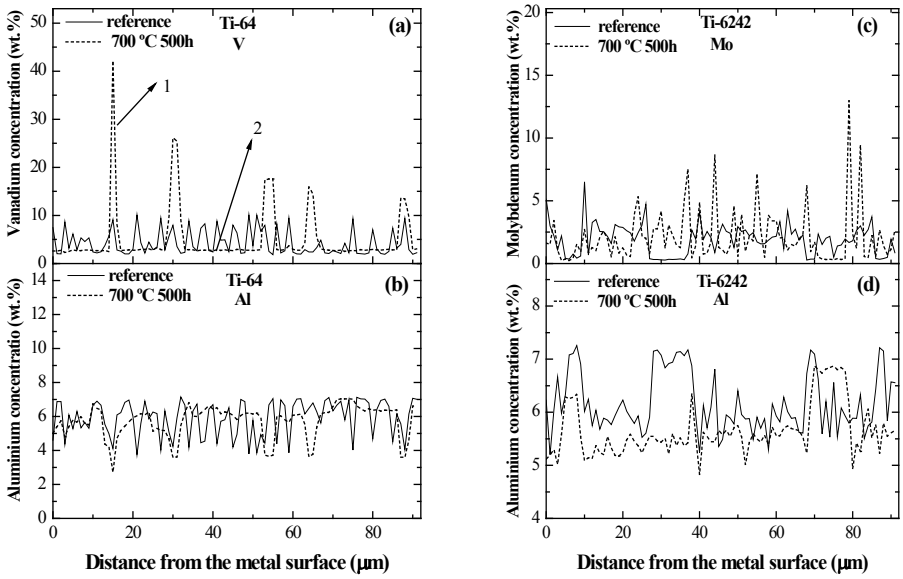

Fig. 12. EPMA (a) vanadium and (b) aluminium concentration profiles in Ti–64 alloy, reference sample (solid lines) and heat treated sample at 700 ºC after 500 hours (dashed lines); EPMA (c) molybdenum and (d) aluminium concentration profiles in Ti–6242 alloy, reference sample (solid lines) and sample heat treated at 700 ºC after 500 hours (dashed lines).

Based on analysis of the EPMA concentration profiles of the β and α stabilizing element for the two alloys shown in Figure 12 two phenomena were observed. In continuation both phenomena will be discussed separately with respect to the alloy where they were noted. In Ti–64, significant rise of the peak heights (i.e. vanadium concentration) occurred, ranging from maximum 12 wt. % in the reference sample to about 42 wt. % at maximum after the treatment at 700 ºC for 500 hours. It was noted that vanadium concentration rise is dependent on the oxygen content in the bulk of the metal. At distances close to the metal surface (15 μm) (see Figure 12(a)), the highest vanadium concentration was observed (42 wt. %), which gradually decreased moving towards the bulk of the sample and reached the average bulk concentration of vanadium about 4.5 wt. % (see Table 1). It was observed that vanadium during the long heat treatment (500 hours) is accumulating in the β phases of the alloy (see Figure 12(a)). Such accumulation is not surprising because the atomic radius of titanium (176 pm) and vanadium (171pm) are very similar [47]. The accumulation of vanadium causes saturation of the β phase with vanadium forming a solid solution. The relatively fast air cooling to room temperature in a few minutes has not affected significantly the concentration of vanadium in the β phase. An increase of the peak and plateau widths in the EPMA vanadium concentration profile for the treatment at 700 ºC for 500 hours was found, compared to the reference sample. This indicates a change in the microctructure, which can be seen in Figure 11 a) and b). Additionally, higher content of iron in β phases was found, ranging from 2–10 wt. % compared with the reference material (see Table 1). It is known that iron contents larger than 0.1 wt. % stabilize β phase at temperatures above 590 ºC. Fe is a β–eutectoid element with 590 ºC as eutectoid temperature below which β–Ti decomposes into α–Ti and intermetallic FeTi. However, if the cooling rate is fast enough, this decomposition

do not occur and β–Ti remains at the grain boundaries forming precipitates, which suppress the grain coarsening [46]. Such β phase rich with vanadium and iron are found in the microstructure of the alpha–case layer in Ti–64 alloy after heat treatment at 700 °C (see Figure 11(b)). It is considered that Ti and V form solid solution at 700 °C and this was confirmed by the Ti–V phase diagram [48]. Additionally, from the Al concentration profiles shown in Figure 12 b) for Ti–64 it can be seen that the sharp peaks in the reference sample become very broad after heat treatment. This result indicates that coarsening of the microstructure in Ti–64 after heat treatment occurred.

The microstructure of Ti–6242 is more complex and the interpretation of the molybdenum and aluminium EPMA concentration profiles was more difficult to conduct (see Figure 12(c) and (d)). No obvious trend was observed between the reference and the heat–treated sample in terms of variation of the molybdenum concentration as in Ti–64 for vanadium. Instead, narrowing of the peaks and broadening of the plateaus width with respect to temperature were observed (see Figure 12(b)). This indicates that molybdenum tends to be in the β phase in a similar manner as vanadium in Ti–64, which is expected because these elements are both strong beta stabilizers. As can be seen from the optical micrographs shown in Figure 11 (c) and (d) there is an increase of the amount of α phase after heat treatment compared to the as–received material. However, the increase was not quantified. Moreover, depletion of aluminium content in the alpha–case layer in Ti–6242 after heat treatment was noted, which confirms that aluminium diffuses outward and contributes to the oxidation resistance by forming dense Al_2O_3 layer on top of the oxide scale.

4. Conclusions

The oxide scale and the alpha–case layer formed after isothermal heat treatment in air at the temperature range 500–700 °C in Ti–64 and Ti–6242 were characterized by means of microscopic techniques. The following conclusions are made:

- The heat treatment of the two alloys at all three tested temperatures resulted in simultaneous formation of oxide scale and alpha–case layer beneath the oxide scale.
- The oxidation of Ti–64 was faster than the oxidation of Ti–6242 alloy at 593 and 700 °C for times up to 500 hours.
- The heat treatment at 700 °C for 500 hours resulted in formation of multi–layered oxide scale in Ti–64, whereas such morphology of the oxides scale was absent in Ti–6242 alloy.
- For both alloys there was good agreement between the metallographically measured and the EPMA estimated alpha–case layer thicknesses at all temperatures and times, except at 700 °C for 500 hours in Ti–6242 where the optically measured alpha case thickness was smaller than that estimated with EPMA.
- Analysis of the EPMA concentration profiles of the main α and β alloying elements showed a re-distribution of alloying elements in the microstructure after heat treatment.
- From the metallographic examination and the EPMA concentration profiles it can also be concluded that the primary α grains in the microstructure of Ti–64 coarsened after heat treatment at 700 °C for 500 hours and that formation of solid solution of vanadium and iron in β phase occurs.

Acknowledgments

The authors kindly acknowledge the Joint European Doctoral Programme in Materials Science and Engineering Programme (DocMASE), Graduate School of Space Technology and the Aeronautical Research Engineering Programme (NFFP) for financial support. The authors would like to acknowledge GKN Aerospace Engine Systems Sweden for its support during the research work and Francois Mattera for assisting in performing the heat treatments. We would like to acknowledge Morten Raanes at Norwegian University of Science and Technology, Norway for performing the EPMA measurements and for fruitful discussions in evaluating the results. Additionally the authors are grateful to Professor Ragnar Tegman for the discussions of the results.

References

[1] Lütjering G. and Williams J. C., **2007,** *Titanium* 2nd Ed., (Berlin, Springer–Verlag).

[2] Leyens C. and Peters M., **2003,** *Titanium and titanium alloys*, (Wiley VCH Verlag GmbH, Weinheim), 187.

[3] Boyer R. R., *An overview on the use of titanium in the aerospace industry*, **1996,** Materials Science and Engineering A213, 103–114.

[4] Donachie M. J., **2000,** *Titanium: A Technical Guide*, (ASM International, Ohio, USA)

[5] Eylon D., Fujishiro S., Postans P. J. and Froes F. H., *High temperature titanium alloys–A review*, **1984,** Journal of Metals, 55–62.

[6] Senoy R. N., Unnam J. and Clark R. K., *Oxidation and embrittlement of Ti–6Al–2Sn–4Zr–2Mo alloy*, **1986,** Oxidation of Metals 26, 105–124.

[7] Unnam J., Senoy R. N. and Clark R. K., *Oxidation of commercial purity titanium*, **1986,** Oxidation of Metals 26, 231–252.

[8] Chan Kwai S., Koike M., Johnson Benjamin W. and Okabe T., *Modelling of alpha–case formation and its effect on the mechanical properties of titanium alloy castings*, **2008,** Metallurgical and Materials Transactions 39A, 171–180.

[9] Shamblen C. E. and Redden T. K., *Air contamination and embrittlement in titanium alloys*, **1968,** The Science, Technology and Application of Titanium (Pergamon Press, Oxford, United Kingdom), 199–208.

[10] Leyens C., Peters M., Weinem D. and Kaysser W. A., *Influence of long–term annealing on tensile properties and fracture of near–α titanium alloy Ti–6Al–2.75Sn–4Zr–0.4Mo–0.45Si*, **1996,** Metallurgical and Materials Transactions 27A, 1709–1717.

[11] Evans R. W., Hull R. J. and Wilshire B., *The effects of alpha–case formation on the creep fracture properties of the high–temperature titanium alloy IMI834*, **1996,** Journal of Materials Processing Technology 56, 492–501.

[12] Pilchak A. L., Porter W. J. and John R., *Room temperature fracture processes of a near–α titanium alloy following elevated temperature exposure*, **2012,** Journal of Materials Science 47, 7235–7253.

[13] Gaddam R., Antti M. L. and Pederson R., *Influence of alpha–case layer on the low cycle fatigue properties of Ti–6Al–2Sn–4Zr–2Mo alloy*, **2014,** Materials Science and Engineering A599, 51–56.

[14] Sung S. Y. and Kim Y. J., *Alpha–case formation mechanism on titanium investment castings*, 2005, Materials Science and Engineering A405, 173–177.

[15] Jordan D., *Study of alpha case formation on heat treated Ti–6–4 alloy*, **2008,** Heat Treating Progress 8, 45–47.

[16] Fujishiro S. and Eylon D., *Improved high temperature mechanical properties of titanium alloys by platinum ion plating*, **1978,** Thin Solid Films 54, 309–315.

[17] Leyens C., Peters M. and Kaysser W. A., *Intermetallic Ti-Al coatings for protection of titanium alloys: oxidation and mechanical behavior*, **1997,** Surface and Coatings Technology 94–95, 34–40.
[18] Gurrappa I. and Gogia A. K., *Development of oxidation resistant coatings for titanium alloys*, **2001,** Materials Science and Technology 17, 581–587.
[19] Du H. L., Datta P. K., Lewis D. B. and Burnel–Gray J. S., *Air oxidation behaviour of Ti–6Al–4V alloy between 650 and 850 °C,* **1994,** Corrosion Science 36, 631–642.
[20] Frangini S., Mignone A. and De Riccardis F., *Various aspects of the air oxidation behaviour of a Ti6Al4V alloy at temperatures in the range 600–700 °C*, **1994,** Journal of Materials Science 29, 714–720.
[21] Sugiura Y., *Growth behaviors of alpha cases in Ti–6Al–4V and Ti–10V–2 Fe–Al alloys during high temperature heat treatment in air*, **2003,** Titan–2003, Science and Technology IV, Weinheim, Wiley–VCH, 2051–2057.
[22] Sai Srinadh K. V. and Singh V., *Oxidation behaviour of the near α–titanium alloy IMI 834,* **2004,** Bulletin of Materials Science 27, 347–354.
[23] Peters P. W. M., Hemptenmacher J. and Todd C., *Oxidation and stress enhanced oxidation of Ti–6–2–4–2*, **2004,** Titan–2003, Science and Technology IV, Weinheim, Wiley–VCH, 2067–2074.
[24] Guleryuz H. and Cimenoglu H., *Oxidation of Ti–6Al–4V alloy*, **2009,** Journal of Alloys and Compounds 472, 241–246.
[25] McReynolds K. S. and Tamirisakandala S., *A study on alpha–case depth in Ti–6Al–2Sn–4Zr–2Mo*, **2011,** Metallurgical and Materials Transactions 42A, 1732–1736.
[26] Jia W., Zeng W., Zhang X., Zhou Y., Liu J. and Wang Q., *Oxidation behavior and effect of oxidation on tensile properties of Ti60 alloy*, **2011,** Journal of Materials Science 46, 1351–1358.
[27] Poquillon D., Armand C. and Huez J., *Oxidation and oxygen diffusion in Ti–6al–4V alloy: Improving measurements during Sims analysis*, **2013,** Oxidation of Metals 79, 249–259.
[28] Zeng S., Zhao A., Jiang H., Fan X., Duan X. and Yan X., *Cyclic oxidation behaviour of the Ti–6Al–4V alloy*, **2014,** Oxidation of Metals 81, 467–476.
[29] Aerospace Series–Test methods–Titanium and titanium alloys–Part 009–Determination of surface contamination (SS–EN 2003–009:2007), Swedish Standards Institute, **2007**.
[30] AMS 4911 L, **2008,** Titanium alloy, sheet, strip and plate 6Al–4V annealed (SAE–AMS/MAM).
[31] AMS 4976 G, **2008,** Titanium alloy, forgings 6.0Al–2.0Sn–4.0Zr–2.0Mo solution and precipitation heat treated (SAE–AMS/MAM).
[32] Leyens C., Peters M. and Kaysser W. A., *Influence of microstructure on oxidation behaviour of near–α titanium alloys*, **1996,** Materials Science and Technology 12, 213–218.
[33] Velasco B. G. and Aswath P. B., *Microstructural stability, microhardness and oxidation behaviour of in situ reinforced Ti–8.5Al–1B–1Si (wt%)*, **1998,** Journal of Materials Science 33, 2203–2214.
[34] Gurrappa I., Manova D. and Gerlach J.W., *Influence of nitrogen implantation on the high temperature oxidation of titanium–base alloys*, **2006,** Surface and Coatings Technology 201, 3536–3546.
[35] Chaze A. M. and Coddet C., *Influence of aluminium on the oxidation of titanium between 550 and 750 °C*, **1990,** Journal of the Less Common Metals 157, 55–70.
[36] Becker S., Rahmel A., Schorr M. and Schutze M., *Mechanism of isothermal oxidation of the intermetallic TiAl and of TiA1 Alloys,* **1992,** Oxidation of Metals 38, 425–464.

[37] Champin B., Graff L. Armand M., Beranger G. and Coddet C., *Oxidation of titanium alloys used at temperatures close to those in turbomachinery*, **1978,** Journal of the Less Common Metals 69, 163–183.

[38] Andersson A. and Andersson S.L.T., *Characterization of vanadium oxide catalysis in relation to activities and selectivities for oxidation and ammooxidation of alkylpyridines,* **1985,** American Chemical Symposium Series 279, 121–142.

[39] Tripp H. P. and King B. W., *Thermodynamic data on oxides at elevated temperatures*, **1955,** Journal of American Ceramic Society 38, 432–437.

[40] E. A. Gulbransen, K. F. Andrew and F. A. Brassart, *Vapor pressure of Molybdenum trioxide*, Journal of the Electrochemical Society 110, **1963**, 242–243.

[41] Kofstad P., **1988,** *High Tepmerature Corrosion*, Springer.

[42] Liu Z. and Welsch G., *Literature survey on diffusivities of oxygen, aluminum, and vanadium in alpha titanium, beta titanium, and in rutile*, **1988,** Metallurgical Transactions 19A, 1121–1125.

[43] Pitt F. and Ramulu M., *Influence of grain size and microstructure on oxidation rates in titanium alloy Ti–6Al–4V under superplastic forming conditions*, **2004,** Journal of Materials Engineering and Performance 13, 727–734.

[44] Gaddam R., Sefer B., Pederson R. and Antti M.L., *Oxidation and alpha case formation in Ti–6Al–2Sn–4Zr–2Mo alloy*, **2014,** submitted.

[45] Reed–Hill R. E., 1988, Physical Metallurgy 2nd Ed., Van Nostrand.

[46] Simbi D. J. and Scully J. C., *The effect of residual interstitial elements and iron on mechanical properties of commercially pure titanium*, **1996,** Materials Letters 26, 35–39.

[47] E. Clementi, D. L. Raimond, W. P. Reinhard, *Atomic screening constants from SCF functions, II., Atoms with 37 to 86 electrons,* **1967,** Journal of Chemical Physics 47, 1300–1307.

[48] Murray J. L., *Phase Diagrams of Binary Titanium Alloys*, ASM International, Metals Park, OH, **1987,** 319–327.